CHROMATIN REGULATION: HOW NUCLEOSOMES FIND THEIR POSITIONS AND THE ROLE OF CHROMATIN BINDING PROTEINS IN CELLULAR QUIESCENCE

by

THOMAS BENJAMIN BAILEY

A DISSERTATION

Presented to the Department of Chemistry and Biochemistry
and the Division of Graduate Studies of the University of Oregon
in partial fulfillment of the requirements
for the degree of
Doctor of Philosophy

December 2022

DISSERTATION APPROVAL PAGE

Student: Thomas Benjamin Bailey

Title: Chromatin Regulation: How Nucleosomes Find Their Positions and the Role of Chromatin Binding Proteins in Cellular Quiescence

This dissertation has been accepted and approved in partial fulfillment of the requirements for the Doctor of Doctor of Philosophy degree in the Department of Chemistry and Biochemstry by:

Diane Hawley	Chairperson
Eric Selker	Advisor
David Garcia	Core Member
Julia Widom	Core Member
Raghuveer Parthasarathy	Institutional Representative

and

Krista Chronister	Vice Provost for Graduate Studies

Original approval signatures are on file with the University of Oregon Division of Graduate Studies.

Degree awarded December 2022

DISSERTATION ABSTRACT

Thomas Benjamin Bailey

Doctor of Philosophy

Department of Chemistry and Biochemistry

December 2022

Title: Chromatin Regulation: How Nucleosomes Find Their Positions and the Role of Chromatin Binding Proteins in Cellular Quiescence

Chromatin is made up of an organism's DNA and DNA binding proteins inside of the nucleus. Nucleosomes are the fundamental unit of chromatin, consisting of a 147 base pair DNA sequence and a protein octamer comprised of 8 histone proteins, two copies of histone H2A, H2B, H3, and H4. Nucleosomes are used to regulate gene expression in both the positioning of the nucleosome along DNA, or the post-translational histone modifications. In the first chapter, we will demonstrate that the chromatin binding protein, Tup1 is essential for nucleosome positioning and H3K23 deacetylation, which is required for entry into cellular quiescence. In the next chapter, we will address how the chromatin remodeler complex, Isw2, precisely positions nucleosomes through direct interactions with transcription factors. In the next chapter, we present an optimized protocol for measuring nucleosome positioning. Finally, we will end on some preliminary data and discussion on the next steps in researching Tup1 and Isw2.

This dissertation contains previously published co-authored material.

CURRICULUM VITAE

NAME OF AUTHOR: Thomas Benjamin Bailey

GRADUATE AND UNDERGRADUATE SCHOOLS ATTENDED:

University of Oregon, Eugene
University of North Carolina – Wilmington, Wilmington, NC

DEGREES AWARDED:

Doctor of Philosophy, 2022, University of Oregon
Bachelor of Science, 2016, University of North Carolina - Wilmington

AREAS OF SPECIAL INTEREST:

Molecular Biology
Cell Biology
Genomics
Genetics

PROFESSIONAL EXPERIENCE:

Graduate Teaching Fellow, University of Oregon, 2016

Graduate Research Assistant, University of Oregon, 2016-2022

GRANTS, AWARDS, AND HONORS:

UNCW Chancellor's Achievement Award (2012 & 2014)

Dean's List (2012 & 2013)

Summer Undergraduate Research and Creativity Award Recipient (2015)

Center for the Support of Undergraduate Research and Fellowship Supplies Award (2014)

National Institute of Health Molecular Biology and Biophysics Training Grant (2018)

PUBLICATIONS:

McKnight, L. E., Crandall, J. G., **Bailey, T. B.**, Banks, O. G. B., Orlandi, K. N., Truong, V. N., Donovan, D. A., Waddell, G. L., Wiles, E. T., Hansen, S. D., Selker, E. U., & McKnight, J. N. (2021). Rapid and inexpensive preparation of genome-wide nucleosome footprints from model and non-model organisms. STAR Protocols, 2(2), 100486. https://doi.org/10.1016/j.xpro.2021.100486

Donovan DA, Crandall JG, Truong VN, Vaaler AL, **Bailey TB**, Dinwiddie D, Banks OG, McKnight LE, McKnight JN. Basis of specificity for a conserved and promiscuous chromatin remodeling protein. Elife. 2021 Feb 12;10:e64061. doi: 10.7554/eLife.64061. PMID: 33576335; PMCID: PMC7968928.

ACKNOWLEDGMENTS

I wish to express sincere appreciation to Laura McKnight and Eric Selker in their help with writing and preparing this manuscript, as well as their guidance in experimental design. In addition, special thanks are due to Kenichi Noma and the members of the Noma lab who provide valuable feedback on experiments and data. I also thank the members of the Institute of molecular Biology for their feedback and support. Lastly, I want to thank Jeff McKnight, without whom none of this work would be possible. This work was supported by a National Institutes of Health training grant T32 GM007759 (to T.B.B), and by NIGMS R01 GM129242 (to J.N.M. and L.E.M).

This thesis is dedicated to Jeff McKnight, whose brilliance, kindness, and humility impacted everyone he knew. You will be forever missed.

TABLE OF CONTENTS

LIST OF FIGURES

Figure Page

LIST OF TABLES

Table Page

CHAPTER I:

INTRODUCTION

Chromatin refers to the combination of DNA, proteins, and RNA found in the nuclei of cells. The most fundamental unit of chromatin is the nucleosome, which is comprised of DNA wrapped around a histone protein octamer (Felsenfeld, 1978). The histone octamer is comprised of two copies of histone H2A, H2B, H3, and H4 (Ramakrishnan, 1997). Cells can make modifications to chromatin, which influences transcription of genes (Ehrensberger & Svejstrup, 2012). This allows cells to adapt to their environment or for multicellular organisms to generate a diverse population of cells from the same underlying sequence of DNA (Ehrensberger & Svejstrup, 2012; Weiner et al., 2015). Aberrations in these processes are associated with disease states, particularly cancer (Beck et al., 2012; Corces et al., 2018; Polak et al., 2015; Valencia & Kadoch, 2019; Weinstein et al., 2013). Modifications to chromatin can take many forms: histone variants can be exchanged, nucleosomes can be repositioned along DNA, histone proteins can be post-translationally modified, and DNA can be chemically modified, to name a few. In this work we will focus on nucleosome positioning and histone post translational modifications and how *S. cerevisiae* utilizes these to induce quiescence as a survival mechanism.

Nucleosome positioning is the translocation of one nucleosome to a new sequence of DNA. Nucleosomes are actively positioned by chromatin remodelers, a class of proteins that have an ATPase motor that is required to move nucleosomes (Lusser & Kadonaga, 2003). Chromatin remodelers slide nucleosomes along DNA to prevent binding of transcription factors or evict transcription factors as the presence of

nucleosomes typically prevents the binding of DNA binding factors (Lorch & Kornberg, 2017). Chromatin remodelers are classified into four distinct families: SWI/SNF (switch/sucrose-non-fermenting), ISWI (imitation switch), CHD (chromodomain-helicase-DNA binding) and INO80 (inositol requiring 80) (Tyagi et al., 2016). In this thesis we will focus on ISW2, a member of the ISWI family of chromatin remodelers and how it plays a key role in regulating nucleosome positions during quiescence.

Histone proteins are heavily post-translationally modified, which allows cells to regulate gene expression. Histone post-translational modifications (PTMs) typically occur on histone tails, however there are also many that occur in the histone fold domain (Rothbart & Strahl, 2014). Histone PTMs are known to regulate the recruitment of chromatin binding proteins, as well as alter the dynamics of histone/DNA interactions. The acetylation mark is one such histone PTM where the acetyl group of acetyl-COA is covalently bound to a lysine. Histones are acetylated by histone acetyl transferases (HATs) and deacetylated by histone deacetylases (HDACs) (Kurdistani & Grunstein, 2003). Because the acetylation neutralizes the positive charge on lysine, it loses affinity for the negatively charged DNA, which make the histone more amenable for transcription factor binding or RNA-polymerase II mediated transcription. Thus, acetyl marks on histone tails are associated with active transcription (Struhl, 1998; Turner, 1991). There are many places on the histone where we see acetyl marks, however for this study we will focus on the acetylation of lysine 23 on histone H3 (H3K32ac). H3K23ac, which is catalyzed by the histone deacetylase complex Rpd3, has been shown to decrease during cellular quiescence. Rpd3 is known to interact with many factors, and we demonstrate

that Tup1, a known Rpd3 interactor, is essential in its function to repress genes during quiescence.

CHAPTER II:

TUP1 IS CRITICAL FOR TRANSCRIPTIONAL REPRESSION IN QUIESCENCE IN *S. CEREVISIAE*

Introduction

Cellular quiescence is a non-proliferative cell state that appears conserved across all life (Marescal & Cheeseman, 2020; Rittershaus et al., 2013; van Velthoven & Rando, 2019). Quiescent cells are distinct from other non-dividing cells, such as senescent and terminally differentiated cells, in that quiescent cells can return to a proliferative state if the right conditions are met. Quiescence is necessary for the survival of unicellular organisms in environments that are unfavorable for proliferation; in fact, most microbes in nature are quiescent (O'Farrell, 2011; Valcourt et al., 2012). In multicellular eukaryotes, quiescence plays a critical role in various cell types including stem cells, fibroblasts, and lymphocytes (Tümpel & Rudolph, 2019; van Velthoven & Rando, 2019; Yao, 2014). The inability to properly regulate quiescence can lead to cancer; additionally, cancer stem cells can become quiescent, leading to drug resistance and the ability to initiate relapse at a later time (Vallette et al., 2019). All quiescent cells have conserved characteristics including transcriptional repression, increased cell density, translational repression, and decreased cell metabolism (de Virgilio, 2012; Gray et al., 2004; Miles et al., 2021; Sun & Gresham, 2021). Many of the components that regulate quiescence are found throughout life and likely have conserved functions; however, some of the fundamental ways cells regulate entry, exit, and maintenance of quiescence are not fully understood (Yanagida, 2009).

Saccharomyces cerevisiae is a well-established model organism for studying cellular quiescence because it can reliably produce a population of quiescent cells (Gray et al., 2004; Sun & Gresham, 2021). Quiescence is notoriously difficult to study in multicellular organisms due to the lack of quiescence-specific biomarkers and because it is difficult to determine which cells are quiescent until they begin dividing again. *S. cerevisiae* can produce a large population of quiescent cells that can be isolated by density centrifugation (Allen et al., 2006). Additionally, budding yeast is capable of surviving mutations that would be lethal in higher order organisms, allowing study of critically important factors in the process of establishing quiescence (Miles et al., 2021; Sun & Gresham, 2021). Because many of the fundamental components that regulate the cell cycle are conserved between budding yeast and higher eukaryotes, we suspect that many players involved in cell cycle arrest are highly conserved.

Tup1-Ssn6 is a transcriptional corepressor complex that globally regulates many cell processes in *S. cerevisiae* (Malavé & Dent, 2006). Tup1 serves mostly as a repressor, although it can also induce gene expression in some contexts depending on its phosphorylation state (Conlan et al., 1999; Proft and Struhl, 2002). Tup1 forms a complex with Ssn6 in which 3-4 Tup1 molecules associate with each Ssn6 molecule (Varanasi et al., 1996). The structure of Tup1 contains an N-terminal helix, which facilitates oligomerization and interacts with histone tails, and a beta-propeller domain composed of seven WD40 domains, which interact with other proteins such as histone deacetylases (HDACs) and DNA binding factors (Sprague et al., 2000). While the detailed mechanism of repression by Tup1 is unknown, some relevant information is available. Tup1 is recruited by sequence-specific transcription factors to DNA (Hanlon et

al., 2011), where it recruits histone deacetylases to generate hypoacetylated regions of chromatin, typically associated with transcriptional repression (Davie et al., 2003; Fleming et al., 2014; Watson et al., 2000; Wu et al., 2001). In addition to HDAC recruitment, Tup1 interacts directly with nucleosomes by binding histone H3 and H4 tails, preferentially to hypoacetylated tails, to stabilize +1 nucleosomes that have been repositioned by Isw2 (Chen et al., 2013; Li & Reese, 2001; Rizzo et al., 2011; Zhang & Reese, 2004b). Tup1 also interacts directly with the Mediator complex through its subunit Hrs1, potentially inhibiting transcription into gene bodies (Papamichos-Chronakis et al., 2000). Lastly, Tup1 is thought to influence transcription by blocking the recruitment of activating factors to chromatin (Parnell & Stillman, 2011; Wong & Struhl, 2011).

Homologues of Tup1-Ssn6 found in higher eukaryotes include Groucho in drosophila, Grg in mice, and TLE1 in humans (Jennings & Ish- Horowicz, 2008). While the beta-propeller domain is well conserved in both sequence and structure, the sequence of the N-terminus is poorly conserved; however, it appears to be structurally conserved in simulations (Jumper et al., 2021; Varadi et al., 2022). Cross-species interactions have been established, where TLE family proteins can pull down yeast Ssn6 from cellular lysate, suggesting strong conservation of structure and function (Flores-Saaib & Courey, 2000; Grbavec et al., 1999). Mice and flies exhibit severe developmental phenotypes in Groucho/TLE null or hypomorphic mutations (Agarwal et al., 2015). Additionally, in humans TLE1 is currently being studied as both a cancer biomarker and a potential cancer therapeutic drug target (Ogawa et al., 2019; Yuan et al., 2017).

During quiescence in yeast, it has been observed that nucleosomes are repositioned and histone tails are deacetylated (McKnight, Boerma, et al., 2015;

McKnight, Breeden, et al., 2015). Tup1 plays a role in histone deacetylation and chromatin remodeling in other contexts (Davie et al., 2003; Zhang & Reese, 2004b); however, it is unclear whether Tup1 contributes to these processes in quiescence. Tup1 has been identified as a gene that is essential for viability of cells in G0 and is implicated in glucose repression in yeast, but there is no known molecular mechanism to explain its role in these processes (Lin et al., 2017; Papamichos- Chronakis et al., 2004; Reimand et al., 2012; Williams et al., 1991; Williams & Trumbly, 1990). Here, we demonstrate that Tup1 is essential for repressing target genes in stationary phase by interacting with Rpd3 and Isw2 to generate regions of repressed chromatin. We also show that cells lacking Tup1 display morphological defects in stationary phase, suggestive of a possible role for Tup1 in mitosis.

Results

Tup1 Relocalizes After Glucose Starvation

Because Tup1 is a master regulator of many processes in *S. cerevisiae*, we sought to investigate the consequences of glucose starvation on Tup1 localization across the genome. We performed ChIP-Seq analysis on a Myc-tagged Tup1 strain during log phase, diauxic shift, and stationary phase (Figure 1A). Ideally, we would work with purified quiescent cells, but due to the unusual clumping of Tup1 deletion strains (Supplementary Figure 1), which is not alleviated by the addition of EDTA, it was impossible to isolate pure populations of quiescent cells. We therefore performed ChIP for Tup1 in stationary phase cells so that direct comparisons could be made to Δtup1 strains. However, we do anticipate that the findings in stationary phase will translate to quiescence because we observed that a fraction of stationary cells in Tup1 knockout

strains are viable and can re-enter the cell cycle when plated on glucose rich media. Additionally, we know that Tup1 knockouts have reduced viability in G0, indicating that Tup1 plays a critical role in quiescence.

In log phase, we observed Tup1 binding to the promoters of roughly 923 genes, including genes for ribosomal protein subunits, tRNAs, and cell wall organization (Figure 1B-C). During diauxic shift, we observed Tup1 at 174 new targets across the genome, where it persisted into stationary phase. Gene ontology analysis revealed that during diauxic shift, Tup1 bound to the promoters of sugar transmembrane transporters, carbohydrate kinases, ATP from ADP factors, zinc transporters, and DNA binding transcription factors (Figure 1D). Motif analysis revealed significant enrichment for binding motifs of 78 transcription factors, including Mig1, which is known to recruit Tup1 to sites of repression (Supplementary Table 1) (Bailey & Grant, 2021; Papamichos-Chronakis et al., 2004; Treitel & Carlson, 1995).

Tup1 Both Activates and Represses Key Targets for Quiescence Initiation

Next, we sought to understand how Tup1 binding correlates with transcriptional changes upon glucose repression. We performed differential expression analysis on RNA-Seq datasets, comparing transcription between wild type and Tup1 knockout strains during diauxic shift and stationary phase (Figure 2A). We were able to detect differential expression of 2102 genes in diauxic shift and 2999 genes during stationary phase in the Tup1 deletion, suggestive of a role for Tup1 in altering transcriptional programming during glucose exhaustion. Of the genes that were significantly differentially expressed in diauxic shift, nearly 60% had at least a 2-fold increase in expression, while the remaining 40% showed significant reduction in expression (Figure 2A). During stationary phase,

only slightly more genes showed increased expression than showed decreased expression (approximately 52% versus 48%). Among genes that are repressed by Tup1, 787 were repressed in both diauxic shift and stationary phase (Figure 2B).

A previous screen for genes required for quiescence in yeast found 137 deletion mutants that were unable to form a quiescent cell population (L. Li et al., 2015). In our experiments, Tup1 was found to regulate expression of 57% of these genes, indicating that Tup1 plays a key role in transcriptional reprogramming during quiescence. Gene ontology analysis revealed that during diauxic shift, Tup1 represses genes associated with transmembrane transport and metabolism of carbohydrates (Figure 2C). We also observed Tup1 repression of genes implicated in transportation of amino acids, metal ions (Zn2+, Mg2+, Cu2+, and Fe2+), vitamins, and fatty acids. While transportation of fatty acids appeared repressed, metabolism of fatty acids appears to be activated by Tup1. In addition to repressing transportation of many components, Tup1 apparently stalls translation by repressing expression of ribosomal protein subunits, ribosome biogenesis genes, and tRNA ligases. During stationary phase, Tup1 represses many of the same genes found in diauxic shift, and also represses additional gene sets including rRNAs and DNA transcription factors associated with gene activation.

By comparing the results from RNA-Seq and ChIP-Seq, we found that Tup1 occupancy does not correlate solely with repression or activation of genes. For example, out of the 981 genes Tup1 releases from in DS, 35% have higher levels of expression in the Tup1 deletion and 25% have lower levels, while 40% are not significantly affected. Perhaps Tup1 release frees up binding for additional factors, which may be repressive or may induce transcription. Of the 176 genes where we detect Tup1 binding during DS, we

find that 131 are differentially expressed. Most (60%) are repressed by Tup1 and less than 15% are activated, demonstrating that Tup1 recruitment to a site during diauxic shift is usually indicative of repression. Because the number of sites bound by Tup1 in the ChIP dataset does not match the number of repressed genes, it is likely that we did not detect all Tup1 binding that occurs during diauxic shift; however, we do not believe that the inability to detect all instances of Tup1 binding fully accounts for this difference. We observed that Tup1 binds to and represses many DNA binding transcription factors including Hap1, Nrg1, and Mig1 (Supplementary Table 1) and downstream effects of the repression of these transcription factors may account for why there are more repressed targets in the RNA-Seq dataset compared to the ChIP-Seq dataset.

Sds3 and Xbp1 Repress Targets in Common With Tup1

Tup1 recruits the Rpd3L complex to sites of repression through DNA-bound transcription factors (Davie et al., 2003; Hanlon et al., 2011; Treitel & Carlson, 1995; Watson et al., 2000). We know that histone deacetylation during quiescence is largely Rpd3L-dependent and that Tup1 interacts with Rpd3L (McKnight, Boerma, et al., 2015). To explore this connection further, we first compared our Tup1 ChIP data to an existing Rpd3 ChIP dataset in quiescent cells (Supplementary Figure 2A) (McKnight, Boerma, et al., 2015). We found substantial overlap in Rpd3 and Tup1 peaks, indicating that they localize to similar targets, if not interact directly. Comparing sites of Tup1 binding in 3-day cultures to Rpd3 binding sites in purified quiescent cells (McKnight, Boerma, et al., 2015), we find that 160 of the 193 Tup1 peaks (94%) overlap with those of Rpd3. We also performed ChIP-Seq for the stress response factor Xbp1, which is required to recruit

Rpd3 at Xbp1 motifs, and compared these data to Tup1 ChIP and found that Xbp1 and Tup1 also share binding sites (Supplementary Figure 2B).

To elucidate the relationship between Tup1 and Rpd3 in quiescence, we knocked out Sds3, an Rpd3L-specific subunit required for deacetylation, and compared RNA-Seq datasets to that of the Tup1 knockout (Figure 3A). Upon deletion of Sds3 we observed that 1680 genes were differentially expressed in diauxic shift (57% repressed by Sds3 and 43% activated) and 3212 are differentially expressed during stationary phase (52% were repressed by Sds3 and 48% were activated). 734 genes that were upregulated upon Sds3 deletion in diauxic shift were also found to be upregulated during the stationary phase. A gene ontology analysis revealed that Sds3 represses many genes in common with Tup1, including those implicated in carbohydrate transport and ribosome biogenesis. Sds3 is different from Tup1 in that it also represses cell cycle-associated genes.

When comparing the two RNA-Seq datasets we found that during diauxic shift, 37% of genes repressed by Sds3 were also repressed by Tup1 ($p < 5.5e-42$) (Figure 3B). During stationary phase, Tup1 represses 41% of genes repressed by Sds3 ($p < 1.6e-65$). This suggests widespread collaboration between Tup1 and Rpd3L in repressing target genes upon glucose starvation.

The transcriptional repressor Xbp1 has been shown to recruit Rpd3L to its binding sites (McKnight, Boerma, et al., 2015). MACS2 (Y. Zhang et al., 2008) peak calling from our ChIP dataset on Xbp1 and Tup1 binding suggests that Tup1 and Xbp1 localize to similar genes (Supplementary Figure 1). We performed ChIP-Seq experiments in strains lacking Xbp1 and found loss of Xbp1 has no effect on Tup1 binding, demonstrating that Xbp1 does not directly recruit Tup1, even though they colocalize (Supplementary Figure

2B). To measure the effect of Xbp1 deletion on transcriptional silencing, we deleted Xbp1 and performed RNA-Seq experiments during diauxic shift and log phase. We observed that in an Xbp1 deletion 528 genes are differentially expressed during diauxic shift, and during stationary phase 1437 genes were differentially expressed (Figure 3A).

Of these genes, 86% were repressed by Xbp1, and 14% were activated. During stationary phase, 51% of differentially expressed genes were repressed by Xbp1 and 49% activated. A gene ontology analysis revealed that Xbp1 is responsible for repressing genes associated with carbohydrate metabolism during diauxic shift, while repressing carbohydrate transport and cell cycle genes during stationary phase. Xbp1 and Tup1 repress 150 ($p < 3.8e-28$) shared genes during diauxic shift and 379 ($p < 2.8e-60$) genes during stationary phase (Figure 3C). Xbp1 represses 153 ($p < 4.8e-45$) genes in common with Sds3 during diauxic shift and 455 ($p < 1.3e-101$) during stationary phase. Xbp1 also regulates cell cycle genes along with Sds3, while Tup1 has no effect on these genes.

Tup1, Sds3, and Xbp1 Are Required for H3K23 Deacetylation at Repressed Genes

Since Tup1 facilitates H3K23 deacetylation in other contexts (Malavé & Dent, 2006), we next wanted to see if Tup1 contributes to the H3K23 deacetylation we observe during quiescence. To determine if Tup1 is required for deacetylation, we performed H3K23ac ChIP-Seq during stationary phase where Tup1, Xbp1, or Sds3 had been deleted. More than half of the genes (535) with changes in acetylation showed differential regulation by Tup1 or Sds3 in our RNA-seq data ($p < 7.97e-6$). Cells with the Sds3 deletion showed global hyperacetylation in the promoter region during the stationary phase (Figure 4A-B). Additionally, Δtup1 cells also showed global hyperacetylation, though not as dramatically as with the Δsds3 strain. It was difficult to see a global effect

of Xbp1 deletion on acetylation levels; however, when we filtered genes with an Xbp1 motif, it appears that deletion of Xbp1 influences acetylation levels as well, although not nearly as dramatically as with loss of Sds3 or Tup1. To determine the effect of acetylation of transcription, we took the 1000 genes with the greatest changes in acetylation levels across all three mutants and compared them to genes repressed by Tup1 or Sds3 in stationary phase (Figure 4C). We observed a strong relationship between genes that are deacetylated in stationary phase and genes that are repressed.

Tup1 and Isw2 Regulate Nucleosome Positions at HXT Family Genes

During quiescence, cells reposition their +1 nucleosomes, either to shrink the nucleosome depleted region (NDR) or to expand it. Shrinking of the NDR is generally regarded as repressive, because it presumably blocks recruitment of DNA transcription factors and RNA polymerase II. Expansion of the nucleosome NDR, on the other hand, presumably facilitates recruitment of RNA polymerase and is associated with active transcription. The vast majority of NDRs shrink during quiescence in yeast, while a few are expanded (McKnight, Breeden, et al., 2015). The chromatin remodeler Isw2 is known to interact with Tup1, and both proteins are required to position nucleosomes in some contexts (Rizzo et al., 2011; Zhang & Reese, 2004b, 2004a). Because Tup1 is involved in +1 nucleosome stabilization in other contexts, we performed MNase- Seq to determine if Tup1 affects the position of nucleosomes in stationary phase. We found that specifically, Tup1 and Isw2 are required to position nucleosomes at the HXT family of glucose transporter genes HXT1, HXT3, HXT8, HXT9, HXT11, HXT13, HXT15, and HXT16 (Figure 5A).

RNA-Seq data revealed that Isw2 is required to repress 106 genes during diauxic shift and 172 genes in stationary phase (Figure 5B). Isw2 represses many shared targets with Tup1: 33% of genes repressed by Isw2 are also repressed by Tup1 in diauxic shift, whereas almost half of the genes repressed by Isw2 in stationary phase are repressed by Tup1. In addition, we found a greater number of mispositioned nucleosomes in the Δisw2 strain, which had mispositioned nucleosomes in the -2, -1, +1, and +2 positions relative to the transcription start site (TSS) (Figure 5C). Our gene ontology analysis of the genes with mis-positioned nucleosomes in the Δisw2 deletion showed that Isw2 regulates nucleosomes in the promoters of genes involved in glucose transport, cell cycle, and DNA repair pathways in stationary phase (Figure 5D).

Deletion of Tup1 or Sds3 Leads to Morphological Defects in Stationary Phase

Due to the multimeric nature of the Tup1-Ssn6 complex, it has been hypothesized that Tup1 may act as a scaffold for long-distance chromatin interactions. We know that during quiescence there are large scale chromatin folding events in yeast (Swygert et al., 2019). We have biochemical evidence that Tup1 may regulate chromatin folding in vitro; however, it is unknown whether this occurs in vivo. We initially wondered if deleting Tup1 would lead to less compaction of chromatin and sought to determine if Δtup1 cells had larger nuclei using fluorescence microscopy and DAPI staining. Although we failed to detect statistically significant changes in nuclei size, we found that Δtup1 cells showed multiple DAPI puncta not observed in wild type cells (Figure 6A-B).

Deletion of Sds3 did not cause this phenotype; however, Δsds3 cells were often misshapen, which we termed "peanut shaped cells" (Figure 6C). Peanut shaped cells have been observed in other mutants, particularly mutants involved in schmoo formation such as AFR1, PEA2, and SPA2 (Chenevert et al., 1994). While Sds3 does not appear to regulate the expression of these genes to a significant extent, Sds3 is involved in regulating the cell cycle, bud site selection, and cell wall organization. While the phenotype between Δsds3 cells and Afr1 mutant appear similar, it is likely caused by different types of misregulation. We did not observe any changes in Δisw2 yeast compared to wild type yeast. The morphological defects observed in both Δtup1 and Δsds3 yeast suggest a potential mitotic defect, leading to aberrant distribution of DNA within nuclei in Δtup1 cells and abnormal cell division in the Δsds3 mutant. While we were unable to uncover the mechanism underlying this phenomenon, these findings may be of interest for further avenues of investigation.

Discussion

Tup1 plays a key role in regulating large scale transcriptional responses to environmental conditions in yeast (Hanlon et al., 2011). Our ChIP-Seq studies with epitope-tagged Tup1 revealed that when glucose is depleted during the diauxic shift, Tup1 releases from numerous chromatin sites where it is bound in log phase and binds new positions that persist into the stationary phase. Tup1 binds some other sites in both log phase and during diauxic shift, typically associated with genes involved in cell wall organization. During log phase, Tup1 is bound to the promoters of ribosomal subunit proteins and tRNAs, which are actively transcribed at this stage but become repressed during diauxic shift; it seems that Tup1 is involved in both gene activation and

repression. During diauxic shift, Tup1 relocalizes to genes associated with carbohydrate metabolism and transport, as well as factors that convert ADP to ATP, zinc transporters, and DNA-binding transcription factors; Tup1 relocalization to these genes represses their expression. The sites occupied by Tup1 regardless of glucose availability all become derepressed in a Tup1 knockout strain, indicating that Tup1 represses these targets. We suspect that repression of transcription factors by Tup1 may play a role in its ability to affect transcription of more factors in addition to those directly associated with its binding sites. Additionally, because Tup1 does not directly interact with DNA, we suspect that ChIP fails to reveal every instance of Tup1 binding.

Tup1 null mutants fail to repress many of the genes required for diauxic shift and establishment of quiescence. Many of the targets that are repressed/activated by Tup1 account for characteristics of quiescent cells. For example, common hallmarks of quiescent cells are fewer ribosomes, stalled translation, cell wall reorganization, and repression of metabolism. Our RNA-Seq data indicate that Tup1 is required to repress genes associated with all of these processes, demonstrating its role in regulating the transition to quiescence. Li et. al performed a genetic screen for factors that are required for quiescence in yeast. We found that Tup1 regulates more than 56% of these factors, further demonstrating the importance of Tup1 in regulating quiescence.

Tup1 regulates metabolism by simultaneously repressing genes involved in RNA, lipid, amino acid, and carbohydrate biosynthetic processes and activating the glyoxylate cycle and fatty acid metabolism. Transmembrane transporters of amino acids, carbohydrates, fatty acids, and metals (specifically magnesium, zinc, copper, and iron) are repressed by Tup1. We also find that two of the three yeast aquaporins are repressed

by Tup1. It has been observed in other organisms that transmembrane transport is related to cellular proliferation (Peters-Regehr et al., 1999; Shyh-Chang & Daley, 2015). These findings indicate that yeast cells repress the vast majority of transmembrane transporters, which likely allows the cells to maintain a controlled intracellular environment in a context where metabolism is dramatically slowed.

The importance of the Rpd3 complex in establishing a quiescent state has been well demonstrated, and one factor that recruits Rpd3 is the transcription factor Xbp1 (McKnight, Boerma, et al., 2015). Xbp1 and Rpd3 share many common targets of repression with Tup1, while simultaneously having targets independent of Tup1. For example, Tup1 and Sds3 both strongly repress tRNA processing factors, ribosomal subunits, transmembrane transport, sugar catabolism, and cell wall components. Xbp1 and Tup1 overlap in their repression of transmembrane transport genes and sugar metabolism. However, Xbp1 and Sds3 strongly repress cell cycle genes, which are unaffected by Tup1.

Histone deacetylation is strongly associated with transcriptional repression in quiescence (McKnight, Breeden, et al., 2015) and we demonstrated the importance of Tup1, Xbp1, and Sds3 to facilitate histone deacetylation. Whether or not histone deacetylation is the main driving force of transcriptional repression is up for debate. We are only able to detect changes in histone deacetylation three days into stationary phase, which raises the possibility that histone deacetylation is not the main driving force in repressing transcription. However, recent findings demonstrate that the acetylome can change within 5 minutes of glucose depletion, so perhaps changes in the acetylome during diauxic shift are too subtle for us to detect (Hsieh et al., 2022; Cai, et al., 2011).

We know that Tup1 and Rpd3 have repressive activities outside of histone deacetylation Malavé, & Dent, 2006), but it is difficult to decipher which mechanism is employed to repress targets. Overall, there is a strong correlation between genes that are repressed and those that lose their acetyl histone marks.

Tup1 and Isw2 both coordinately regulate nucleosome positions in the promoter regions of HXT family genes. Our RNA-Seq dataset revealed that these genes are also repressed by Tup1 and Isw2, suggesting that repositioning of nucleosomes by Isw2 and Tup1 at these genes leads to repression. Interestingly, these are the only genes in which both Tup1 and Isw2 affect nucleosome positions; deletion of Tup1 has little effect on the positions of nucleosomes at any other genes. We see a greater number of nucleosomes that are affected by Isw2 in genes involved in DNA repair pathways, glucose transport, and cell cycle process. We found that in a Sds3 knockout, cells form peanut shapes, indicative of a cell attempting to divide but ultimately failing to complete the process. Sds3 regulates many cell cycle genes, and it seems likely that failure to repress key cell cycle genes leads to the incomplete cell divisions we observed.

The multiple DAPI puncta observed in Tup1 knockout cells warrant further investigation. One possibility is that these cells have multiple nuclei or fragments of nuclei, which could be the result of a failure to properly segregate chromosomes during mitosis. Another possibility is these puncta are fragments of a broken-down nucleus, which is the result of cell cycle dysregulation. In any case, the observation highlights the importance of Tup1 in regulating the exit from the cell cycle. Taken together these results indicate that Tup1 is critical for gene repression in the exit from the cell cycle and establishment of quiescence.

It has been demonstrated that the Tup1 homologue GRG5 is critical for embryonic stem cell fate decisions in mice (Chanoumidou et al., 2018). Additionally, TLE1 is associated with many cancers in humans, including synovial carcinoma, lung cancer, breast cancer, glioblastoma, gastric cancer, and pancreatic cancer (Yuan et al., 2017). This indicates a role of Tup1/Groucho/TLE family proteins in determining cell fate in higher eukaryotes. Perhaps a conserved role of Tup1 family proteins is to regulate entry and exit from the cell cycle, which may explain why dysregulation of Groucho of TLE in higher eukaryotes leads to cancer.

Materials and Methods

Generation of Deletion Strains

All yeast strains were generated from the parent strain *S. cerevisiae* W303 RAD5+ (ATCC 208352). Null mutants were generated by replacing the gene of interest with antibiotic resistance markers amplified from pAG vectors (Longtine et al., 1998). FLAG- and Myc- tagged strains were made from a pFA6a vector containing their respective sequences. We then inserted the tags through homologous recombination of PCR products using selectable drug markers (Longtine et al., 1998).

Growth Conditions

S. cerevisiae W303 cultures were streaked from glycerol stocks onto yeast extract peptone dextrose (YPD) plates and grown at 30° C. Individual colonies were picked and used to inoculate 25 mL YPD with shaking at 30° C. These cultures were grown to an O.D. of 0.6 to 0.8 for log phase cultures. Diauxic shift cultures were obtained by monitoring glucose levels with glucose test strips (Precision Laboratories). Cells were

harvested two hours after there was no detectable glucose. Stationary phase cultures were prepared by growing yeast for three days in YPD medium.

Chromatin Immunoprecipitation

Chromatin immunoprecipitation was performed as previously described (Rodriguez et al.; 2014). 100 OD-mL of cells were crosslinked in 1% formaldehyde for 20 minutes at 30° C. Cells were then quenched with a final concentration of 125 mM glycine, pelleted, and frozen at -80° C. Cells were lysed in a Bead Beater (Biospec) for two minutes with acid- washed glass beads, diameter 425-600 m (Sigma Aldrich) in the presence of protease inhibitors (Proteoloc Protease Inhibitor Cocktail, Expedeon) and then sheared in a Bioruptor sonicator for a total of 30 min (high output 30 sec on 30 sec off for 10 minutes 3x) and then centrifuged. The sheared chromatin supernatant was incubated with antibodies bound to G protein beads (Invitrogen). The crosslinks were reversed, overnight at 65° C and the sample was treated with 20 g RNase A for two hours at 45° C and 100 g Proteinase K for *4* hours at 55° C, and then purified using Qiagen MinElute columns. DNA samples were quantified using a Qubit fluorescence assay and libraries were prepared using a NuGEN Ovation Ultralow kit. Sequencing was performed by the University of Oregon Genomics and Cell Characterization Core Facility on an Illumina NextSeq500 on the 37 cycle, paired-end setting, yielding approximately 10-20 million paired- end reads per sample.

RNA Extraction

Cells were removed from -80° C and ground with a mortar and pestle in liquid nitrogen. RNA was extracted using hot acid-phenol (Uppuluri et al., 2007) and cleaned up using

the RNeasy kit (Qiagen). Libraries were prepared using the NuGEN Universal Plus mRNA kit. Sequencing was performed by University of Oregon Genomics and Cell Characterization Core Facility on an Illumina NextSeq500 with 37 cycles of paired-end setting. Paired end reads were filtered and aligned to the *S. cerevisiae* sacSer3 genome using bowtie2 (Langmead & Salzberg, 2012). Differential expression analysis was performed using DESeq2 (Love et al., 2014).

Micrococcal Nuclease Digestion

We utilized our rapid MNase protocol (McKnight et al., 2021). In short, cross-linked cells were permeabilized by zymolyase digestion then treated with MNase and Exonuclease III. Next, the samples were treated with RNaseA and Proteinase K and purified using the Qiagen MinElute PCR Cleanup kit.

DAPI Staining and Fluorescence Microscopy

Staining and microscopy was performed as described by Swygert et al. (2019). Cells were fixed in 3.7% formaldehyde for 20 min at 4° C in 0.1 M KPO4 pH 6.4 buffer. Cells were washed twice in sorbitol citrate (1.2 M sorbitol, 100 mM K2HPO4, 36.4 mM citric acid) and incubated with 2.5 µg of Zymolyase for 30 minutes. Cells were added to polytetrafluoroethylene (PFTE) slides with 0.1% polylysine then washed with ice cold methanol and acetone. Next 5 µL of DAPI mount (0.1 µg/ml DAPI, 9.25 mM p-phenylenediamine, dissolved in PBS, and 90% glycerol) was added to the well. Images were taken on a Zeiss LSM 880 confocal microscope with Airyscan. Images were analyzed and processed using Imaris software (Oxford Instruments). Two biological replicates were used for each strain.

Computational Analysis

All alignments were performed using Bowtie2 (Langmead & Salzberg, 2012). Further analysis was performed using deepTools including generation of heatmaps (Ramírez et al., 2016). For ChIP, data was normalized to RPKM and gene tracks were visualized using Integrated Genome Browser (Freese et al., 2016). Peak picking from ChIP data was performed using MACS2 (Y. Zhang et al., 2008). Venn diagrams were generated using euler.com (Larson, 2020). Motif analysis was performed using SEA in MEME-suite (Bailey & Grant, 2021). Gene ontology was performed using Gorilla (Eden, 2015). We chose the two unranked lists option with our target set being genes that were present in our peak calling or genes that were differentially expressed in our RNA-seq datasets. Our background set included all transcripts that were detected in RNA-seq. Additionally we chose all enriched GO terms.

Author Contributions

Conceptualization, T.BB., E.U.S., J.N.M.; Methodology, T.B.B, L.E.M., J.N.M.; Investigation, T.B.B., P.A.A., L.E.M., J.N.M.; Additional Resources, E.U.S.; Writing - Original Draft, T.B.B.; Writing - Reviewing and Editing, T.B.B., E.U.S.; L.E.M.; Visualization, T.B.B., L.E.M.; Supervision, E.U.S., J.N.M., L.E.M.; Project Administration, L.E.M., J.N.M.; Funding Acquisition, J.N.M.

Data Availability

The datasets generated during this study are available at GEO under accession code GSE210934.

Acknowledgments

The authors thank the Genomics Core (GC3F) at the University of Oregon for high throughput sequencing services. The authors also thank Christine Cucinotta (Fred Hutchinson Cancer Research Center) and Hideki Tanizawa, Osamu Iwasaki, Ken-Ichi Noma for helpful discussions related to this work. Additionally we thank Christine Cucinotta and Alison Greenlaw for tracking down Rpd3 data for us. This work was supported by a National Institutes of Health training grant T32 GM007759 (to T.B.B), and by NIGMS R01 GM129242 (to J.N.M. and L.E.M).

CHAPTER III:

BASIS OF SPECIFICITY FOR A CONSERVED AND PROMISCUOUS CHROMATIN REMODELING PROTEIN

Introduction

Chromatin consists of the nucleic acids and proteins that make up the functional genome of all eukaryotic organisms. The most basic regulatory and structural unit of chromatin is the nucleosome. Each nucleosome is defined as an octamer of histone proteins, which is wrapped by approximately 147 base pairs of genomic DNA (Luger et al., 1997; Kornberg, 1974). The specific positioning of nucleosomes on the underlying DNA can have significant effects on downstream processes, such as promoter accessibility and molecular recruitment, which ultimately serve to alter gene expression (Lai and Pugh, 2017). Despite decades of research, the mechanisms leading to precise nucleosome locations in cells are still being defined.

Nucleosome positioning is dynamically established by a group of enzymes known as ATP-dependent chromatin remodeling proteins (ChRPs) (Zhou et al., 2016). Extensive biochemical and structural characterization has been performed on this group of proteins from various families (Clapier et al., 2017). The chromodomain-helicase-DNA binding (CHD) and imitation switch (ISWI) families of ChRPs have been characterized as nonspecific nucleosome sliding and spacing factors *in vitro* (Stockdale et al., 2006; Hauk et al., 2010; McKnight et al., 2011; Kagalwala et al., 2004; Lusser et al., 2005; Tsukiyama et al., 1999; Pointner et al., 2012). In yeast, flies, and mammals, ChRPs generate evenly spaced nucleosome arrays at transcription start sites and organize

genomic chromatin at other defined boundaries (Pointner et al., 2012; Lee et al., 2007; Mavrich et al., 2008a; Valouev et al., 2011; Krietenstein et al., 2016; Wiechens et al., 2016; Baldi et al., 2018; Gkikopoulos et al., 2011; Zhang et al., 2011). However, relatively little is known about the in vivo biological regulation of these spacing factors, and it is not understood how they can accurately and reproducibly position nucleosomes throughout the genome in different cellular contexts.

A widely accepted model is that ChRPs pack nucleosome arrays against a noninteracting barrier, such as an unrelated DNA binding protein or another nucleosome (Krietenstein et al., 2016; Zhang et al., 2011; Mavrich et al., 2008b). In this way, general regulatory factors (GRFs) could establish chromatin landscapes with differing nucleosome arrays in response to changes in the cellular environment. In support of this model, nucleosome arrays near GRFs and other DNA binding elements appear to be phased relative to the binding motifs of the sequence-specific DNA binding factors in cells and in biochemically reconstituted cell-free systems (Krietenstein et al., 2016; Baldi et al., 2018; Yan et al., 2018). This model suggests that boundaries of nucleosome arrays are determined by the binding of barrier factors. Implicit in this barrier model are the assumptions that ChRPs act as nonspecific nucleosome spacing machines throughout the genome and that specific ChRP and GRF interactions are not required to establish nucleosome positions. While this model provides a good explanation for how phased nucleosome arrays can be established throughout the genome by a combination of DNA binding factors and nonspecific chromatin remodeling factors, the fundamental assumptions of the barrier model have not been thoroughly tested.

It has been shown through genetic and recent biochemical experiments that members of the ISWI family of ChRPs functionally interact with transcription factors *in vivo* (Krietenstein et al., 2016; Gelbart et al., 2005; Goldmark et al., 2000; Fazzio et al., 2001; Yadon et al., 2013). One of the most well-defined interacting partners of ISWI proteins is the meiotic repressorof unscheduled meiotic gene expression (Ume6), which is found in yeasts. It has been previously demonstrated that Ume6 and Isw2, an ISWI-containing ChRP complex in *Saccharomyces cerevisiae* (homologous to the ATP-dependent chromatin assembly factor [ACF] complex in humans and flies), share genetic targets of repression and likely interact physically (Goldmark et al., 2000). While interactions with sequence-specific DNA binding proteins can potentially determine precise nucleosome targeting and final nucleosome positions (Donovan et al., 2019; Bowman and McKnight, 2017; McKnight et al., 2016), the mechanisms through which physical interactions between Isw2 and any genomic recruitment factor like Ume6 influence nucleosome positioning activity in cells have not been defined. For example, it is not known how these physical interactions occur or what role they play in the biochemical outcomes of chromatin remodeling reactions.

In this work, we have successfully identified the mechanism of interaction between Isw2 and Ume6 in *S. cerevisiae*. By taking a protein dissection approach combined with genome-wide nucleosome profiling, we have identified a previously uncharacterized helical domain in Ume6 that allows for Isw2 binding, specific genomic recruitment, and precise nucleosome positioning outcomes. We further demonstrate that conserved attributes of this helical domain are observed in the cell cycle regulator Swi6, which we identified as a new Isw2-recruitment adapter protein that allows for specific

nucleosome positioning at Mbp1/Swi6 (MBF) and Swi4/Swi6 (SBF) targets. We have also determined that the transcription factor-interacting interface of Isw2/ACF-like remodeling complexes contains a few key and highly conserved residues within the WAC (WTSF/Acf1/cbp146) domain. Finally, we show that these residues, which are essential for directional, sequence-specific remodeling, were lost in the evolution of the Drosophila lineage, where extensive biochemical, genetic, and genomic characterization has been performed on the ITC1 ortholog ACF.

Results

Isw2 activity in cells is inconsistent with known biochemistry and the barrier model for nucleosome packing

We wished to understand how the conserved Isw2 protein complex in yeast behaves genome-wide and at specific promoter nucleosomes at target sites. Yeast Isw2 has been characterized extensively in biochemical assays, which all suggest that it has nonspecific DNA binding, ATP hydrolysis, nucleosome sliding, mononucleosome centering, and nucleosome spacing activities (Stockdale et al., 2006; Kagalwala et al., 2004; Lusser et al., 2005; Tsukiyama et al., 1999; Dang and Bartholomew, 2007; Dang et al., 2006; Hota et al., 2013; Kassabov et al., 2002; Zofall et al., 2004; Zofall et al., 2006). These nonspecific nucleosome mobilizing activities suggest that the Isw2 protein should be able to organize nucleosome arrays against a barrier across the genome in yeast cells since (1) it is estimated that there are enough Isw2 molecules for every 10–20 nucleosomes in the genome (Gelbart et al., 2005), (2) Drosophila melanogaster ACF, an Isw2 ortholog, can organize nucleosomes into evenly spaced arrays (Baldi et al., 2018), and (3) other nonspecific and related nucleosome spacing factors can globally space

nucleosomes in yeast and other organisms (Pointner et al., 2012; Wiechens et al., 2016; Gkikopoulos et al., 2011; Zhang et al., 2011). To first determine how Isw2 positions nucleosomes in *S. cerevisiae*, we examined nucleosome positioning activity in an isw1/chd1 deletion background to eliminate known and potentially overlapping global spacing factors and thus highlight 'isolated positioning activity' by Isw2. When examining the positioning of nucleosomes with and without Isw2 at all yeast pre-initiation complex sites (PICs), it is evident that Isw2 activity is specialized at only a subset of target sites (Figure 7A). As seen previously (Gkikopoulos et al., 2011; Ocampo et al., 2016), no global nucleosome spacing or organizing activity is detected by Isw2 alone (Figure 7). Close inspection of Isw2-targeted PICs suggests that Isw2 can only organize a single PIC-proximal nucleosome, while subsequent nucleosomes become more poorly phased as the distance from the initially positioned nucleosome increases (Figure 7A). Importantly, the PICs that display specific Isw2-directed activity are bound by Isw2, while those lacking any detectable nucleosome organization by Isw2 are unbound (Figure 7A, middle panel).

It has been shown that Isw2 associates with sequence-specific DNA binding factors, such as the transcriptional repressor Ume6 (Goldmark et al., 2000; Fazzio et al., 2001). Isw2 activity at Ume6-bound loci has been previously characterized as precise, with Isw2 reproducibly moving nucleosomes until the predicted edge of the nucleosome core particle is 30 base pairs from the center of the Ume6 binding motif (McKnight et al., 2016). Because of the connection to Ume6, we examined nucleosome positions in an isw1/chd1 background in the presence and absence of Isw2 to determine whether Isw2 is similarly restricted at known target sites. Again, we determined that Isw2 is efficient at

positioning the Ume6-proximal nucleosome but positioning of nucleosomes decays rapidly as the distance from the proximal nucleosome increases, suggesting that Isw2 may only position single nucleosomes at target sites (Figure 7B, clusters 1 and 3). Nucleosomes also appear always to be positioned toward Ume6 motifs as nucleosome positions in the absence of Isw2 are always more distal to the Ume6 motif than when Isw2 is present. Finally, these nucleosomes are positioned with the dyad only separated from the Ume6 motif by 100 nucleotides rather than the ~200 nucleotides that would be expected between dyads in a nucleosome array based on Isw2 preferentially leaving 60 base pairs of linker DNA between nucleosomes in vitro (Kagalwala et al., 2004; Tsukiyama et al., 1999). Of note, a subset of Ume6-bound sites do not display Isw2-dependent nucleosome remodeling (Figure 7B, cluster 2). We have observed slightly reduced chromatin immunoprecipitation (ChIP) signal for Ume6 at these sites (Figure 7). We speculate that for cluster 2 sites where Ume6 is bound, the Isw2 complex might in fact be recruited but that the nearest nucleosome is too distant from the recruitment site, making it out of reach of the remodeler and thus resulting in no change in nucleosome position at these sites.

The observations that (1) Isw2 is solely required to move single nucleosomes at target sites, (2) Isw2 does not have global nucleosome spacing/organizing activity, and (3) Isw2 moves nucleosomes within 100 nucleotides of bound Ume6 suggest that Isw2 behavior in cells is distinct from our understanding of Isw2 activity from decades of biochemical characterization. Similarly, these specific movements toward Ume6 (a barrier) are inconsistent with previous biophysical studies, where ISWI proteins were shown to move nucleosomes away from inert DNA-bound factors (Li et al., 2015).

Because of these inconsistencies, we wished to know if Isw2 followed the ‘barrier model’ for positioning nucleosomes at Ume6-bound targets. Initially to test this, we created a variant Ume6 construct where all residues were deleted except for the DNA binding domain. This Ume6(Δ2–763) construct binds to the same targets as full-length Ume6 (Figure 7). However, Isw2 does not appear to have any activity on global Ume6-proximal nucleosomes in the presence of the Ume6 DNA binding domain alone as nucleosomes in this strain occupy identical positions when Ume6 or Isw2 are completely absent (Figure 7B). In the presence of full-length Ume6, the Isw2 complex appears to be necessary and sufficient for moving motif-proximal nucleosomes as nucleosome positions in the ISW2/isw1/chd1 strain could apparently achieve identical motif-proximal nucleosome positions as the wild-type strain. Additionally, the CHD1/isw1/isw2 and ISW1/chd1/isw2 strains were unable to move any Ume6-proximal nucleosomes (Figure 7), which strongly argues that Ume6 is not acting as a passive barrier against which nucleosome spacing factors can pack nucleosomes. Instead, these data are more consistent with the recent characterization of Isw2 as a ‘puller' (Kubik et al., 2019), with Ume6 being a DNA-bound factor that may immobilize Isw2 to create leverage for ‘pulling’. Consistent with this immobilized pulling model and consistent with the directional movement of single nucleosomes toward Ume6-bound sites, artificially tethered chromatin remodeling proteins were previously shown to always move nucleosomes toward target sites (Donovan et al., 2019). We suspected that Ume6 and Isw2 likely interact in a specific fashion to faithfully select and precisely move single-target nucleosomes toward a recruitment motif (Figure 7C).

A small helical epitope is necessary and sufficient for Isw2-directed nucleosome positioning at Ume6 targets

To determine which region(s) on Ume6 are required for specific nucleosome positioning by Isw2, we initially created a panel of N-terminal Ume6 truncations to determine when nucleosome positioning by Isw2 is lost (Figure 8). This initial truncation panel was motivated by the poor overall conservation of the Ume6 protein even within related yeasts, as well as the disordered structure predicted by Phyre2 (Kelley et al., 2015). Our truncation panel indicated that Isw2 activity was retained if the N-terminus was deleted to residue 322 but lost when deleted to residue 508. Closer inspection of the residues between 322 and 508 revealed a conserved region with a proline-rich segment followed by a predicted alpha helix, altogether spanning Ume6 residues 479–508 (Figure 8A). Deletion of residues 2–479 preserved Isw2-positioned nucleosomes at Ume6 sites, while an internal deletion of 480–507 in the context of an otherwise full-length Ume6 abrogated nucleosome positioning by Isw2 (Figure 8). Importantly, Ume6 Δ2–479 and Ume6 Δ2–508 showed identical binding as measured by ChIP (Figure 8), indicating that the loss of nucleosome positioning is not due to the loss of Ume6 binding.

Since this region is proximal to the characterized Sin3-binding domain in Ume6 (Washburn and Esposito, 2001), we wished to validate that the newly determined Isw2-recruitment helix is independent from the Sin3-binding domain. Ume6 recruits both Isw2 and Sin3-Rpd3 for full repression of target genes (Goldmark et al., 2000; Fazzio et al., 2001). If either Isw2 or Sin3-Rpd3 is present, there is partial repression at Ume6-regulated genes. However, if Sin3-Rpd3 and Isw2 are both lost, Ume6 targets are fully de-repressed. We examined transcriptional output at Ume6 genes in Ume6(Δ2–479) +/–

Rpd3 and Ume6(Δ2–508) +/– Rpd3. Transcription was modestly increased at Ume6 targets in Ume6(Δ2–508)/RPD3+ compared to Ume6(Δ2–479)/RPD3+ (Figure 8), which would be expected if only Isw2 is lost when residues 479–508 are deleted. More convincingly, only a modest increase in transcription was seen at Ume6 targets in the Ume6(Δ2–479)/Δrpd3 strain, suggesting that Isw2 is still present, while the Ume6(Δ2–508)/Δrpd3 strain displayed extreme induction of Ume6-regulated genes, suggesting that both Isw2 and Rpd3 activity are absent (Figure 8B).

Finally, we wanted to know if the predicted helix consisting of Ume6 residues 479–508 was sufficient to bring Isw2 nucleosome positioning activity to Ume6 target sites. To test this, we employed the SpyCatcher/SpyTag system (Zakeri et al., 2012), which creates a spontaneous covalent bond between a short SpyTag peptide and a SpyCatcher domain. We fused the SpyTag peptide to the C-terminus of Ume6(Δ2–596), a construct that is incapable of positioning motif-proximal nucleosomes (Figure 8). We then appended Ume6 residues 479–508 to the C-terminus of the SpyCatcher domain and introduced this fusion on a yeast expression plasmid driven by the ADH1 promoter. In yeast cells, this would create a fusion protein in which the helical element is ectopically displayed on the C-terminus of a DNA binding competent but nucleosome-positioning-deficient construct, connected via a SpyTag-SpyCatcher linker. This fusion protein was capable of fully recapitulating Isw2-positioned nucleosomes at a subset of Ume6 sites (Figure 8C). Perhaps not surprisingly, considering the non-native positioning of the recruitment helix in this fusion construct, not all Ume6 sites were able to gain proper nucleosome positioning with this chimeric system (Figure 8). We conclude that the region spanning residues 479–508 in Ume6 is a yeast-conserved Isw2-recruitment

domain and is required and sufficient for recruiting Isw2 nucleosome positioning activity to Ume6 targets.

Discussion

An interacting barrier model for nucleosome array establishment

Collectively, our results give rise to an 'interacting barrier model' as an alternative means of genomic nucleosome positioning by introducing a targeted interaction between an epitope contained within condition-specific transcription factors and ISWI-type ChRPs. We show that a recruitment factor, the sequence-specific repressor Ume6, harbors a helical domain that interacts with the N-terminus of the Isw2 accessory protein Itc1. Further, we reveal this geometrically restricts the binding of the Isw2 catalytic subunit to a motif-proximal nucleosome. The complex then remodels the nucleosome, repositioning it to a specific distance from the Ume6 recognition motif. At this point and for reasons to be elucidated, this complex is strained or inactivated, and it fails to remodel any further, leaving the nucleosome in a precise location with respect to the bound recruitment factor. The activity of Isw2 and the interacting barrier sets the absolute phase of a nucleosome array that is propagated by true nonspecific spacing activities of Chd1 and Isw1 in yeast, as previously described (Gkikopoulos et al., 2011; Zhang et al., 2011; Ocampo et al., 2016). This 'interacting barrier model' of chromatin organization is more comparable to the factor-targeted activities of SWI/SNF than the nonspecific array spacing of CHD family remodelers and is potentially conserved through humans based on conservation of key interacting residues in Itc1 and the observation that Isw2 orthologs can precisely position nucleosomes adjacent to specific factors in the human genome (Wiechens et al., 2016). Together, we show that coupling between an epitope on an interacting barrier and

a conserved chromatin remodeling protein leads to robust, directional, and specific nucleosome organization at genomic regulatory elements.

Small epitopes in transcription factors organize large chromatin domains

Our data suggest that some small peptide domains embedded within transcription factors can nucleate nucleosome arrays of over 1 kb in length *in vivo* through an interaction with evolutionarily conserved ChRPs. Unlike the arrays established by nonspecific ChRPs, these nucleosome arrays are organized in a sequence-specific and directional manner. Establishing large swaths of chromatin structure by appending a small epitope on a genome-associated protein creates opportunity for diversity with few evolutionary constraints. Changes in relatively small DNA binding motifs, and the small peptide sequences with which they interact, can have a large impact on chromatin structure. Supporting this notion, we were able to identify a strikingly similar motif to that found in Ume6 in the unrelated cell cycle regulator Swi6, which we identified as a new Isw2-recruitment adapter for Swi4 and Mbp1. For these reasons, we find it likely that more ChRP-interacting motifs will be discovered in multiple transcription factors from a variety of organisms, and these motifs may play a significant role in sequence-specific nucleosome positioning for precisely phased and tunable nucleosome arrays in eukaryotic genomes. Importantly, the identification of such epitopes in human cells could lead to the development of targeted drugs to specifically disrupt defined remodeler–transcription regulator interactions.

Materials and Methods

Yeast strains and plasmids

All yeast strains were derived from the parent strain *S. cerevisiae* W303 RAD5+. Gene deletions were made by replacing the gene of interest with antibiotic resistance markers amplified from pAG vectors. C-terminal deletions of genes were also made by replacing the region to be deleted with antibiotic resistance markers. N-terminal gene deletions were made by first replacing the region to be deleted with a URA3 marker, and then counterselecting with 5-fluoroorotic acid (FOA) to delete the URA3. Ume6-helix was introduced to yeast through plasmid transformation of a p416 vector containing the Ume6 helix fused to the SpyCatcher protein (Zakeri et al., 2012). To make SpyTagged yeast strains, a C-terminal 3x FLAG tag followed by the SpyTag sequence (AHIVMVDAYKPTK) (Zakeri et al., 2012) was cloned into a pFA6a vector. Tags were then inserted at the endogenous locus of interest by homologous recombination of PCR products from the respective tagging vectors using selectable drug markers.

Growth conditions

Cells were grown at 30°C and 160 rpm in yeast extract–peptone–2% glucose (YPD) medium unless otherwise indicated. Strains were streaked from glycerol stocks onto 2% agar YPD plates and grown at 30°C for 2–3 days. An isolated colony was then grown overnight in 25 ml of YPD. This pre-culture was used to inoculate 25 ml of YPD at an OD600 of 0.2, which was grown to an OD600 of 0.6–0.8 for chromatin analysis. Yeast containing nonintegrating plasmids (p416) were grown in SD (-) Ura overnight, diluted to OD600 = 0.2 in YPD and grown to OD600 = 0.6–0.8 for chromatin analysis. Cells were then fixed with 1% formaldehyde and harvested for chromatin analysis unless otherwise indicated. Strains were streaked from glycerol stocks onto 2% agar YPD plates and

grown at 30°C for 2–3 days. An isolated colony was then grown overnight in 25 ml of YPD. This pre-culture was used to inoculate 25 ml of YPD at an OD_{600} of 0.2, which was grown to an OD_{600} of 0.6–0.8 for chromatin analysis. Yeast containing nonintegrating plasmids (p416) were grown in SD (-)Ura overnight, diluted to OD_{600} = 0.2 in YPD and grown to OD_{600} = 0.6–0.8 for chromatin analysis. Cells were then fixed with 1% formaldehyde and harvested for chromatin analysis.

Micrococcal nuclease digestions and library construction

Micrococcal nuclease digestions were performed with a minimum of two biological replicates as previously described (Rodriguez et al., 2014). Briefly, cells were grown to mid-log phase and fixed with 1% formaldehyde. Chromatin was digested with 10, 20, and 40 units of MNase for 10 min. Proper nuclease digestion of DNA was analyzed by agarose gel, and samples with approximately 80% mononucleosomes were selected for library construction. After reversal of crosslink, RNase treatment, calf intestine phosphatase (NEB, Ipswich MA, USA) treatment, and proteinase K digestion, mononucleosome-sized fragments were gel-purified and resulting DNA was used to construct libraries with the NuGEN Ovation Ultralow kit per the manufacturer's instructions. Libraries were sequenced at the University of Oregon's Genomics and Cell Characterization Core Facility on an Illumina NextSeq500 on the 37 cycle, paired-end, High Output setting, yielding approximately 10–20 million paired reads per sample.

Chromatin immunoprecipitation and library construction

Chromatin immunoprecipitation was performed with biological replicates as previously described (Rodriguez et al., 2014). Briefly, cells were grown to mid-log phase, fixed with 1% formaldehyde, and lysed by bead-beating in the presence of protease inhibitors. Chromatin was fragmented by shearing in a Bioruptor sonicator (Diagenode, Denville NJ, USA) for a total of 30 min (high output, 3 × 10′ cycles of 30 s on, 30 s off). Sonication conditions were optimized to produce an average fragment size of ~300 base pairs. FLAG-tagged protein was immunoprecipitated using FLAG antibody (Sigma, St. Louis MO, USA) and Protein G magnetic beads (Invitrogen, Waltham MA, USA). After crosslink reversal and proteinase K digestion, DNA was purified using Qiagen MinElute columns and quantified by Qubit High-Sensitivity fluorometric assay. Libraries were prepared using the NuGEN Ovation Ultralow kit by the manufacturer's instructions and sequenced at the University of Oregon's Genomics and Cell Characterization Core Facility on an Illumina NextSeq500 with 37 cycles of paired-end setting, yielding approximately 10 million single-end reads per sample. Only the first read (R1) of each paired read was taken for downstream alignments and processing.

RNA extraction and library construction

For RNA-Seq (minimum two biological replicates), RNA was purified by hot acid phenol extraction followed by polyA selection and strand-specific library construction using the NuGEN Universal Plus mRNA Kit according to the manufacturer's instructions. Libraries were sequenced on an Illumina NextSeq500 on the 37 cycle, paired-end, high-output setting. Paired-end reads were quality filtered for adapter contamination and low-quality ends using trimmomatic (Bolger et al., 2014). After quality filtering, an average

of 10.5 million reads per paired-end sample remained. Surviving reads were mapped to the *S. cerevisiae* reference genome (Cunningham et al., 2015) using STAR (V.2.5.3) (Dobin et al., 2013). Gene counts were quantified from uniquely aligning reads using HTSeq (V.0.9.1) (Anders et al., 2015). Differential gene expression was performed using DESeq2 (V.1.22.2) (Love et al., 2014), and expression graphs were generated using ggplot2 (Wickham, 2016).

Data processing and analysis

MNase sequencing data were analyzed as described previously (McKnight and Tsukiyama, 2015). Briefly, paired-end reads were aligned to the *S. cerevisiae* reference genome (Cunningham et al., 2015) using Bowtie 2 (Langmead and Salzberg, 2012) and filtered computationally for unique fragments between 100 and 200 bp. Dyad positions were calculated as the midpoint of paired reads, then dyad coverage was normalized across the *S. cerevisiae* genome for an average read/bp of 1.0. Dyad coverage is displayed in all figures. Nucleosome alignments to transcription Ume6 binding sites were performed by taking average dyad signal at each position relative to all 202 intergenic instances of a Ume6 motif center (WNGGCGGCWW). PIC locations were obtained from Rhee and Pugh, 2012. For ChIP-Seq data, single-end reads were aligned to the *S. cerevisiae* reference genome with Bowtie 2 and total read coverage was normalized such that the average read at a genomic location was 1.0. ChIP peaks were called using a 400 bp sliding window with a threshold average enrichment within the window of 3.0. Data were visualized using Integrated Genome Browser (Freese et al., 2016). The datasets

generated during this study are available in the GEO Database with accession code GSE149804.

Bridge from Chapter 3 to Chapter 4

In this chapter we explored how Isw2 regulates nucleosome positions using MNase. In the following chapter, we will discuss an optimized method that we developed to improve the traditional MNase method.

CHAPTER IV:

RAPID AND INEXPENSIVE PREPARATION OF GENOME-WIDE NUCLEOSOME FOOTPRINTS FROM MODEL AND NON-MODEL ORGANISMS

Introduction

MNase-seq (micrococcal nuclease sequencing) is used to map nucleosome positions in eukaryotic genomes to study the relationship between chromatin structure and DNA-dependent processes. Current protocols require at least two days to isolate nucleosome-protected DNA fragments. We have developed a streamlined protocol for *S. cerevisiae* and other fungi which takes only three hours. Modified protocols were developed for wild fungi and mammalian cells. This method for rapidly producing sequencing-ready nucleosome footprints from several organisms makes MNase-seq faster and easier, with less chemical waste.

Methods

Before you begin:

TIMING: [0.5–2 h]

Here, we describe the protocol for use in budding yeast in liquid culture, which was optimized from a previously published protocol (Rodriguez et al, 2014). We have also adapted this streamlined protocol for use with *S. cerevisiae* growing on a plate, *S. cerevisiae* quiescent cells, *S. pombe*, *N. crassa*, wild mushrooms, *C. elegans*, *D.*

rerio fin cells, and mammalian cells. The key changes to adapt the protocol to other cell stages or organisms are noted in the relevant step of the protocol.

1. If needed, prepare buffers (see materials and equipment for recipes).

    a. The following stock solutions can be prepared ahead of time and stored for an extended period at 25°C: 2M sorbitol, 1M Tris pH 7.5, 2.5M glycine, STOP buffer.

    b. Stock solutions of Proteinase K (20 mg/mL) and RNase A (10 mg/mL) can be prepared ahead of time and stored for an extended time at −20°C.

    c. MNase (20 units/μL) and MNase digestion buffer can be aliquoted and stored long-term at −80°C. We have observed that MNase aliquots are stable for at least a year, but have not tested longer storage.

2. Ensure that the formaldehyde being used is less than 3 months old.

3. 2 days before the start of the experiment (day -2), streak the strain(s) of interest onto appropriate selection plates and incubate at 30°C. Sick strains, or strains grown in synthetic medium, may take longer to grow.

Note: If isolating quiescent (Q) cells, you will need an additional 3 days before starting the experiment, so cells need to be streaked out at least a week prior.

4. The day before the experiment (day -1), start an overnight culture of yeast in YPD or other appropriate media; grow at 30°C with shaking for 18–20 h.

Note: If isolating Q cells, start an overnight culture on day -4 or earlier, as the culture must grow for at least 3 days to reach quiescence.

Note: If working from yeast on a plate, instead of an overnight culture, make a large patch (1cm × 3 cm) on a plate with appropriate selection if needed; sick strains may take up to 48 h to grow.

Preparing cell pellets

TIMING: [3–5 h]

5. On Day 0 (or Day 1, if proceeding directly to crosslinking) dilute an overnight culture of yeast to an OD_{600} = 0.2–0.3 in 25 mL of YPD, or other appropriate media. Grow at 30°C with shaking, to an OD_{600} = 0.8–1.

Note: For more slowly growing strains, a larger volume may be used and grown to a lower OD_{600}; ensure at least one doubling takes place before pelleting. The goal is to have 20 OD∗mL of cells (i.e., 20ml of OD_{600} = 1, or 25ml of OD_{600} = 0.8).

6. Pellet 20 OD∗mL of cells in a 50-mL conical tube at 3000×*g* for 5 min.

7. Carefully remove supernatant. Resuspend pellet in 1 mL of deionized water and transfer to a 1.5-mL microcentrifuge tube.

Optional: If time permits, you can proceed directly to the crosslinking protocol at this point instead of pelleting, flash freezing and storing the cells ahead of time; there is a Pause Point after crosslinking.

8. Pellet at 20,000 × *g* for 1 minute in a microcentrifuge. Remove supernatant.

9. Flash freeze the pellet in liquid nitrogen and store it at −80°C. Samples are stable for at least 2 or 3 months at −80°C; we have not tested longer storage times.

MNase (20 units/μL) and MNase digestion buffer can be aliquoted and stored long-term at −80°C. We have observed that MNase aliquots are stable for at least a year, but have not tested longer storage.

Ensure that the formaldehyde being used is less than 3 months old.

2 days before the start of the experiment (day -2), streak the strain(s) of interest onto appropriate selection plates and incubate at 30°C. Sick strains, or strains grown in synthetic medium, may take longer to grow.

Note: If isolating quiescent (Q) cells, you will need an additional 3 days before starting the experiment, so cells need to be streaked out at least a week prior.

The day before the experiment (day -1), start an overnight culture of yeast in YPD or other appropriate media; grow at 30°C with shaking for 18–20 h.

Note: If isolating Q cells, start an overnight culture on day -4 or earlier, as the culture must grow for at least 3 days to reach quiescence.

Note: If working from yeast on a plate, instead of an overnight culture, make a large patch (1cm × 3 cm) on a plate with appropriate selection if needed; sick strains may take up to 48 h to grow.

Preparing cell pellets

TIMING: [3–5 h]

On Day 0 (or Day 1, if proceeding directly to crosslinking) dilute an overnight culture of yeast to an OD600 = 0.2–0.3 in 25 mL of YPD, or other appropriate media. Grow at 30°C with shaking, to an OD600 = 0.8–1.

Note: For more slowly growing strains, a larger volume may be used and grown to a lower OD600; ensure at least one doubling takes place before pelleting. The goal is to have 20 OD∗mL of cells (i.e., 20ml of OD600 = 1, or 25ml of OD600 = 0.8).

Pellet 20 OD∗mL of cells in a 50-mL conical tube at 3000×g for 5 min.

Note: See Table 2 for information on input of different cell types.

Carefully remove supernatant. Resuspend pellet in 1 mL of deionized water and transfer to a 1.5-mL microcentrifuge tube.

Optional: If time permits, you can proceed directly to the crosslinking protocol at this point instead of pelleting, flash freezing and storing the cells ahead of time; there is a Pause Point after crosslinking.

Pellet at 20,000 × g for 1 minute in a microcentrifuge. Remove supernatant.

Flash freeze the pellet in liquid nitrogen and store it at −80°C. Samples are stable for at least 2 or 3 months at −80°C; we have not tested longer storage times.

Prepare cross-linked cells

TIMING: [20−**30 min]**

In this step, formaldehyde is used to capture interactions between DNA and nucleosomes. The crosslinking reaction is then quenched by glycine. For yeast, cells are generally crosslinked with formaldehyde to maintain nucleosome positions throughout the subsequent steps, though it has been debated whether these crosslinks can efficiently trap nucleosome positions without introducing artifacts (Henikoff et al., 2011; Cole et al., 2012). It may be preferable to crosslink cells on the same day as growth, though we have

achieved good results with the method below. Due to natural variation in cells, we recommend performing the experiment on three biological replicates.

MNase-seq of mammalian cells does not require crosslinking. We performed experiments on the cell line PLB-895 (Tucker et al., 1987) both with and without crosslinking and there was no noticeable difference in visualization of nucleosome footprints (Figure 6), though we recommend doing a side-by-side comparison when working with a new cell type for the first time, if possible.

1. Thaw MNase digestion buffer on ice; you will need 100 µL per sample plus another 10 µL per 10 samples to dilute the ExoIII.

2. Resuspend cell pellet in 1 mL of deionized water.

Note: Crosslinking is optional for mammalian cells; if skipping this step, proceed directly to step 8

3. Add 27 µL of 37% formaldehyde to a final concentration of 1%. Rotate end-over-end for 15 min at 25°C.

    a. While the cells are cross-linking, prepare spheroplast buffer; you will need 1 mL per sample with 2 mg zymolyase per mL.

4. To quench the crosslinking reaction, add 50 µL of 2.5M glycine for a final concentration of 125 mM.

5. Pellet at 20,000 × g for 1 minute in a microcentrifuge and remove supernatant carefully.

Pause Point: At this point, cells can be flash frozen in liquid nitrogen and stored at −80°C. Samples are stable for at least 2 or 3 months at −80°C; we have not tested longer storage times.

Make spheroplasts and digest chromatin

TIMING: [3−**4 h]**

In this step, the cell walls of fungi are broken and nuclei are permeabilized to allow micrococcal nuclease (MNase) to access and digest extranucleosomal DNA. Permeabilization is required for fungi but not for mammalian cells, *C. elegans*, or *D. rerio*; for non-fungal samples proceed directly to step 8. [Troubleshooting Problem 1:]

After permeabilization, accessible regions of genomic DNA are digested by MNase, and the ends of the resulting nucleosome fragments are trimmed by Exonuclease III to reduce variation in size, which enables consistent, high-resolution identification of the nucleosome dyad at the center of the core particle. [Troubleshooting Problem 2:]

Cellular RNA is removed, formaldehyde crosslinks are reversed, and protein is digested prior to DNA purification. Finally, the residual 3’ phosphates (from MNase cleavage activity) are removed prior to genomic library construction.

6. Resuspend the pellet of crosslinked cells (fresh or previously frozen) in 1 mL spheroplast buffer plus 2 mg zymolyase to permeabilize the cell walls. Rotate at 25°C for 15 min.

a. While the sample incubates, dilute ExoIII 1:10 (from 100 U/µL stock) in MNase digestion buffer; you will need 3 µL of diluted ExoIII per sample. Keep on ice.

b. Thaw MNase (3 µL per sample), RNase (3 µL per sample), and Proteinase K (10 µL per sample) on ice.

Note: For yeast taken directly from a plate, increase spheroplasting incubation time to 30 min. For purified Q cells, spheroplast for 60 min and increase the amount of zymolyase to 10 mg.

7. Pulse-pellet (15 seconds at 20,000 × *g*); carefully remove supernatant.

8. Add 100 µL digestion buffer + 3 µL MNase (20 U/µL; 60U total) + 3 µL ExoIII (10 U/µL). Incubate at 37°C for 10 min to digest chromatin.

Note: For yeast from a plate, use 1.5µl MNase. For Q cells, use 0.2µl MNase and incubate for 2–10 min (see troubleshooting 3 for more information on optimizing this protocol for Q cells).

Critical: Exact timing of digestion across samples is essential for consistency. To achieve an identical start time for digest, we recommend pipetting the MNase into the open lid of the microcentrifuge tube, and then briefly spinning all the tubes down so that the enzyme reaches each sample at precisely the same time.

9. Stop digestion with 12.5 µL STOP buffer.

Note: We have eliminated SDS from the STOP buffer and switched the order of the Proteinase K and RNAse A steps in order to streamline the protocol. Traditionally, SDS

was included in the STOP buffer and then Proteinase K was added (Rodriguez et al, 2014); both of these components are used to break down protein in the sample, but they also inactivate RNAse, necessitating an additional purification step before proceeding to the RNAse step. In our version, EDTA and EGTA are sufficient to halt crosslinking, and no extra purification is needed.

10. Add 3 µL RNase A (10 mg/mL stock). Incubate at 42°C for 30 min.

11. Add 12.5 µL 10% SDS + 10 µL Proteinase K (20 mg/mL stock) to digest protein and reverse crosslinks. Incubate at 65°C for 45 min.

Note: For uncrosslinked mammalian cells, the incubation time is reduced to 15 min

12. Add 700 µL Buffer PB (from Qiagen kit). Purify using a single Qiagen MinElute PCR column. Follow protocol instructions, with the exception of the elution step. Elute with 12 µL 1× CutSmart buffer (NEB; diluted from 10× stock)

Note: For wild mushrooms, after adding Buffer PB centrifuge the sample for 2 min at 20,000 × *g* to further clear remaining cellular debris. Apply the supernatant to the MinElute column.

13. Add 1 µL Quick CIP. Incubate for 10 min at 37°C.

14. Add 7 µL Orange Loading Dye (NEB) and run the entire sample on a 2% agarose gel.

Critical: The use of Orange Loading Dye and a 2% gel is required for visualization and separation of the digested bands.

Note: Using a 7cm × 10cm or 15cm × 10cm TAE-agarose gel in TAE, it takes approximately 40 min at 100V to get proper separation of bands

15. Cut out the mononucleosome band, gel extract with a Qiagen MinElute column. Follow protocol instructions, with the exception of the elution step. Elute with 12 μL EB.

16. Quantify with PicoGreen or other preferred method; store at −80°C. DNA yield typically ranges from 10-50 ng total. This sample is now ready for preparing libraries; we use 5 ng of input with the Ovation Ultralow Library System V2 (from NuGEN), though we have successfully sequenced libraries prepared from as little as 0.5 ng input. There are a variety of options for preparation of libraries, and this protocol can likely feed into whatever pipeline you are currently using. We have not tested how long samples are stable at −80°C, but we usually prepare library samples within a month.

Expected outcomes

The first step toward validating the nucleosome footprints obtained using this protocol is assessing the quality of the digests on agarose gel (Step 14). Figure 9 shows an example of well-digested DNA, where bands are evident for the tri-, di-, and mono-nucleosomal fragments. Some variation is acceptable, but over- or under-digested DNA may yield poor quality data (see troubleshooting, Problem 2).

After preparing libraries from the S. cerevisiae samples obtained using our new rapid protocol and a previously published protocol (Rodriguez et al., 2014), we sequenced them and analyzed the data using our standard protocol (McKnight and Tsukiyama 2015;

Donovan et al., 2019). We compared our data to previously published datasets (Donovan et al., 2019; McKnight et al., 2016) for wild type and isw2 yeast (Figure 10). We chose Isw2-deficient yeast because Isw2 is required for nucleosome shifts at specific target loci, which allows us to determine if our protocol can recapitulate Isw2-specific nucleosome positions at transcription start sites. For all samples, nucleosome organization at transcription start sites (TSSs) displayed the stereotypical structure, with a nucleosome-depleted region flanked by packed nucleosome arrays (Figure 10A). Comparison of nucleosome positions at Isw2 targets showed that nucleosomes were detected at strain-specific but not protocol-specific locations (Figure 10B). Both the rapid protocol and the standard protocol recovered strain-specific nucleosome positioning at Ume6 binding sites, a known Isw2-recruitment protein (Goldmark et al., 2000) across the genome (Figures 10C and 10D).

We also applied the rapid MNase protocol to purified quiescent cells (Allen et al., 2006), or Q cells. As previously observed, quiescent yeast required longer spheroplasting with an increased amount of zymolyase (McKnight et al., 2015) to compensate for a highly fortified cell wall (Li et al., 2015). We also tested different amounts of time for the MNase digest (Figure 11A), as we found our Q cell protocol required more adjustments to get acceptable footprints, which were not entirely consistent across samples of Q cells prepared on different days. We hypothesize that this is because isolation of Q cells involves several steps and therefore produces more heterogeneous cell samples. For this reason we recommend testing different MNase digest times and/or amounts of MNase when processing Q cells to obtain properly-digested nucleosomes. We found that we could also reproducibly recover nucleosome footprints from patches of yeast grown on

agar plates, or “colony MNase” (Figure 11B) and the captured nucleosome positions accurately reflect nucleosome positioning across the yeast genome (Figures 11C and 11D). Similar to liquid culture, the rapid colony MNase protocol can also detect Isw2-specific nucleosome events genome-wide (Figures 11E and 11F). It is important to note that colony MNase is not appropriate for all types of experiments, and researchers should consider whether stationary or log-phase cells are more appropriate for their needs.

Without any protocol modifications, we were able to recover a well-defined and appropriately digested nucleosome ladder from wild type *S. pombe* cells (Figure 12A). We compared our sequencing data set with previously published MNase-seq data sets from S. pombe (DeGennaro et al., 2013; Steglich et al., 2015). Genomic nucleosome dyad positions from samples prepared by the rapid MNase protocol were the same as seen previously (Figure 12B). In addition, global nucleosome positioning at S. pombe TSSs was nearly identical across data sets (Figure 12C). We also performed the rapid MNase protocol on crosslinked, germinated *N. crassa* (Figure 12D). Importantly, we verified that the genomic nucleosome positions we obtained were similar to previously published *N. crassa* data sets (Seymour et al., 2016; Klocko et al., 2019) (Figure 12E).

Table 1 summarizes some of the key differences between standard MNase protocols for various model fungi and our rapid protocol. In each instance, significantly less starting material is required for the rapid protocol, and in most cases the standard protocol uses phenol/chloroform extraction followed by ethanol precipitation for purification of the DNA; the use of a MinElute column shortens the time for purification considerably. The rapid protocol eliminates phenol and chloroform and also usually uses less formaldehyde, significantly decreasing the amount of hazardous reagents used

overall and also reducing hazardous waste. Additionally, standard protocols for *N. crassa* require isolation of nuclei or a chromatin fraction, along with the use of protease inhibitors. The rapid protocol uses conidia without further preparation, greatly reducing the time and effort involved in preparing the starting material, and protease inhibitors are not required. Notably, one standard method for preparing MNase samples from *N. crassa* (Klocko et al, 2019) does not use formaldehyde, but we have observed that crosslinking improves the quality of the sequencing data and provides more distinct peaks for nucleosome positions (Figure 12E, top row versus bottom row). No standard method exists for MNase of *S. cerevisiae* or *S. pombe* from a patch of cells on a plate, so we could not make a comparison to our rapid "colony MNase".

We wished to design a rapid protocol that was standardized across species, so we performed experiments on a variety of locally foraged wild fungi and were able to obtain well-spaced nucleosome footprints (Figure 13). It is important to note that the size of the mononucleosome band is usually between 100 and 200 bp, but this product might run slightly larger in different organisms, as in lane 2 of Figure 13A. Because we did not sequence this sample, we cannot be absolutely certain that this band reflects mononucleosomal fragments, but we are reasonable sure. We also tested *C. elegans, D. rerio* fin cells, and the cell line PLB-895 (Tucker et al., 1987); while we do not have gel images for the C. elegans or D. rerio samples, we saw a prominent mononucleosome band for both of these organisms after a single test using the same protocol as for mammalian cells (with crosslinking), and we are confident that this protocol can be easily adapted for sequencing-quality nucleosome footprints. For PLB-895 cells, we performed the protocol with crosslinking in order to better compare it to our other samples (Figure

13A), but we also prepared samples without crosslinking as this is the more standard practice for MNase of mammalian cells (Figure 13B); there is no obvious difference visually. A 1-day MNase protocol already exists for mammalian cells (Ramani et al., 2019), but ours is significantly shorter and provides a promising standardized alternative to previously published protocols across organisms. We did not sequence these nucleosome fragments in the interest of time and cost, along with the lack of annotated genomes for wild fungi, but we encourage users to test the rapid protocol in their model organism of choice.

Quantification and statistical analysis

Libraries were sequenced at the University of Oregon's Genomics and Cell Characterization Core Facility on an Illumina NextSeq500 on the 37 cycle, paired-end, High Output setting, yielding approximately 10–20 million paired reads per sample. MNase sequencing data were analyzed as described previously (McKnight and Tsukiyama 2015). Paired-end reads were aligned to the S. cerevisiae sacCer3 (Yates et al, 2019), S. pombe (Wood et al., 2002), or N. crassa (Galagan et al., 2003) reference genome with Bowtie 2 (Langmead and Salzberg 2012), and filtered computationally for unique fragments between 100 and 200 bp. Dyad positions were calculated as the midpoint of alignment coordinates, then dyad coverage was normalized across the genome for an average read/bp of 1.0. Nucleosome alignment to the Ume6 binding site, WNGGCGGCWW, was performed by taking average dyad signal at each position relative to all intergenic instances of a motif center. Intergenic instances of the Ume6 motif were found using the Saccharomyces Genome Database Pattern Matching tool (https://yeastgenome.org/nph-patmatch). Transcription start sites were obtained from

published datasets for S. cerevisiae (Nagalakshmi et al., 2008) and S. pombe (Thodberg et al., 2019). Previously-published S. cerevisiae data (SRX5086833, (Donovan et al., 2019); SRX1176421, (McKnight et al., 2016)), S. pombe data (SRX554384 (Steglich et al., 2015); SRX331943, (DeGennaro et al 2013)), and N. crassa data (SRX1596291, (Seymour et al., 2016); SRX2822417, (Klocko et al., 2019)) were downloaded from the Sequence Read Archive (SRA) and analyzed using our computational pipeline to identify nucleosome dyad positions. Data were visualized using Integrated Genome Browser (Freese et al., 2016). Sequencing data from this work can be accessed at the GEO database under accession code GSE141676.

Limitations

When testing our protocol on new organisms, we adjusted the following parameters to obtain acceptable nucleosome footprints: input amount (number of cells), spheroplasting time (for fungi), amount of zymolyase, and amount of MNase. More detailed protocols for preparation of input samples from other organisms is available upon request.

Troubleshooting

Problem 1

Genomic DNA is not being digested, as evidenced by a very high molecular weight band on the agarose gel and little or no signal for nucleosome footprints, as in Figure 15.

Potential solution

This most likely is the result of cells not being permeabilized. We suggest extending the incubation time for the spheroplasting step (Step 6) or increasing the amount of zymolyase per mL of buffer in 1-mg increments. Another option is to perform this step at 37°C rather than at 25°C. After spheroplasting, the solution should be much less opaque than it was prior to this step, so it is possible to troubleshoot this step without completing the entire protocol. Furthermore, there are likely organisms that may require additional steps to help permeabilize cells, particularly if the cells possess zymolyase-resistant cell walls. Previous work has demonstrated success using cryogrinding as the cell-breaking step (Gonzalez and Scazzocchio 1997; Givens et al., 2011).

Problem 2

The DNA is over- or under-digested, as evidenced by too much or too little signal for the mononucleosome band. Examples of under-digested samples are shown in lanes B, C, and E of Figure 16. Examples of over-digested samples are shown in lanes D and F. Lane A shows a sample where fewer than 20 OD of cells were pelleted initially.

Potential solution

MNase activity can vary across lots and vendors, so it is critical to calibrate the MNase concentration to give the desired extent of digestion. We recommend performing a test of 3 samples with either 2 μL, 3 μL, or 4 μL of MNase (20 U/μL stock) in Step 6 for S. cerevisiae; different amounts of MNase should be chosen for other types of samples based on Table 2. When running these tests, it is not necessary to treat samples with CIP, so Step 13 of the protocol can be skipped. An ideal digest will result in signal

for mono-, di-, and tri-nucleosome fragments, with the most signal for the mono-nucleosome band, as in Figure 9.

Sometimes it is necessary to adjust the amount of MNase used in the protocol based on your specific enzyme activity, particularly when working with an organism that we have not tested. It is worth noting that often it is still possible to excise the mononucleosome band and obtain high-quality data of over-digested samples, but it is preferable to work with appropriately digested footprints, and the extent of digestion should be consistent across samples that are being compared in a particular experiment.

If the ratio of mono- to di-nucleosome bands appears to be correct, the issue may actually be that too few cells were used, as in lane A of Figure 16. Within an organism, the number of cells used could vary depending on the growth conditions or media composition, as evidenced by the adjustments needed for colony MNase (Table 2). It therefore possible that specific conditions or mutant strains may require subtle changes to digestion or input amount, particularly if it is challenging to accurately quantify the initial number of cells.

Problem 3

Quiescent cells produce improperly-digested footprints. Similar to Problem 2, if DNA appears under- or over-digested for quiescent cells, there are additional steps we took to optimize these samples.

Potential solution

Assuming that the MNase activity has been calibrated as in Problem 2, there are additional considerations when processing quiescent cells. We found that quiescent cells

isolated on different days were not consistently digested, so we recommend preparing multiple MNase samples as standard practice, and testing different incubation times for MNase digest in Step 8, as shown in Figure 11A. For the sample shown in Figure 11A, the mononucleosome band from the 5-minute sample was excised, but for other Q cells the 5-minute time point was over- or under-digested. As indicated in the protocol, using multiple different quiescent cells, we observed a range of 2–10 min to yield appropriate footprints, but due to the variability we have seen, it is conceivable that the optimum range might be shifted for quiescent samples prepared in another lab, as the technique seems sensitive to small changes. In our hands, once we optimized the amount of MNase, the same amount of MNase worked for a variety of Q cell samples.

Problem 4

Unexpectedly low DNA yield, as evidenced by faint bands or no signal on the agarose gel.

Potential solution

Increase the input amount when preparing the sample. Assuming calculations for input were correct, we recommend doubling or even tripling the amount of sample as a test. Yeast cells in log phase versus quiescence, for example, give slightly different OD readings, and sometimes sick strains, certain mutants, or yeast grown in different medium vary in size, so the OD reading and pellet size do not accurately reflect the number of cells and therefore amount of DNA in the sample. Furthermore, the amount of input required can vary drastically for different organisms, so for a sample type that we have not tested, optimization of the amount of input will be necessary.

Problem 5

Instead of nucleosome footprints, only a large smear is visible on the agarose gel.

Potential solution

This is likely due to RNA and/or residual protein in the sample. We most often see this with improperly digested RNA and suggest first increasing the incubation time with RNAse A in Step 10. If that is not effective, increase the incubation time with Proteinase K in Step 11. Another possibility is that the RNAse A and/or Proteinase K stocks have lost activity, and these may need to be re-made.

Bridge from Chapter 4 to Chapter 5

In this chapter we demonstrate an improved MNase method that is more efficient. Next, we will discuss some preliminary MNase data from our lab and future directions for experiments.

CHAPTER V:

PRELIMINARY DATA AND FUTURE DIRECTIONS WITH ISW2

Results

In chapter 3 we found that Isw2 uses transcription factors to reposition nucleosomes. We hypothesized that we could expand this model to show how Isw2 may use a similar mechanism to reposition nucleosomes during quiescence. The idea is that sequence-specific transcription factors are induced during quiescence which would interact with Isw2 and help it space nucleosomes into their quiescence-specific positions. This would demonstrate that state-specific nucleosome positions can be regulated by by transcription factor/chromatin remodeler interactions.

We hypothesized that the transcription factor from chapter 2, Xbp1, could interact with Isw2 to position nucleosomes for quiescence. Xbp1 is a member of the SWI4/MBP1 family of transcription factors and SWI4 and MBP1 both interact with Isw2 to position nucleosomes (Mai & Breeden, 1997). Xbp1 is induced during quiescence and is critical for transcriptional repression. Preliminary analysis of nucleosome positions at Xbp1 motifs demonstrated that nucleosomes are repositioned at these sites are repositioned during quiescence, suggesting an interaction between Isw2 and Xbp1. MNase-seq was subsequently performed on an Xbp1 knockout mutant in the stationary phase and revealed that Xbp1 has little to no effect on nucleosome positions, except in the promoters of Gic2 and Pis1 (Figure 17a). It unclear whether Xbp1 is affecting nucleosome positions in this context due to a direct interaction with Isw2, or because it regulates a factor that interacts with Isw2. We do observe Xbp1 peaks at the promoters

of Gic2 in our ChIP-seq peak calling data, indicating Xbp1 does bind to this region, however there is no evidence of Xbp1 binding at the Pis1 promoter. However, most genes bound by Xbp1 show no change in nucleosome positions in the Xbp1 knockout. If Xbp1 were directly interacting with Isw2 to reposition nucleosomes, we would expect to see a much larger, global change in nucleosome positions in the absence of Xbp1 (Figure 17b). Perhaps Xbp1 only repositions nucleosomes at these two points, or there is redundancy in other promoters. Either way, there are many nucleosomes that undergo positioning during quiescence where there is no clear mechanism.

To find transcription factors that interact with Isw2 during quiescence, we immunoprecipitated the catalytically dead Isw2 K215R with a Flag epitope and used mass-spec to identify any binding partners. We were able to pull down peptides from the transcription factors Stp6, Wtm1, Tra1, Stp5, and T2fa, and Taf14 in our mass spec data. Whether or not these factors functionally interact with Isw2 is unknown and remains to be investigated.

One problem with identifying interactions between Isw2 and transcription factors is that the Isw2/transcription factor interaction is likely very transient and difficult to capture. Additionally, the interaction likely favors transcription factors remaining bound to DNA instead of being pulled down with Isw2. To address this, we came up with the idea of engineering a photoactivatable crosslinker azidomethylphenylalanine into the WAC domain of Itc1 (Maza et al., 2016; Shao et al., 2015). This will be done through unnatural amino acid substitution using the UAA e. coli amber “TAG” codon at key sites within the WAC domain. This would allow us to induce a covalent interaction between the Isw2 complex subunit Itc1 and the transcriptions factors of interest. These

experiments would provide a library of transcription factors that interact with Isw2 and can be done in a variety of contexts and provide a promising future direction for understanding how Isw2 positions nucleosomes. MNase-seq data on how Isw2 positions nucleosomes has already been discussed in Chapter 2. To validate the crosslinking-mass spec data we can compare motifs near nucleosomes positioned by Isw2 and determine which transcription factors interact with Isw2 and have motifs near positioned nucleosomes. When there are candidates based on these criteria, we can advance to deleting these transcription factors and using MNase to determine if they are responsible for positioning nucleosomes.

CHAPTER VI:

CONCLUSION

Altogether, these chapters address the role of Tup1 in establishing a quiescent state through histone deacetylation and nucleosome positioning. We provide a mechanism for nucleosome positioning using the Isw2 complex and additionally provide an improved method for measuring nucleosome positions. Future experiments are needed to understand how Isw2 positions nucleosomes during stationary phase, which is laid out in Chapter V. This work fills in many gaps in our understanding of the role of chromatin interacting proteins in regulating transcription in various cellular contexts. We know that many of these factors (e.g. Tup1, Isw2, and Rpd3) are well conserved across eukaryotes and their respective roles in *S. cerevisiae* are also conserved in higher order eukaryotes. Understanding the mechanisms of how chromatin binding proteins effect gene regulation lay important groundwork for understanding human disease.

APPENDIX

Chapter II Figures

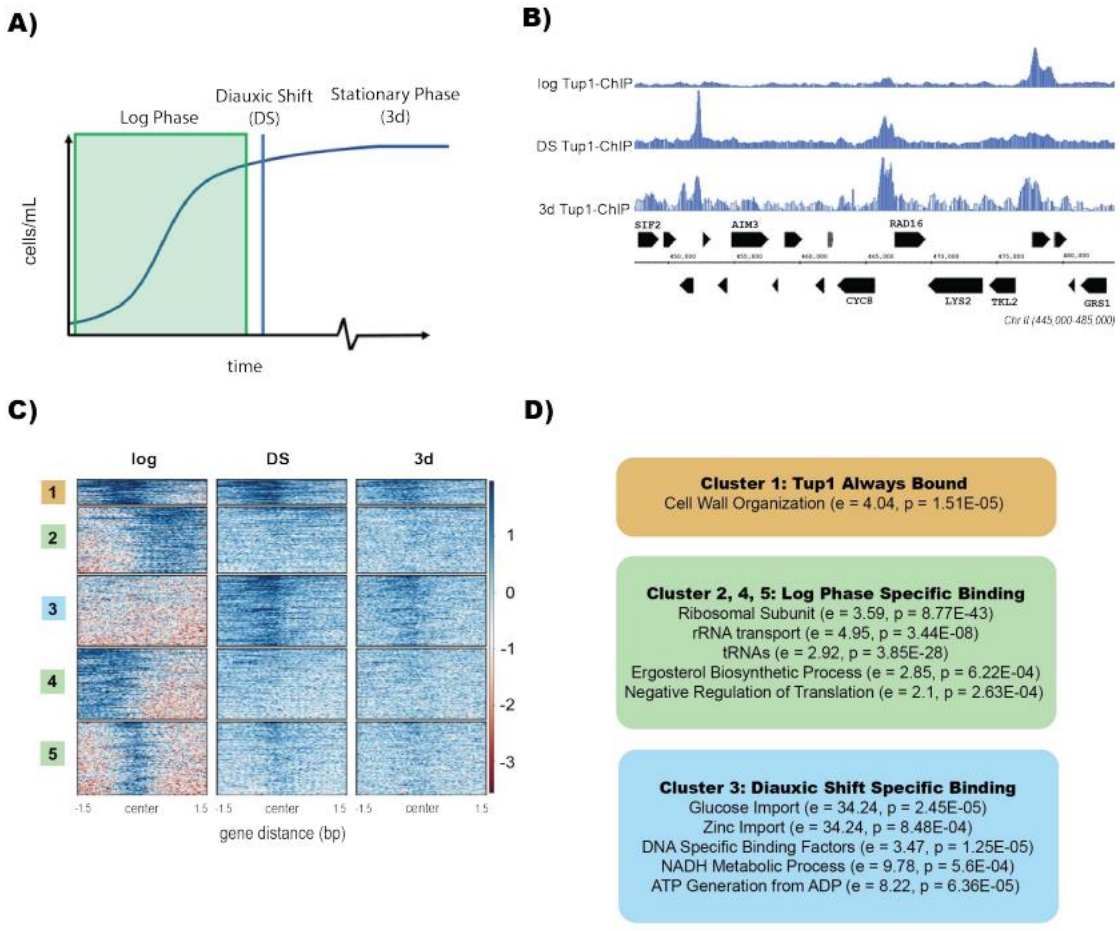

Fig. 1. Tup1 Relocalizes After Glucose Starvation. (A) Illustration of a yeast growth curve indicating diauxic shift (DS) and stationary phase (3d). (B) Integrated Genome Browser (IGB) tracks representative of Tup1-myc ChIP-Seq during log phase, diauxic shift, and stationary phase. (C) ChIP-Seq heatmap of Tup1 binding during log phase, diauxic shift, and stationary phase. Heatmap was clustered using deeptools and sorted by binding intensity. (D) Gene ontology analysis from GOrilla of Tup1 binding locations with relative enrichment (e) and p-value (p) indicated for each term.

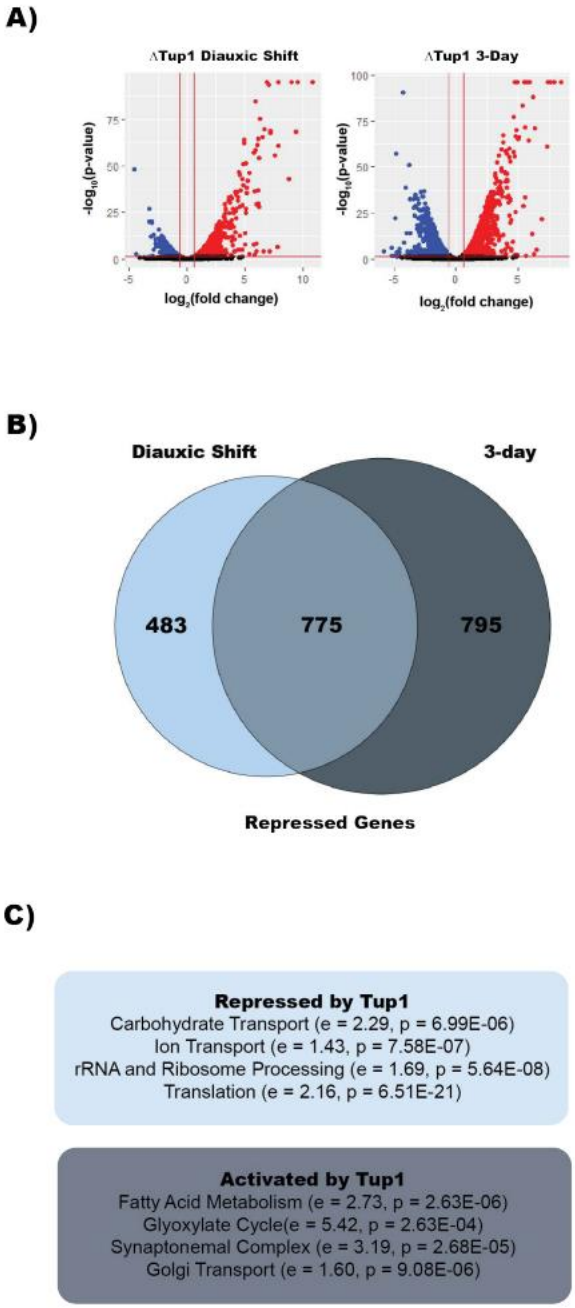

Fig. 2. Tup1 Activates and Represses Key Targets for Quiescence Initiation. (A) Volcano plots of RNA-Seq differential expression data comparing a Tup1 deletion to wild type. Expression changes are based on two biological replicates. (B) Venn diagram comparing genes that are repressed by Tup1 in diauxic shift to those repressed in stationary phase. (C) Gene ontology analysis from GOrilla of transcripts affected by Tup1 in both diauxic shift and stationary phase with relative enrichment (e) and p-value (p) indicated for each term.

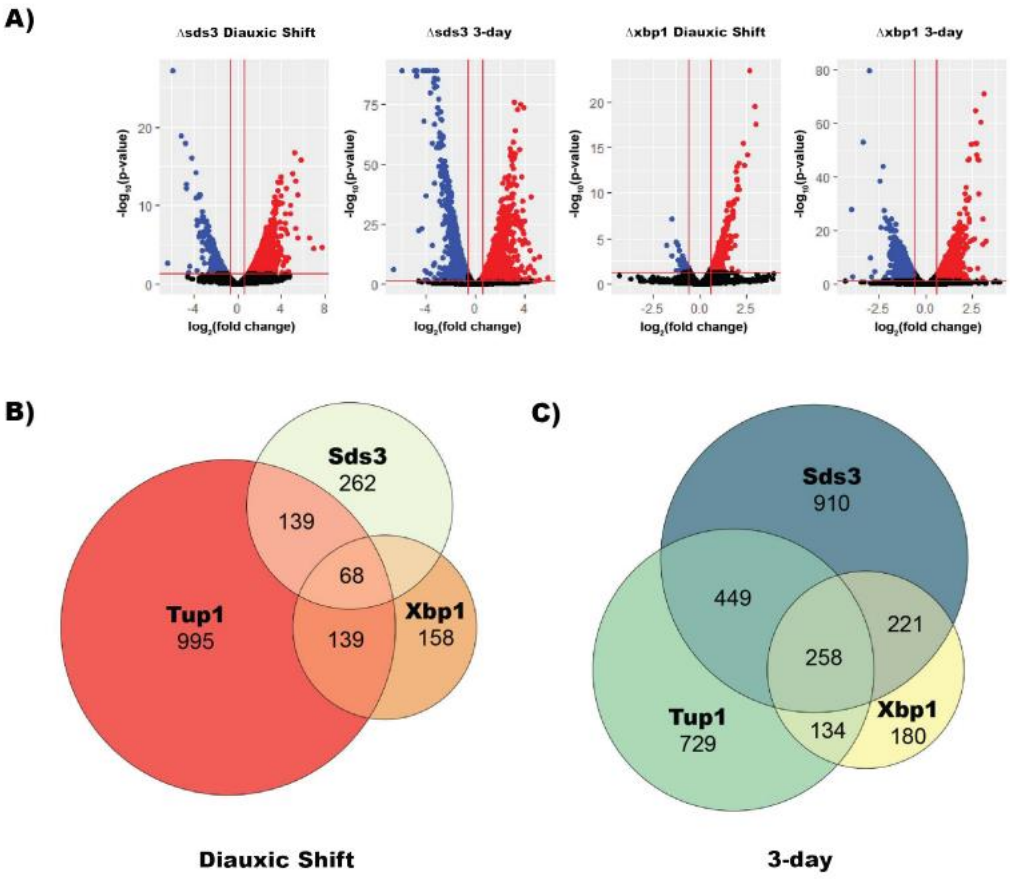

Fig. 3. Sds3 and Xbp1 Repress Targets in Common with Tup1. (A) Volcano plots of RNA-Seq differential expression data comparing Xbp1 and Sds3 deletions to wild type in both diauxic shift and stationary phase. Expression changes are based on two biological replicates. (B) Venn diagram of transcripts repressed by Tup1, Sds3, and Xbp1 in diauxic shift. (C) Venn diagram of transcripts repressed by Tup1, Sds3, and Xbp1 in stationary phase.

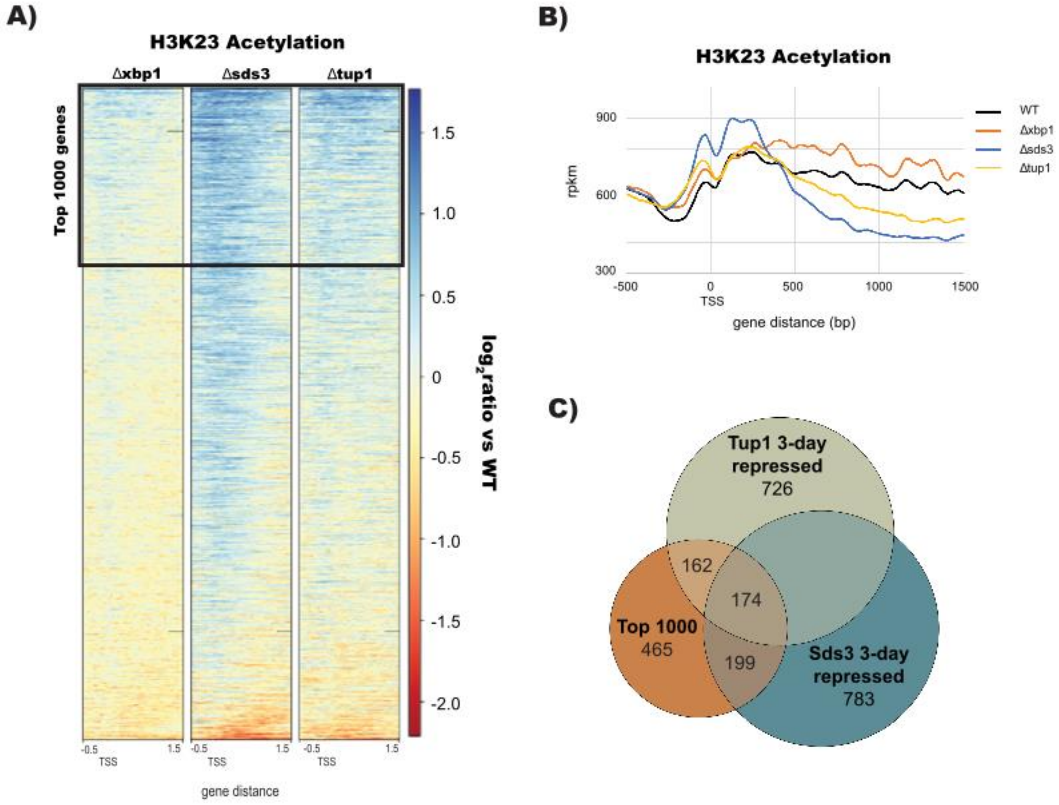

Fig. 4. Tup1, Sds3, and Xbp1 are Required for H3K23 Deacetylation at Repressed Genes. (A) Heatmap showing the change in H3K23ac levels in deletion mutants compared to wild-type across all yeast genes. (B) H3K23ac profile levels across gene promoters, integrated across all yeast genes. (C) Venn diagram comparing the 1000 genes with the largest change in H3K23ac to genes repressed by Tup1 and Sds3 in stationary phase.

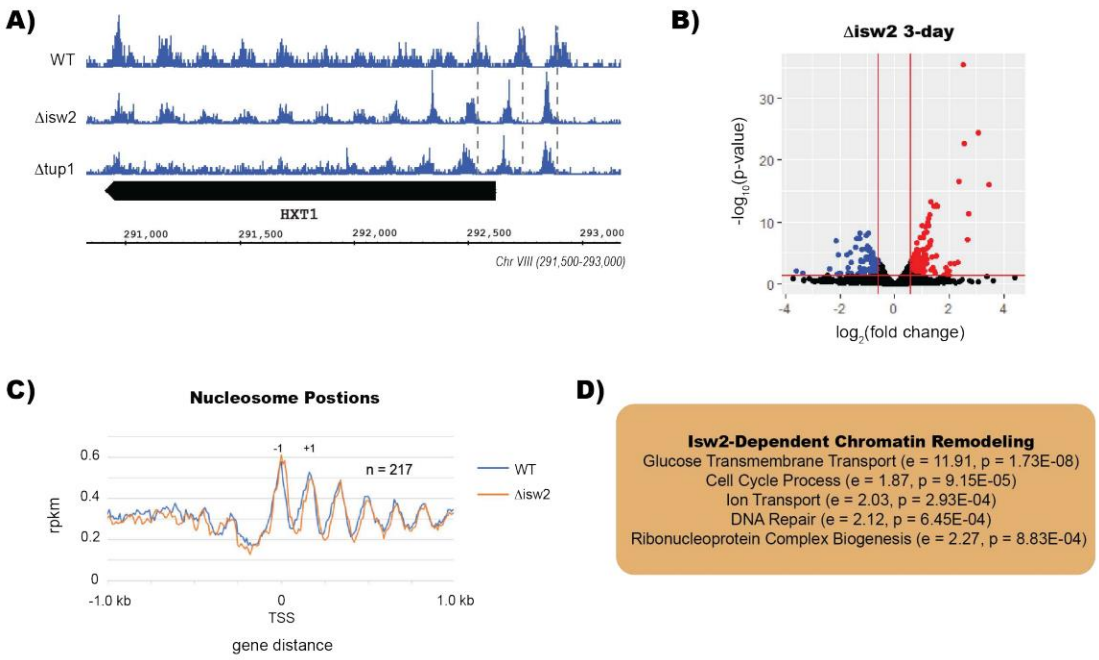

Fig. 5. Tup1 and Isw2 Regulate Nucleosome Positions at HXT Family Genes. (A) Integrated Genome Browser (IGB) tracks of MNase-Seq in wild type, Δisw2, and Δtup1 in stationary phase. Dashed gray lines indicate wild type nucleosome positions. (B) Volcano plot of Δisw2 deletion in stationary phase demonstrating shifted nucleosomes at the HXT1 locus. (C) MNase-Seq dyad signal across 217 genes with shifted nucleosomes in Δisw2 during stationary phase. "-1" indicates the first nucleosome upstream of the TSS, while "+1" indicates the first nucleosome downstream of the TSS. (D) Gene ontology terms for genes with shifted nucleosome positions in Δisw2 yeast at stationary phase, with relative enrichment (e) and p-value (p) indicated for each term.

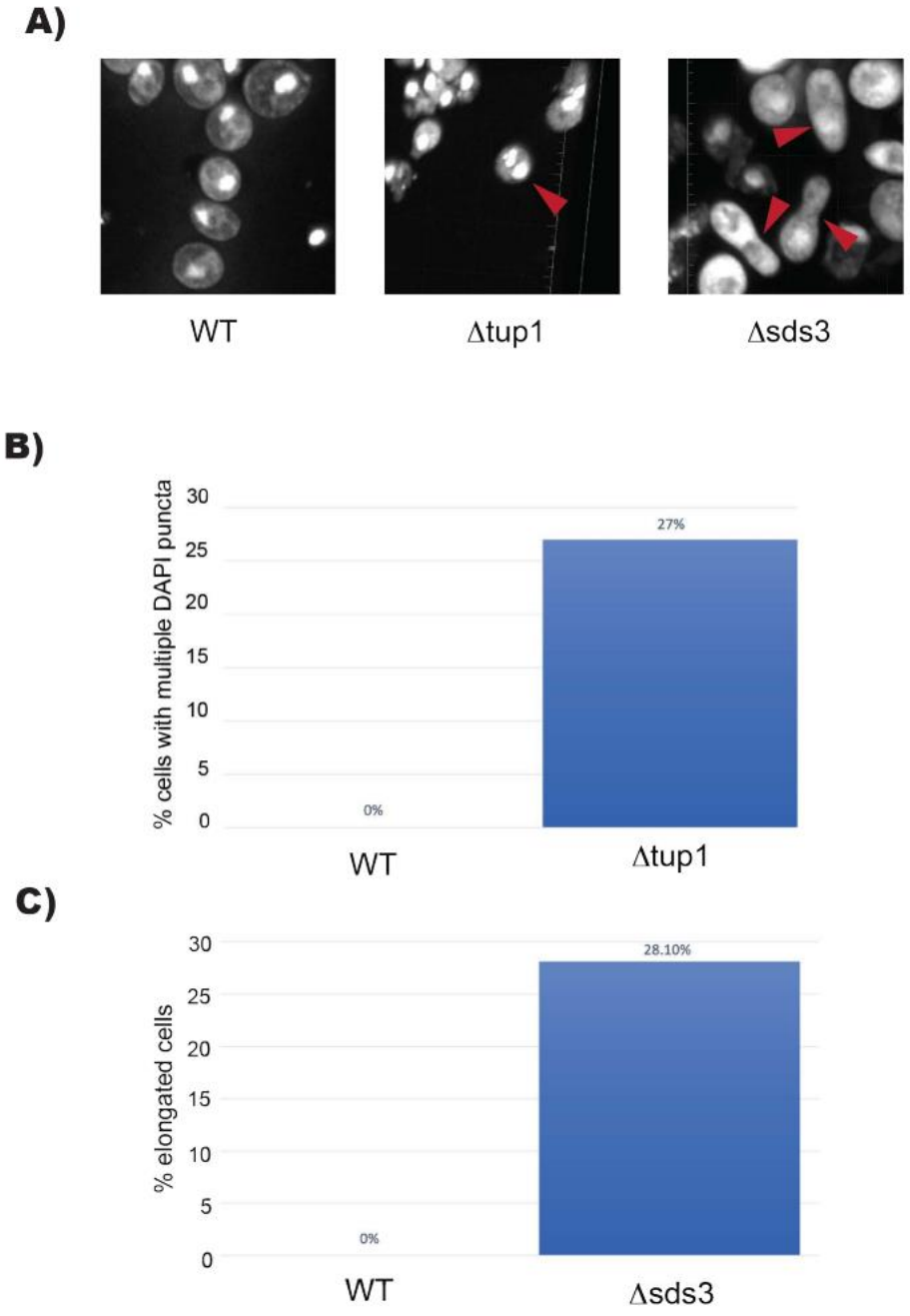

Figure 6. Deletion of Tup1 or Sds3 Leads to Morphology Defects in Stationary Phase. (A) Fluorescence microscopy of DAPI stained nuclei across the genome at 67x magnification in wild type, Δtup1, and Δsds3 yeast. (B) Quantification of Δtup1 cells with multiple DAPI puncta. (C) Quantification of peanut-shaped cells in Δsds3 yeast.

Chapter III Figures

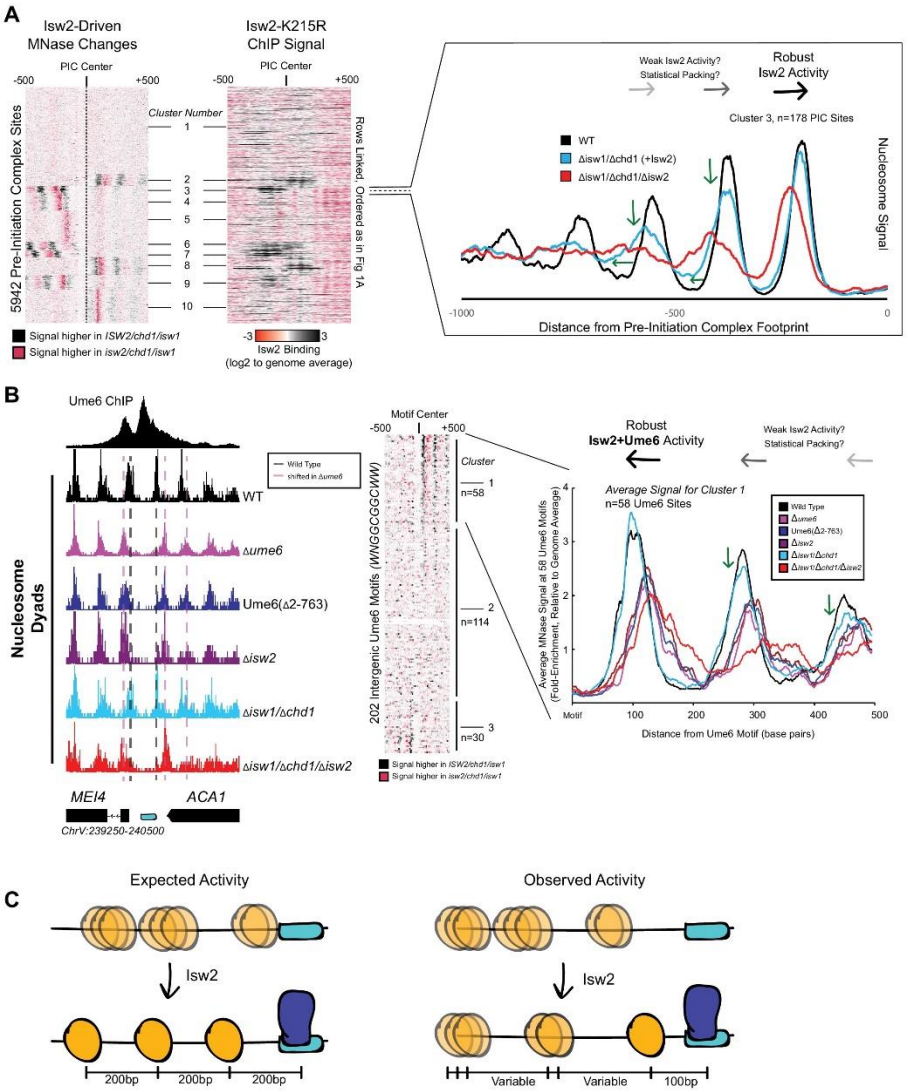

Figure 7. Isw2 is a specialist remodeler that positions single nucleosomes at target sites.(**A**) (Left) Clustered heatmap showing differences in nucleosome dyad signal between *isw2*/*isw1*/*chd1* and *ISW2*/*isw1*/*chd1* strains at 5942 pre-initiation complex sites (PICs). Black indicates positions where Isw2 preferentially positions nucleosomes compared to the strain lacking Isw2. (Middle) Heatmap of ISW2(K215R) ChIP signal, with rows linked to the PIC data on the left, shows that Isw2-dependent nucleosome changes overlap with regions where Isw2 is present. (Right) Average nucleosome dyad signal for wild type (WT) (black), *isw1*/*chd1* (cyan), and *isw2*/*isw1*/*chd1* (red) strains for the 178 PIC sites in cluster 3. Black arrows denote Isw2-driven nucleosome shifts. Green arrows indicate rapid decay of positioning at PIC-distal nucleosomes in the *ISW2*/*isw1*/*chd1* mutant. (**B**) (Left) Genome Browser image showing nucleosome dyad signal at a *u*nscheduled *m*eiotic gene *e*xpression (Ume6) motif (cyan rectangle) for indicated strains. Vertical gray dashed line denotes the motif-proximal WT nucleosome positions while vertical pink dashed line indicates the nucleosome positions in the absence of Ume6 or Isw2. (Center) Clustered heatmap showing the difference in

nucleosome dyad signal between *isw2*/*isw1*/*chd1* and *ISW2*/*isw1*/*chd1* strains at 202 intergenic Ume6 motifs. Black indicates positions where Isw2 preferentially positions nucleosomes compared to strains lacking Isw2. (Right) Average nucleosome dyad signal for indicated strains at Ume6 motifs in cluster 1. Black arrows indicate direction of nucleosome positioning by Isw2. Green arrows signify decreased positioning of motif-distal nucleosomes in the *ISW2*/*isw1*/*chd1* strain (cyan) compared to WT (black). (**C**) (Left) Cartoon depicting the expected activity of Isw2 at barrier elements according to current biochemical data and nucleosome positioning models. Isw2 is thought to move nucleosomes away from bound factors and space nucleosomes with an approximately 200 base pair repeat length. (Right) Cartoon of the observed activity of Isw2 at target sites where only a motif-proximal single nucleosome is precisely positioned but distal nucleosomes are not well-spaced by Isw2.

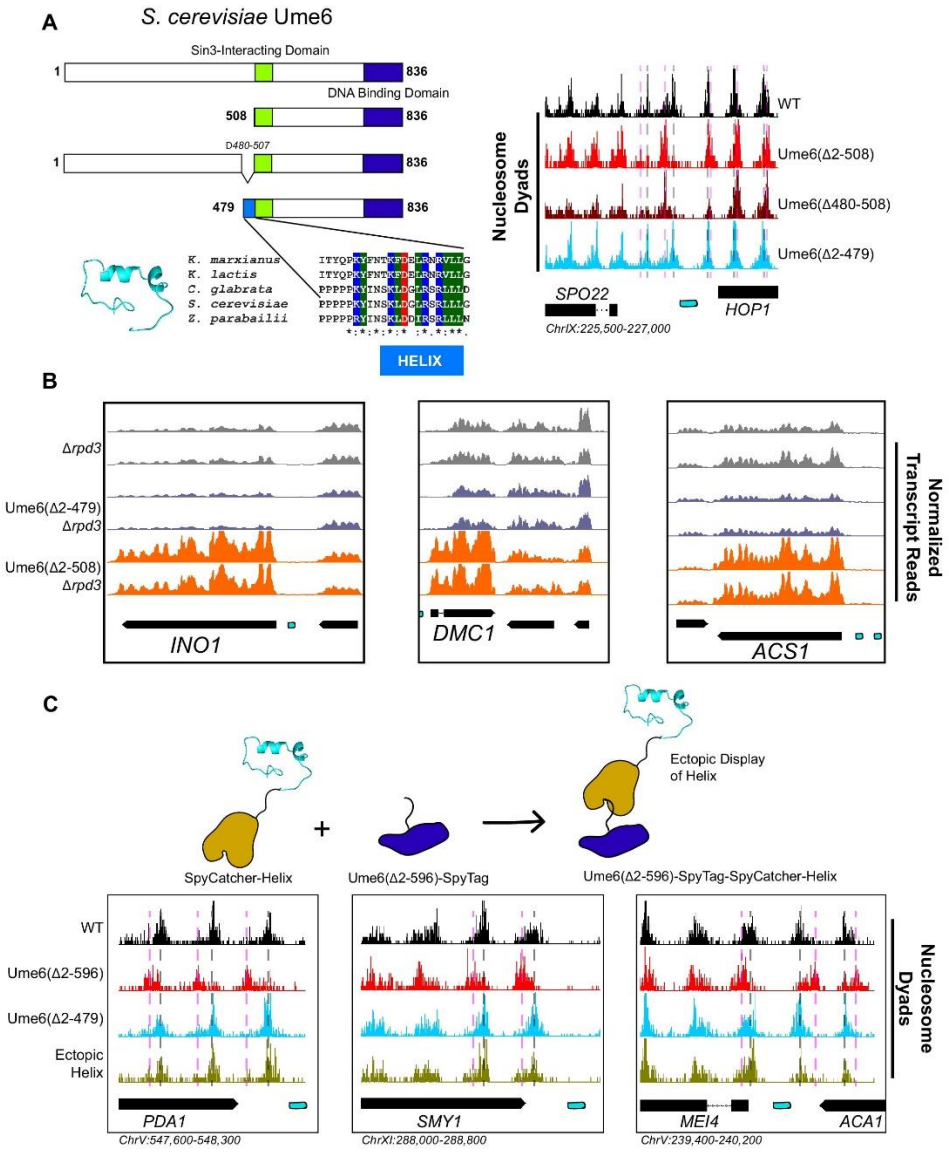

Figure 8. A small predicted helix is the Isw2-recruitment epitope in unscheduled meiotic gene expression (Ume6). (**A**) (Top left) Schematic diagram of Ume6 truncation and deletion constructs used to identify the Isw2-recruitment epitope, with the known Sin3-interacting domain depicted as a green square, the DNA binding domain as a dark blue rectangle, and the putative Isw2-recruitment helix as a light blue rectangle. (Bottom left) Modeled helical peptide (by Phyre2) and sequence conservation of the identified Isw2-recruitment motif in Ume6 constructs from other yeasts. Asterisks denote invariant residues. (Right) Nucleosome dyad signal for Ume6 truncation and deletion strains indicates deletion of the region from residues 480 to 507 completely abrogates nucleosome positioning by Isw2 at Ume6 target sites. Vertical dashed gray lines denote wild-type (WT) positions of nucleosomes while vertical dashed pink lines indicate *isw2* or *ume6*-deficient positions of nucleosomes. (**B**) Genome Browser image showing transcript abundance at three Ume6 target sites for yeast strains lacking Rpd3 with WT Ume6 (gray), Ume6(Δ2–479) (blue), and Ume6(Δ2–508) (orange). Grossly

increased transcription is seen when residues 480–507 are deleted, consistent with expected transcriptional increase associated with loss of Isw2 and Rpd3. Upstream repression sequence (URS) sites are indicated as cyan rectangles. No significant increase in transcription is detected when Ume6 residues 2–479 are deleted. Biological replicates are shown to highlight reproducibility. (**C**) (Top) Cartoon schematic for ectopic display of the Isw2-recruiting helix (residues 480–507) to the C-terminus of a truncated Ume6 construct lacking Isw2-directed nucleosome positioning. A short SpyTag is appended to the C-terminus of the Ume6 construct and residues 480–507 are fused to the SpyCatcher domain and introduced on a yeast expression vector. (Bottom) Nucleosome dyad signal demonstrating recovery of Isw2-directed nucleosome positions at a subset of Ume6 target genes by the ectopically displayed helical element. Vertical dashed gray lines denote WT positions of nucleosomes while vertical dashed pink lines indicate *isw2* or *ume6*-deficient positions of nucleosomes. URS sites are indicated as cyan rectangles.

Chapter IV Figures

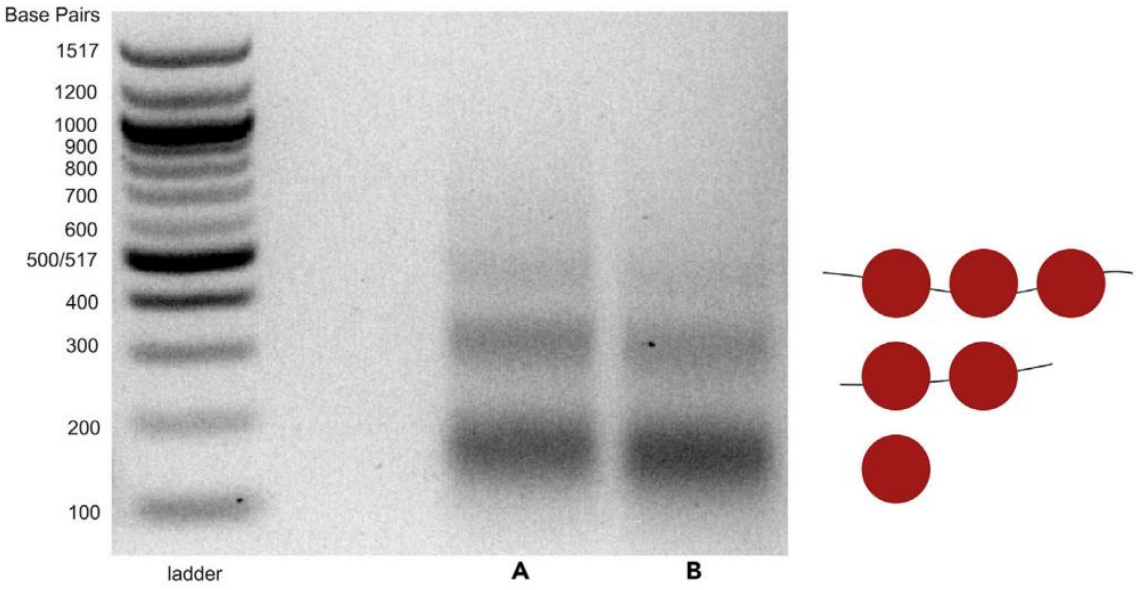

Figure 9. Sample gel showing properly digested nucleosome footprints. Agarose gel showing nucleosome footprints recovered from liquid culture of S. cerevisiae using the rapid MNase protocol. (A) and (B) are replicates from the same WT yeast strain.

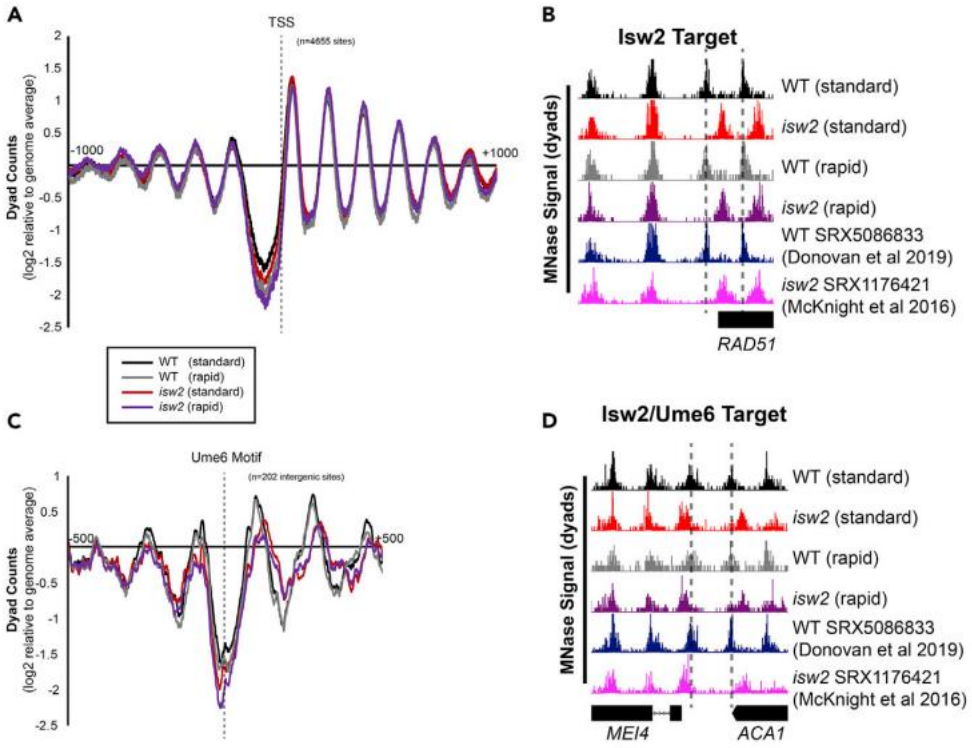

Figure 10. Rapid MNase can accurately map nucleosome positions in S. cerevisiae cells (A) Nucleosome dyad signal at 4655 yeast transcription start sites (TSSs) are plotted for WT and isw2 nucleosomes harvested using a standard or rapid protocol. (B) Example Genome Browser image showing the standard method and rapid method can map Isw2-directed nucleosome positions similar to published data sets at the RAD51 locus. Dashed lines indicate Isw2-positioned nucleosomes. (C) Nucleosome dyad signal at 202 intergenic Ume6 target sites showing rapid and standard MNase methods can accurately identify global changes in nucleosome structure at an Isw2 recruitment motif. (D) Genome Browser image showing all methods correctly identify Isw2-positioned nucleosomes at the MEI4-ACA1 locus, a Ume6 target site. Dashed lines indicate Ume6- and Isw2- positioned nucleosomes.

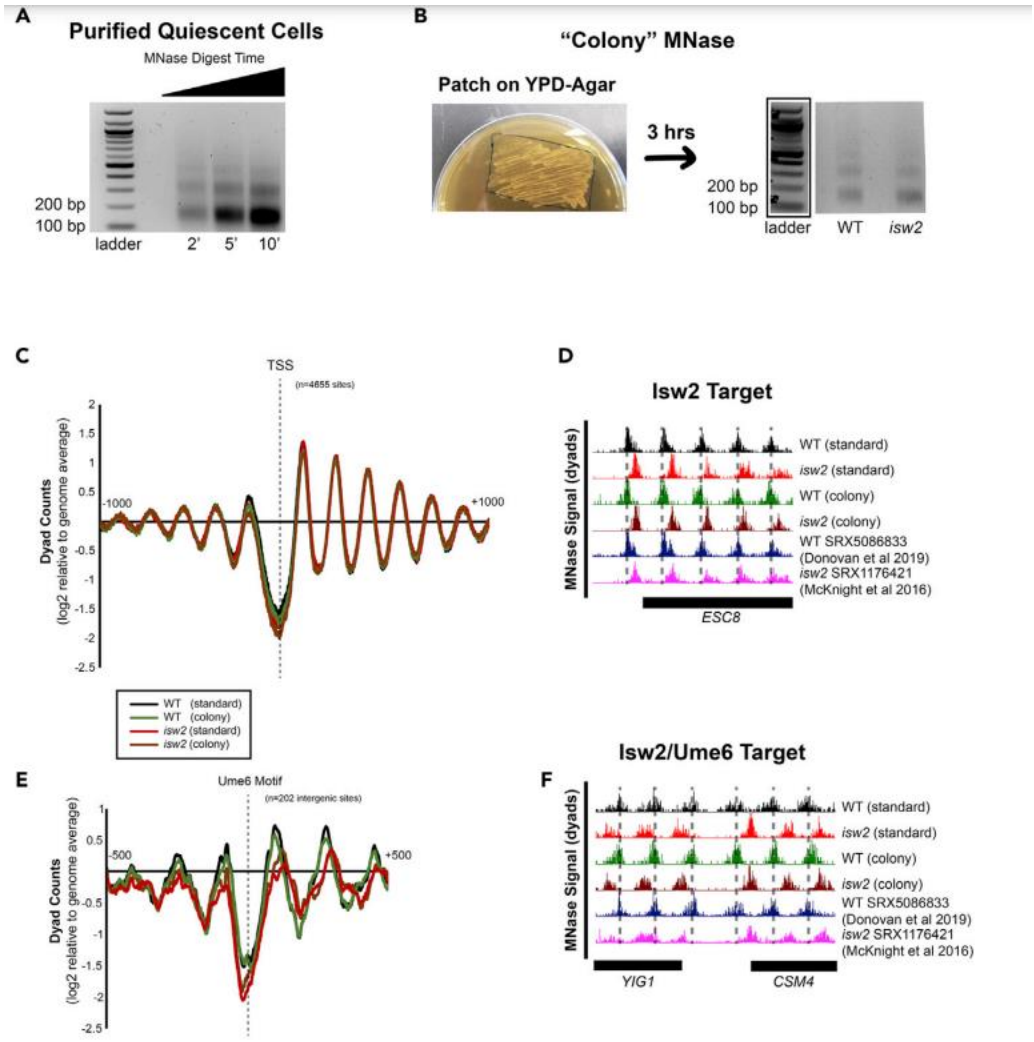

Figure 11. Rapid MNase can recover nucleosome footprints from isolated quiescent cells and yeast patches (A) Representative gel showing nucleosome footprints recovered from purified quiescent cells using the rapid MNase protocol. (B) Representative gel (right) showing nucleosome footprints recovered from a fresh patch of yeast collected from YPD-Agar (left). (C) Nucleosome dyad signal at transcription start sites (TSSs) comparing standard and patch- recovered ‘‘colony’’ MNase footprints. (D) Example Genome Browser image showing ‘‘colony’’ MNase footprints can accurately identify Isw2-directed nucleosome positions at the ESC8 locus compared to the standard MNase protocol and published data sets. (E) Nucleosome dyad signal at 202 intergenic Ume6 target sites showing ‘‘colony’’ MNase can accurately identify global changes at an Isw2 recruitment motif. (F) Genome Browser image showing colony MNase can similarly identify Isw2-positioned nucleosomes at the YIG1- CSM4 locus, an example Ume6 target site. Dashed lines indicate Ume6- and Isw2-positioned nucleosomes.

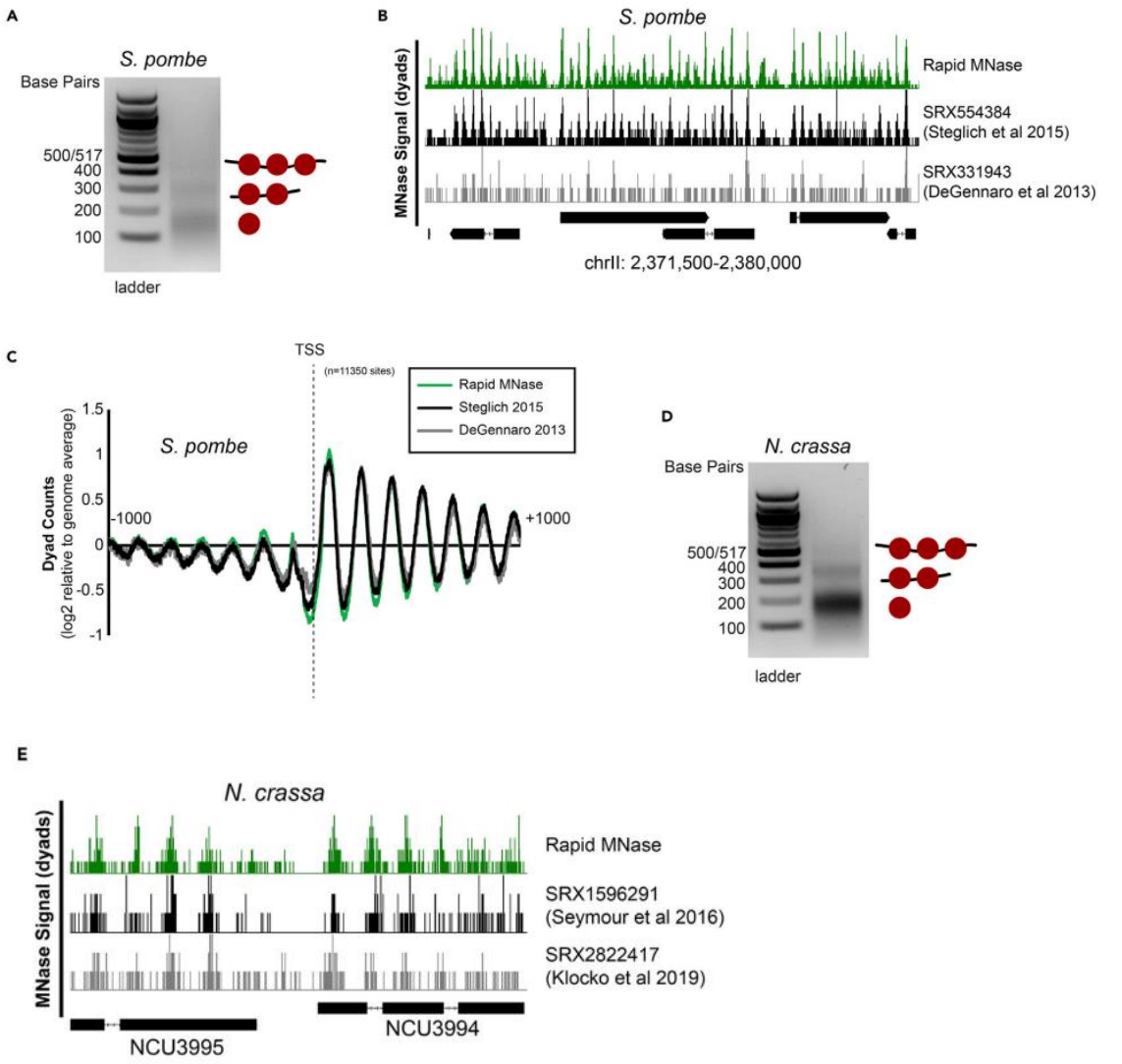

Figure 12. Rapid MNase can accurately map nucleosome positions in S. pombe and N. crassa (A) Agarose gel showing example nucleosome footprints recovered from S. pombe using the rapid MNase protocol. (B) Genome Browser image comparing nucleosome dyad positions on S. pombe chrII recovered for the rapid MNase protocol (top) and previously published data sets. (C) Alignment of nucleosome dyads at 11,350 transcription start sites (TSSs) for rapid MNase-recovered nucleosome footprints and previously published data sets. (D) Agarose gel showing example nucleosome footprints recovered from N. crassa using the rapid MNase protocol. (E) Genome Browser image comparing nucleosome dyad positions at the N. crassa NCU3995-NCU3994 locus for the rapid MNase protocol (top) and previously-published data sets.

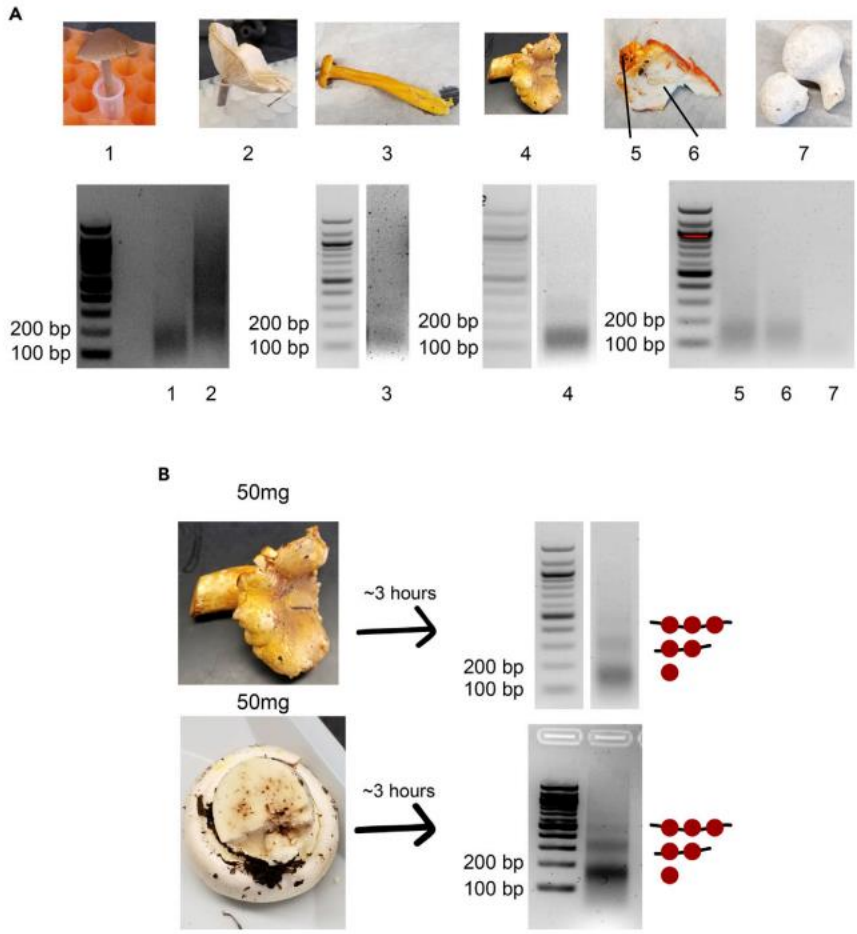

Figure 13. Nucleosome footprints can be rapidly recovered from wild mushroom samples (A) Images of locally-foraged wild mushrooms that were subjected to the rapid MNase protocol (top). Sample 5-6 consists of a distinct surface fungal specimen (5) growing on a host specimen (6). Recovered nucleosome footprints for corresponding mushrooms are shown (bottom). Speculative identities for these samples are (1) Panaeolus foenisceii, (2) unknown, (3) Craterellus tubaeformis, (4) Cantharellus formosus, (5) Hypomyces lactifluorum, (6) Russula brevines, (7) Lycoperdon perlatum. (B) Optimized rapid MNase for specimen 4 (chanterelle) was achieved using 50 mg of tissue leading to well-digested nucleosome footprints (top). The optimized protocol was performed on 50 mg of a previously-untested specimen leading to well-digested nucleosome footprints (bottom). Speculative identity of these samples are Cantharellus formosus (top) and Agricus xanthodermus (bottom).

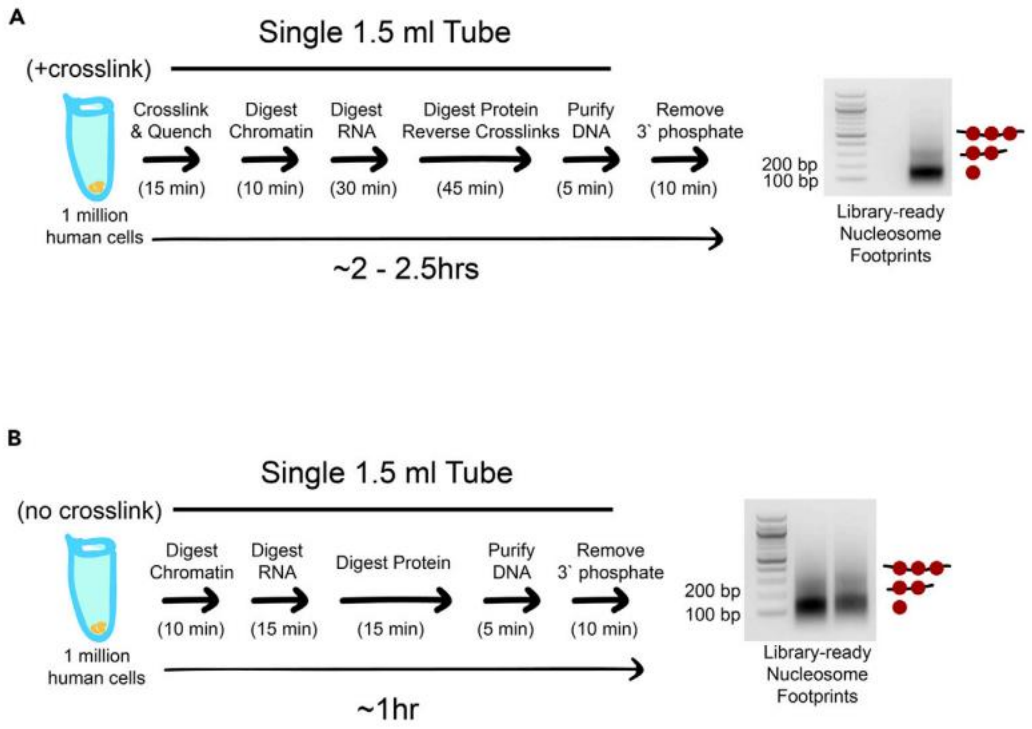

Figure 14. The rapid MNase protocol can be performed on human cells with or without crosslinking (A) Cartoon schematic showing rapid MNase protocol and associated nucleosome footprints for 1 million human cells from the diploid myeloid leukemia cell line PLB-895. The protocol is identical to the yeast liquid culture protocol except that there is no zymolyase treatment. (B) Cartoon schematic showing rapid MNase protocol for PLB-895 cells and associated nucleosome footprints when the crosslinking and crosslinking reversal steps are omitted and other steps are shortened. The crosslink-free protocol can provide nucleosome footprints that are ready for library construction in less than an hour. Left lane: 1.5 million cells input; right lane: 1 million cells input.

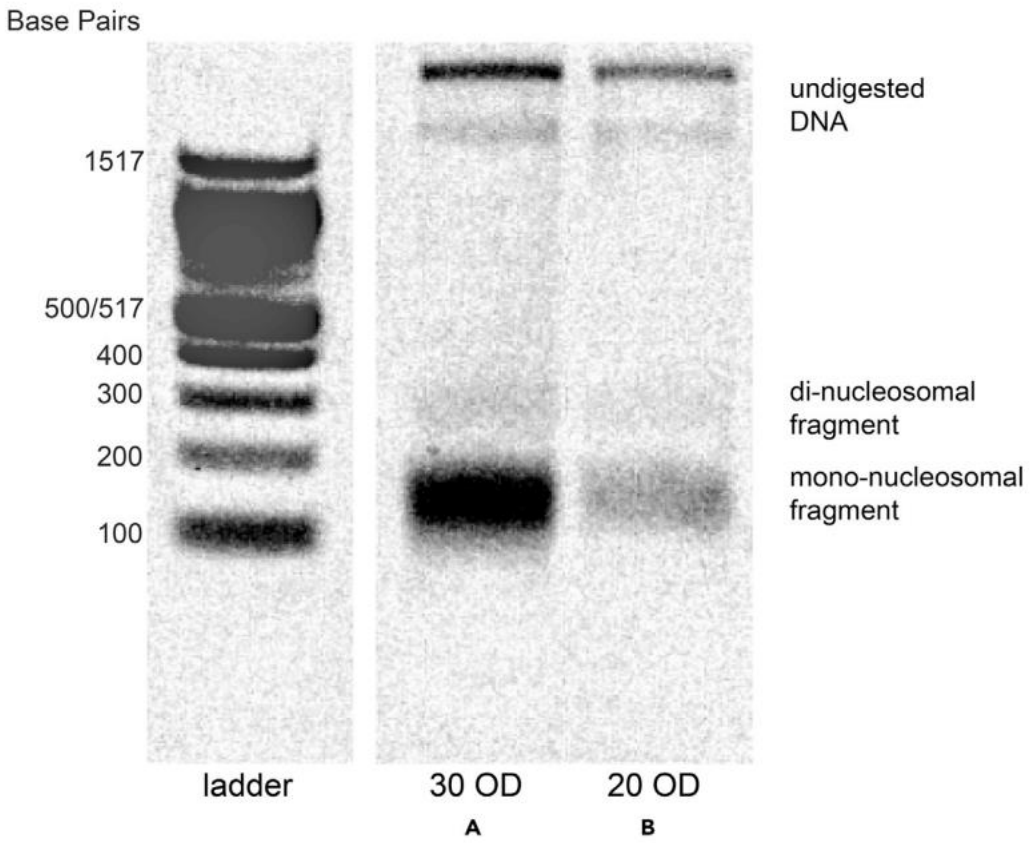

Figure 15. Sample gel showing intact genomic DNA and partial nucleosome footprints from non-permeabilized cells. Agarose gel showing example nucleosome footprints recovered from patches of S. cerevisiae using unoptimized ‘‘rapid colony MNase’’ protocol (2 mg of zymolyase for 15 mi) using an input of (A) 30 OD pellet of yeast, or (B) 20 OD pellet of yeast.

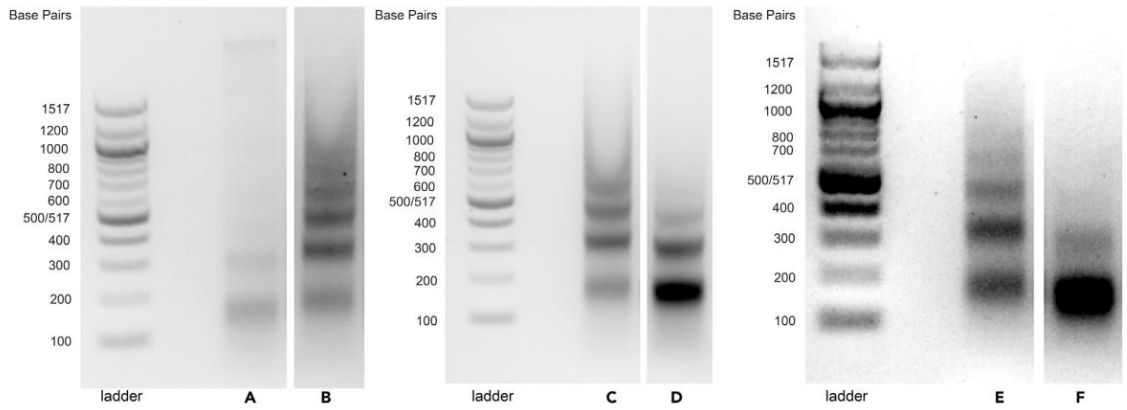

Figure 16. Sample gel showing under- and over-digested nucleosome footprints. Agarose gel showing example nucleosome footprints recovered from S. cerevisiae liquid culture using the rapid MNase protocol (A) Only 15 OD of cells were used as input. (B) Under-digested sample. (C) Under-digested sample. (D) Over-digested sample. (E) Under-digested sample. (F) Over-digested sample.

Chapter V Figures

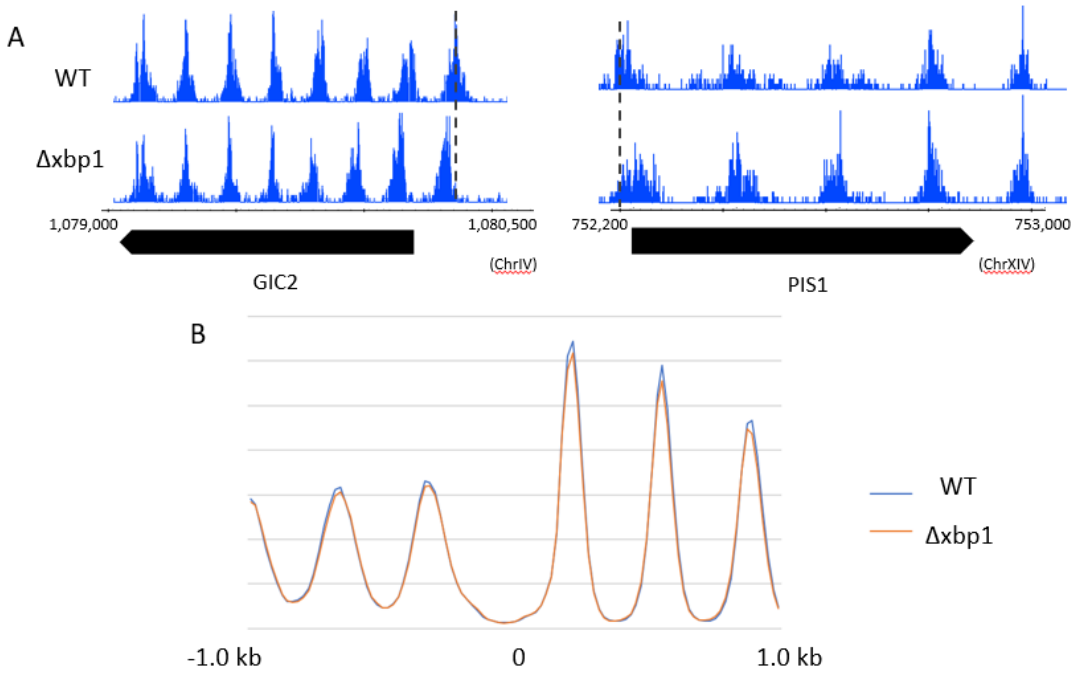

Figure 17: Xbp1 has little effect on nucleosome positions. A. MNase-seq at Gic2 and Pis1 in wild-type and Xbp1 knockouts. B. Nucleosome phase arrays of global nucleosome distributions in wildtype cells and Xbp1 knockouts.

Supplementary Tables and Figures

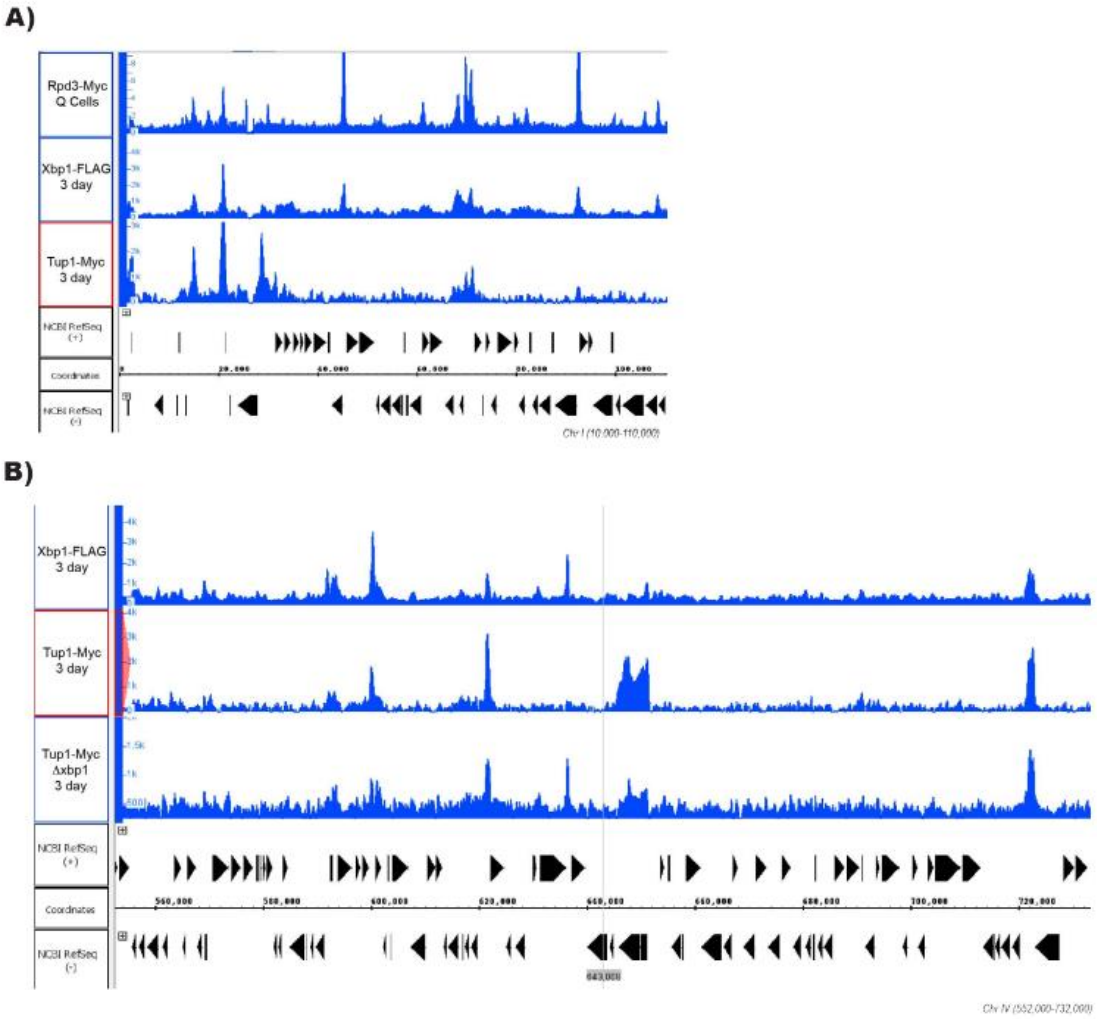

Supplementary Figure 1. Rpd3, Xbp1, and Tup1 Colocalize in Glucose-Starved Yeast. (A) Integrated Genome Browser (IGB) tracks representative of ChIP-Seq for Rpd3-Myc in quiescent cells (Q cells), Xbp1-FLAG in stationary phase (3 day), and Tup1-Myc in stationary phase (3 day). Rpd3-Myc data is from McKnight, Boerma et al. 2015. (B) Integrated Genome Browser (IGB) tracks representative of ChIP-Seq in stationary phase (3 day) for Xbp1-FLAG, Tup1-Myc, and Tup1-Myc in a Δxbp1 background.

ALT_ID	CONSENSUS	TP	TP%	FP	FP%	ENR_RATIO	SCORE_THR	PVALUE	LOG_PVALUE	EVALUE	LOG_EVALUE	QVALUE	LOG_QVALUE
Urc2p	HCGGAGWTA	57	29.23	12	6.15	4.46	13	3.330E-08	-17.22	0.0000243	-10.62	0.0000134	-11.22
Rap1p	ACACCCAYACAYYY	64	32.82	16	8.21	3.82	12	5.430E-08	-16.73	0.0000398	-10.13	0.0000134	-11.22
Tod6p	ADCGCGATGAGSTNHNV	28	14.36	1	0.51	14.5	13	7.890E-08	-16.36	0.0000577	-9.76	0.0000134	-11.22
Dot6p	ANGANGCGATGAGSTGH	24	12.31	0	0	25	16	8.090E-08	-16.33	0.0000592	-9.73	0.0000134	-11.22
Mot3p	TAGGTA	65	33.33	18	9.23	3.47	12	1.920E-07	-15.47	0.000141	-8.87	0.0000254	-10.58
Urc2p	CNTCGGAGATAWTT	57	29.23	15	7.69	3.63	12	5.610E-07	-14.39	0.000411	-7.8	0.0000619	-9.69
Met32p	ANTGTGGCGB	53	27.18	14	7.18	3.6	11	1.460E-06	-13.44	0.00107	-6.84	0.000138	-8.89
Rox1p	TCTATTGTTTCCC	54	27.69	15	7.69	3.44	8.8	2.160E-06	-13.05	0.00158	-6.45	0.000179	-8.63
Ste12p	TTGAAACAATGAAACG	50	25.64	13	6.67	3.64	8.4	2.430E-06	-12.93	0.00178	-6.33	0.000179	-8.63
Stp4p	DNNNNTTCAGCCGYACBAGNG	70	35.9	25	12.82	2.73	11	3.830E-06	-12.47	0.0028	-5.88	0.000253	-8.28
Tec1p	ACATTCTTACATTCTT	64	32.82	22	11.28	2.83	7.5	5.630E-06	-12.09	0.00412	-5.49	0.000339	-7.99
Azf1p	AAAAAGAAA	60	30.77	20	10.26	2.9	12	7.180E-06	-11.84	0.00526	-5.25	0.000396	-7.83
Matalpha2p	ATTGTT	76	38.97	30	15.38	2.48	8.9	8.230E-06	-11.71	0.00603	-5.11	0.000419	-7.78
YGR067C	GHGGGG	75	38.46	30	15.38	2.45	9.6	1.170E-05	-11.35	0.0086	-4.76	0.000556	-7.5
Upc2p	CTCGTWTAG	83	42.56	36	18.46	2.27	11	1.800E-05	-10.92	0.0132	-4.33	0.000795	-7.14
Srd1p	CNNTTTGTAGATCYCAH	72	36.92	29	14.87	2.43	10	1.960E-05	-10.84	0.0143	-4.25	0.000809	-7.12
Mot3p	WAGGTA	67	34.36	26	13.33	2.52	11	2.140E-05	-10.75	0.0157	-4.15	0.000835	-7.09
Pdr1p	TCCGCGGA	48	24.62	15	7.69	3.06	11	2.880E-05	-10.46	0.0211	-3.86	0.000953	-6.96
Pdr3p	TCCGCGGA	48	24.62	15	7.69	3.06	11	2.880E-05	-10.46	0.0211	-3.86	0.000953	-6.96
Rap1p	GGRTGTACGG	48	24.62	15	7.69	3.06	10	2.880E-05	-10.46	0.0211	-3.86	0.000953	-6.96
Ste12p	ATGAAACAATGAGACA	26	13.33	4	2.05	5.4	14	3.950E-05	-10.14	0.0289	-3.54	0.00115	-6.77
Msn1p	AATGTCCH	54	27.69	19	9.74	2.75	12	3.980E-05	-10.13	0.0291	-3.54	0.00115	-6.77
YKL222C	BAACGGARATAANNC	54	27.69	19	9.74	2.75	12	3.980E-05	-10.13	0.0291	-3.54	0.00115	-6.77
Tec1p	TTCTCACATTCTTC	71	36.41	30	15.38	2.32	9.1	4.720E-05	-9.96	0.0345	-3.37	0.00129	-6.65
Zap1p	TTCTTTATGGT	45	23.08	14	7.18	3.07	14	4.880E-05	-9.93	0.0357	-3.33	0.00129	-6.65
Hap1p	TAWCTCCG	55	28.21	20	10.26	2.67	12	5.110E-05	-9.88	0.0374	-3.29	0.0013	-6.64
Gat3p	AAATBRGATCTACAAGCTG	81	41.54	38	19.49	2.1	9.8	8.830E-05	-9.34	0.0646	-2.74	0.00216	-6.14
Tye7p	TGCRTCACGTGAYGCNNC	22	11.28	3	1.54	5.75	13	1.000E-04	-9.21	0.0732	-2.61	0.00236	-6.05
YML081W	CCCCDCH	107	54.87	57	29.23	1.86	10	1.110E-04	-9.1	0.0816	-2.51	0.00254	-5.97
Ste12p	CGTTTCA	68	34.87	30	15.38	2.23	13	1.280E-04	-8.96	0.0937	-2.37	0.00282	-5.87
Yrm1p	ACGGAAAT	66	33.85	29	14.87	2.23	12	1.510E-04	-8.8	0.11	-2.2	0.00322	-5.74
Yox1p	TWAATTR	29	14.87	7	3.59	3.75	7.4	2.080E-04	-8.48	0.152	-1.88	0.00423	-5.47
Arg81p	AAGTGCAACTGACTGCGA	25	12.82	5	2.56	4.33	7.6	2.110E-04	-8.47	0.154	-1.87	0.00423	-5.47
Sfl1p	THNHDNATAGAAGAAATAWDW	32	16.41	9	4.62	3.3	13	2.910E-04	-8.14	0.213	-1.55	0.00567	-5.17
Stp4p	TGCGCTABC	72	36.92	35	17.95	2.03	11	3.620E-04	-7.93	0.265	-1.33	0.00684	-4.99
Hcm1p	ATMAACAA	63	32.31	29	14.87	2.13	10	3.970E-04	-7.83	0.291	-1.24	0.00731	-4.92
Stp3p	GCTAGCGCA	55	28.21	24	12.31	2.24	12	4.800E-04	-7.64	0.351	-1.05	0.00859	-4.76
Lys14p	CNCAAAATTCCGBGCGNT	47	24.1	19	9.74	2.4	12	5.470E-04	-7.51	0.4	-0.92	0.00953	-4.65
Abf1p	RTCRYYY	51	26.15	22	11.28	2.26	10	6.690E-04	-7.31	0.49	-0.71	0.0114	-4.48
Fzf1p	YGSMNMCTATCAYTTYY	40	20.51	15	7.69	2.56	11	7.060E-04	-7.26	0.517	-0.66	0.0117	-4.45
Pdr8p	TCCGHGGA	88	45.13	49	25.13	1.78	9.2	9.120E-04	-7	0.668	-0.4	0.0147	-4.22
Rds2p	ANNNNGAAAAYCCGAGNNNNT	55	28.21	26	13.33	2.07	11	1.240E-03	-6.69	0.909	-0.1	0.0196	-3.93
Gsm1p	ANCTCCG	65	33.33	34	17.44	1.89	9.5	1.810E-03	-6.32	1.32	0.28	0.0262	-3.64
Mig1p	ATTTTGCGGGG	58	29.74	29	14.87	1.97	10	1.820E-03	-6.31	1.33	0.29	0.0262	-3.64
Mig2p	ATTTTGCGGGG	58	29.74	29	14.87	1.97	10	1.820E-03	-6.31	1.33	0.29	0.0262	-3.64
Mig3p	ATTTTGCGGGG	58	29.74	29	14.87	1.97	10	1.820E-03	-6.31	1.33	0.29	0.0262	-3.64
Gcr1p	CWTCC	52	26.67	25	12.82	2.04	9	2.000E-03	-6.21	1.46	0.38	0.0282	-3.57
Cep3p	YTCGGAAA	78	40	44	22.56	1.76	12	2.090E-03	-6.17	1.53	0.43	0.0288	-3.55
Cup2p	HTHNNGCTGD	27	13.85	9	4.62	2.8	12	2.490E-03	-5.99	1.83	0.6	0.0337	-3.39
Stb5p	CGGTGTTA	30	15.38	11	5.64	2.58	10	2.780E-03	-5.89	2.03	0.71	0.0368	-3.3
Rlm1p	CTAWWWWTAG	39	20	17	8.72	2.22	10	3.060E-03	-5.79	2.24	0.81	0.0397	-3.23
Tbf1p	ARCCCTAA	64	32.82	35	17.95	1.81	11	3.420E-03	-5.68	2.5	0.92	0.0435	-3.13
YKL222C	AACGGARAT	73	37.44	42	21.54	1.72	11	3.730E-03	-5.59	2.73	1.01	0.0466	-3.07
Arg80p	CCTCTAAAGG	51	26.15	26	13.33	1.93	9.2	4.100E-03	-5.5	3	1.1	0.0503	-2.99
Srd1p	GTAGWTC	42	21.54	20	10.26	2.05	9.6	4.800E-03	-5.34	3.51	1.26	0.0578	-2.85
Mcm1p	TTACCNAATTNGGTAA	110	56.41	72	36.92	1.52	4	4.960E-03	-5.31	3.63	1.29	0.0578	-2.85
Ixr1p	KTTSAAYKGTTYASA	105	53.85	68	34.87	1.54	6.6	4.970E-03	-5.3	3.64	1.29	0.0578	-2.85
Abf1p	AGCCGTAAATAGTTATCTTCCAAG	33	16.92	14	7.18	2.27	0.15	5.130E-03	-5.27	3.76	1.32	0.0586	-2.84
Aft2p	CGCACCC	101	51.79	66	33.85	1.52	9.4	6.670E-03	-5.01	4.88	1.59	0.0749	-2.59
Yap1p	ASGTAATT	108	55.38	72	36.92	1.49	10	7.240E-03	-4.93	5.3	1.67	0.0799	-2.53
Nrg2p	HAGGGTCB	50	25.64	27	13.85	1.82	11	7.970E-03	-4.83	5.83	1.76	0.0865	-2.45
Cad1p	TTACGTAAT	152	77.95	109	55.9	1.39	7.5	8.230E-03	-4.8	6.02	1.8	0.0879	-2.43
Pdr3p	VCGGAA	47	24.1	25	12.82	1.85	8.8	8.600E-03	-4.76	6.3	1.84	0.0894	-2.41
Dal81p	GAAAATTGCGTT	55	28.21	31	15.9	1.75	10	8.780E-03	-4.74	6.43	1.86	0.0894	-2.41
Dal82p	GAAAATTGCGTT	55	28.21	31	15.9	1.75	10	8.780E-03	-4.74	6.43	1.86	0.0894	-2.41
Met32p	TGTGGCDB	132	67.69	93	47.69	1.41	8.9	9.450E-03	-4.66	6.92	1.93	0.0948	-2.36
Rds1p	CCBBTCGGCCGAAVDNCD	89	45.64	58	29.74	1.53	7.2	1.000E-02	-4.61	7.32	1.99	0.0988	-2.31
Rlm1p	TAWWWWTAGM	81	41.54	52	26.67	1.55	9.2	1.110E-02	-4.51	8.09	2.09	0.103	-2.27
Met32p	ABTGTGGC	67	34.36	41	21.03	1.62	10	1.120E-02	-4.49	8.22	2.11	0.103	-2.27
Mig1p	TTATTTCTGGGG	108	55.38	74	37.95	1.45	6.4	1.130E-02	-4.48	8.28	2.11	0.103	-2.27
Mig2p	TTATTTCTGGGG	108	55.38	74	37.95	1.45	6.4	1.130E-02	-4.48	8.28	2.11	0.103	-2.27
Mig3p	TTATTTCTGGGG	108	55.38	74	37.95	1.45	6.4	1.130E-02	-4.48	8.28	2.11	0.103	-2.27
Mot3p	AAGGWT	50	25.64	28	14.36	1.76	11	1.140E-02	-4.48	8.32	2.12	0.103	-2.27
Msn1p	AATGTCC	39	20	20	10.26	1.9	12	1.190E-02	-4.43	8.69	2.16	0.106	-2.24
Stb5p	CGGKGTTATA	73	37.44	46	23.59	1.57	9.9	1.210E-02	-4.41	8.89	2.19	0.107	-2.23
Rdr1p	TNNGNCNTGCGGAWATNNNNC	60	30.77	36	18.46	1.65	12	1.280E-02	-4.36	9.39	2.24	0.111	-2.2
Rph1p	AANNNDAWTTAGGGGKGNA	84	43.08	55	28.21	1.52	9.5	1.290E-02	-4.35	9.41	2.24	0.111	-2.2

Supplementary Table 1: Motif Analysis of Tup1 ChIP in Stationary Phase (3 day)
TP = The number of primary sequences matching the motif / the number of primary sequences (the percentage of primary sequences matching the motif) TP% = The percentage of primary sequences matching the motif with scores greater than or equal to the optimal match score threshold FP = The number of control sequences matching the

motif / the number of primary sequences (the percentage of control sequences matching the motif) FP% = The percentage of control sequences matching the motif with scores greater than or equal to the optimal match score threshold ENR_RATIO = The relative enrichment ration of the motif in the primary vs. control sequences, defined as Ratio = ((TP+1)/(NPOS+1)) / ((FP+1)/(NNEG+1)), where NPOS is the number of primary sequences in the input, and NNEG is the number of control sequences in the input SCORE_THR = The match score threshold giving the optimal p-value. This is the score threshold used by SEA to determine the values of “TP” and “FP”.

REFERENCES CITED

Agarwal, M., Kumar, P., & Mathew, S. J. (2015). The Groucho/Transducin-like enhancer of split protein family in animal development. IUBMB Life, 67(7), 472–481. https://doi.org/10.1002/iub.1395

Allen, C., Buttner, S., Aragon, A.D., Thomas, J.A., Meirelles, O., Jaetao, J.E., Benn, D., Ruby, S.W., Veenhuis, M., Madeo, F., et al. (2006). Isolation of quiescent and nonquiescent cells from yeast stationary-phase cultures. J. Cell Biol. 174, 89–100.

Anders S, Pyl PT, Huber W. 2015. HTSeq–a Python framework to work with high-throughput sequencing data. Bioinformatics 31:166–169. DOI: https://doi.org/10.1093/bioinformatics/btu638, PMID: 25260700

Bailey, T. L., & Grant, C. E. (2021). SEA: Simple Enrichment Analysis of motifs. BioRxiv, 2021.08.23.457422. https://www.biorxiv.org/content/10.1101/2021.08.23.457422v1

Baldi S, Jain DS, Harpprecht L, Zabel A, Scheibe M, Butter F, Straub T, Becker PB. 2018. Genome-wide rules of nucleosome phasing in Drosophila. Molecular Cell 72:661–672. DOI: https://doi.org/10.1016/j.molcel.2018.09.032, PMID: 30392927

Beck, S., Bernstein, B. E., Campbell, R. M., Costello, J. F., Dhanak, D., Ecker, J. R., Greally, J. M., Issa, J. P., Laird, P. W., Polyak, K., Tycko, B., & Jones, P. A. (2012). A blueprint for an international cancer epigenome consortium. A report from the AACR cancer epigenome task force. Cancer Research, 72(24), 6319–6324. https://doi.org/10.1158/0008-5472.CAN-12-3658

Bolger AM, Lohse M, Usadel B. 2014. Trimmomatic: a flexible trimmer for illumina sequence data. Bioinformatics 30:2114–2120. DOI: https://doi.org/10.1093/bioinformatics/btu170, PMID: 24695404

Bowman GD, McKnight JN. 2017. Sequence-specific targeting of chromatin remodelers organizes precisely positioned nucleosomes throughout the genome. BioEssays 39:e201600183. DOI: https://doi.org/10.1002/bies.201600183

Breeden L. 1996. Start-specific transcription in yeast. Current Topics in Microbiology and Immunology 208:95–127. DOI: https://doi.org/10.1007/978-3-642-79910-5_5, PMID: 8575215

Cai, L.; Sutter, B. M.; Li, B.; Tu, B. P. (2011). Acetyl-CoA Induces Cell Growth and Proliferation by Promoting the Acetylation of Histones at Growth Genes. Molecular Cell, 42(4), 426–437. https://doi.org/10.1016/j.molcel.2011.05.004.Acetyl-CoA

Cam, H.P., and Whitehall, S. (2016). Micrococcal nuclease digestion of schizosaccharomyces pombe chromatin. Cold Spring Harb. Protoc. 2016, 996–1000.

Chanoumidou, K., Hadjimichael, C., Athanasouli, P., Ahlenius, H., Klonizakis, A., Nikolaou, C., Drakos, E., Kostouros, A., Stratidaki, I., Grigoriou, M., & Kretsovali, A. (2018). Groucho related gene 5 (GRG5) is involved in embryonic and neural stem cell state decisions. Scientific Reports, 8(1), 1–16. https://doi.org/10.1038/s41598-018-31696-9

Chen, K., Wilson, M. A., Hirsch, C., Watson, A., Liang, S., Lu, Y., Li, W., & Dent, S. Y. R. (2013). Stabilization of the promoter nucleosomes in nucleosome-free regions by the yeast Cyc8-Tup1 corepressor. Genome Research, 23(2), 312–322. https://doi.org/10.1101/gr.141952.112

Chenevert, J., Valtz, N., & Herskowitz, I. (1994). Identification of genes required for normal pheromone-induced cell polarization in Saccharomyces cerevisiae. Genetics, 136(4), 1287–1296. https://doi.org/10.1093/genetics/136.4.1287

Clapier CR, Cairns BR. 2012. Regulation of ISWI involves inhibitory modules antagonized by nucleosomalepitopes. Nature 492:280–284. DOI: https://doi.org/10.1038/nature11625, PMID: 23143334

Clapier CR, Iwasa J, Cairns BR, Peterson CL. 2017. Mechanisms of action and regulation of ATP-dependent chromatin-remodelling complexes. Nature Reviews Molecular Cell Biology 18:407–422. DOI: https://doi.org/10.1038/nrm.2017.26, PMID: 28512350

Cole, H.A., Howard, B.H., and Clark, D.J. (2012). Genome-wide mapping of nucleosomes in yeast using paired-end sequencing. Methods Enzymol. 513, 145–168.

Fazzio, T.G., Kooperberg, C., Goldmark, J. P., Neal, C, Basom, R., Delrow, J., Tsukiyama, T., Widespread collaboration of Isw2 and Sin3-Rpd3 chromatin remodeling complexes in transcriptional repression. Molecular and Cellular Biology 21:6450–6460. DOI: https://doi.org/10.1128/MCB.21.19.6450-6460.2001, PMID: 11533234

Conlan, R. S., Gounalaki, N., Hatzis, P., & Tzamarias, D. (1999). The Tup1-Cyc8 Protein Complex Can Shift from a Transcriptional Co-repressor to a Transcriptional Co-activator. Journal of Biological Chemistry, 274(1), 205–210. https://doi.org/10.1074/jbc.274.1.205

Corces, M. R., Granja, J. M., Shams, S., Louie, B. H., Seoane, J. A., Zhou, W., Silva, T. C., Groeneveld, C., Wong, C. K., Cho, S. W., Satpathy, A. T., Mumbach, M. R., Hoadley, K. A., Robertson, A. G., Sheffield, N. C., Felau, I., Castro, M. A. A., Berman, B. P., Staudt, L. M., … Chang, H. Y. (2018). The chromatin accessibility landscape of primary human cancers. Science, 362(6413). https://doi.org/10.1126/science.aav1898

Cunningham F, Amode MR, Barrell D, Beal K, Billis K, Brent S, Carvalho-Silva D, Clapham P, Coates G, FitzgeraldS, Gil L, Giro´ n CG, Gordon L, Hourlier T, Hunt SE, Janacek SH, Johnson N, Juettemann T, Ka¨ha¨ri AK, Keenan S,et al. 2015. Ensembl 2015. Nucleic Acids Research 43:D662–D669. DOI: https://doi.org/10.1093/nar/gku1010, PMID: 25352552

Dang W, Bartholomew B. 2007. Domain architecture of the catalytic subunit in the ISW2-nucleosome complex. Molecular and Cellular Biology 27:8306–8317. DOI: https://doi.org/10.1128/MCB.01351-07, PMID: 17908792

Dang W, Kagalwala MN, Bartholomew B. 2006. Regulation of ISW2 by concerted action of histone H4 tail and extranucleosomal DNA. Molecular and Cellular Biology 26:7388–7396. DOI: https://doi.org/10.1128/MCB.01159-06, PMID: 17015471

Davie, J. K., Edmondson, D. G., Coco, C. B., & Dent, S. Y. R. (2003). Tup1-Ssn6 Interacts with Multiple Class I Histone Deacetylases in Vivo. Journal of Biological Chemistry, 278(50), 50158–50162. https://doi.org/10.1074/jbc.M309753200

de Virgilio, C. (2012). The essence of yeast quiescence. FEMS Microbiology Reviews, 36(2), 306–339. https://doi.org/10.1111/j.1574-6976.2011.00287.x

DeGennaro, C.M., Alver, B.H., Marguerat, S., Stepanova, E., Davis, C.P., Ba¨ hler, J., Park, P.J., and Winston, F. (2013). Spt6 regulates intragenic and antisense transcription, nucleosome positioning, and histone modifications genome-wide in fission yeast. Mol. Cell Biol. 33, 4779–4792.

Dobin A, Davis CA, Schlesinger F, Drenkow J, Zaleski C, Jha S, Batut P, Chaisson M, Gingeras TR. 2013. STAR:ultrafast universal RNA-seq aligner. Bioinformatics 29:15–21. DOI:https://doi.org/10.1093/bioinformatics/bts635, PMID: 23104886

Donovan DA, Crandall JG, Banks OGB, Jensvold ZD, Truong V, Dinwiddie D, McKnight LE, McKnight JN. 2019. Engineered chromatin remodeling proteins for precise nucleosome positioning. Cell Reports 29:2520–2535. DOI: https://doi.org/10.1016/j.celrep.2019.10.046, PMID: 31747617

Ehrensberger, A. H., & Svejstrup, J. Q. (2012). Reprogramming chromatin. Critical Reviews in Biochemistry and Molecular Biology, 47(5), 464–482. https://doi.org/10.3109/10409238.2012.697125

Fazzio TG, Kooperberg C, Goldmark JP, Neal C, Basom R, Delrow J, Tsukiyama T. 2001. Widespread

Felsenfeld, G. (1978). Chromatin. Nature, 271(412), 115–121. http://10.0.4.56/009059999108902%5Cnhttp://search.ebscohost.com/login.aspx?direct=true&db=hia&AN=3788411&amp%5Cnlang=fr&site=ehost-live

Fleming, A. B., Beggs, S., Church, M., Tsukihashi, Y., & Pennings, S. (2014). The yeast Cyc8-Tup1 complex cooperates with Hda1p and Rpd3p histone deacetylases to robustly repress transcription of the subtelomeric FLO1 gene. Biochimica et Biophysica Acta - Gene Regulatory Mechanisms, 1839(11), 1242–1255. https://doi.org/10.1016/j.bbagrm.2014.07.022

Flores-Saaib, R. D., & Courey, A. J. (2000). Analysis of Groucho-histone interactions suggests mechanistic similarities between Groucho- and Tup1-mediated repression. Nucleic Acids Research, 28(21), 4189–4196. https://doi.org/10.1093/nar/28.21.4189

Foord R, Taylor IA, Sedgwick SG, Smerdon SJ. 1999. X- ray structural analysis of the yeast cell cycle regulator Swi6 reveals variations of the ankyrin fold and has implications for Swi6 function. Nature Structural Biology 6:157–165. DOI: https://doi.org/10.1038/5845, PMID: 10048928

Freese, N. H., Norris, D. C., & Loraine, A. E. (2016). Integrated genome browser: Visual analytics platform for genomics. Bioinformatics, 32(14), 2089–2095. https://doi.org/10.1093/bioinformatics/btw069

Fyodorov DV, Kadonaga JT. 2002. Binding of Acf1 to DNA involves a WAC motif and is important for ACFmediated chromatin assembly. Molecular and Cellular Biology 22:6344–6353. DOI: https://doi.org/10.1128/MCB.22.18.6344-6353.2002, PMID: 12192034

Galagan, J.E., Calvo, S.E., Borkovich, K.A., Selker, E.U., Read, N.D., Jaffe, D., FitzHugh, W., Ma, L.J., Smirnov, S., Purcell, S., et al. (2003). The genome sequence of the filamentous fungus Neurospora crassa. Nature 422, 859–868.

Gelbart ME, Bachman N, Delrow J, Boeke JD, Tsukiyama T. 2005. Genome-wide identification of Isw2 chromatin-remodeling targets by localization of a catalytically inactive mutant. Genes & Development 19:942–954. DOI: https://doi.org/10.1101/gad.1298905, PMID: 15833917

Givens, R.M., Mesner, L.D., Hamlin, J.L., Buck, M.J., and Huberman, J.A. (2011). Integrity of chromatin and replicating DNA in nuclei released from fission yeast by semi-automated grinding in liquid nitrogen. BMC Res. Notes 4, 499.

Gkikopoulos T, Schofield P, Singh V, Pinskaya M, Mellor J, Smolle M, Workman JL, Barton GJ, Owen-Hughes T. 2011. A role for Snf2-related nucleosome-spacing enzymes in genome-wide nucleosome organization. Science 333:1758–1760. DOI: https://doi.org/10.1126/science.1206097, PMID: 21940898

Goldmark JP, Fazzio TG, Estep PW, Church GM, Tsukiyama T. 2000. The Isw2 chromatin remodeling complex represses early meiotic genes upon recruitment by Ume6p. Cell 103:423–433. DOI: https://doi.org/10.1016/S0092-8674(00)00134-3, PMID: 11081629

Gonzalez, R., and Scazzocchio, C. (1997). A rapid method for chromatin structure analysis in the filamentous fungus Aspergillus nidulans. Nucleic Acids Res. 25, 3955–3956.

Gray, J. V, Petsko, G. A., Johnston, G. C., Ringe, D., Singer, R. A., & Werner-washburne, M. (2004). “Sleeping Beauty”: Quiescence in Saccharomyces cerevisiae. Society, 68(2), 187–206. https://doi.org/10.1128/MMBR.68.2.187

Grbavec, D., Lo, R., Liu, Y., Greenfield, A., & Stifani, S. (1999). Groucho/transducin-like Enhancer of split (TLE) family members interact with the yeast transcriptional co-repressor SSN6 and mammalian SSN6-related proteins: Implications for evolutionary conservation of transcription repression mechanisms. Biochemical Journal, 337(1), 13–17. https://doi.org/10.1042/0264-6021:3370013

Hanlon, S. E., Rizzo, J. M., Tatomer, D. C., Lieb, J. D., & Buck, M. J. (2011). The stress response factors Yap6, Cin5, Phd1, and Skn7 direct targeting of the conserved co-repressor Tup1-Ssn6 in S. cerevisiae. PLoS ONE, 6(4). https://doi.org/10.1371/journal.pone.0019060

Hauk G, McKnight JN, Nodelman IM, Bowman GD. 2010. The chromodomains of the Chd1 chromatin remodeler regulate DNA access to the ATPase motor. Molecular Cell 39:711–723. DOI: https://doi.org/10.1016/j.molcel.2010.08.012, PMID: 20832723

Henikoff, J.G., Belsky, J.A., Krassovsky, K., MacAlpine, D.M., and Henikoff, S. (2011). Epigenome characterization at single base-pair resolution. Proc. Natl. Acad. Sci. U S A 108, 18318– 18323.

Hota SK, Bhardwaj SK, Deindl S, Lin YC, Zhuang X, Bartholomew B. 2013. Nucleosome mobilization by ISW2 requires the concerted action of the ATPase and SLIDE domains. Nature Structural & Molecular Biology 20:222–229. DOI: https://doi.org/10.1038/nsmb.2486, PMID: 23334290

Hsieh, W. C., Sutter, B. M., Ruess, H., Barnes, S. D., Malladi, V. S., & Tu, B. P. (2022). Glucose starvation induces a switch in the histone acetylome for activation of gluconeogenic and fat metabolism genes. Molecular Cell, 82(1), 60-74.e5. https://doi.org/10.1016/j.molcel.2021.12.015

Hwang WL, Deindl S, Harada BT, Zhuang X. 2014. Histone H4 tail mediates allosteric regulation of nucleosome remodelling by Linker DNA. Nature 512:213–217. DOI: https://doi.org/10.1038/nature13380, PMID: 25043036

Ito T, Levenstein ME, Fyodorov DV, Kutach AK, Kobayashi R, Kadonaga JT. 1999. ACF consists of two subunits, Acf1 and ISWI, that function cooperatively in the ATP-dependent catalysis of chromatin assembly. Genes & Development 13:1529–1539. DOI: https://doi.org/10.1101/gad.13.12.1529, PMID: 10385622

Jennings, B. H., & Ish-Horowicz, D. (2008). The Groucho/TLE/Grg family of transcriptional co-repressors. Genome Biology, 9(1), 205. https://doi.org/10.1186/gb-2008-9-1-205

Jumper, J., Evans, R., Pritzel, A., Green, T., Figurnov, M., Ronneberger, O., Tunyasuvunakool, K., Bates, R., Žídek, A., Potapenko, A., Bridgland, A., Meyer, C., Kohl, S. A. A., Ballard, A. J., Cowie, A., Romera-Paredes, B., Nikolov, S., Jain, R., Adler, J., … Hassabis, D. (2021). Highly accurate protein structure prediction with AlphaFold. Nature, 596(7873), 583–589. https://doi.org/10.1038/s41586-021-03819-2

Kagalwala MN, Glaus BJ, Dang W, Zofall M, Bartholomew B. 2004. Topography of the ISW2-nucleosome complex: insights into nucleosome spacing and chromatin remodeling. The EMBO Journal 23:2092–2104. DOI: https://doi.org/10.1038/sj.emboj.7600220, PMID: 15131696

Kassabov SR, Henry NM, Zofall M, Tsukiyama T, Bartholomew B. 2002. High-resolution mapping of changes in histone-DNA contacts of nucleosomes remodeled by ISW2. Molecular and Cellular Biology 22:7524–7534. DOI: https://doi.org/10.1128/MCB.22.21.7524-7534.2002, PMID: 12370299

Kelley LA, Mezulis S, Yates CM, Wass MN, Sternberg MJ. 2015. The Phyre2 web portal for protein modeling, prediction and analysis. Nature Protocols 10:845–858. DOI: https://doi.org/10.1038/nprot.2015.053, PMID: 25950237

Klocko, A.D., Uesaka, M., Ormsby, T., Rountree, M.R., Wiles, E.T., Adhvaryu, K.K., Honda, S., and Selker, E.U. (2019). Nucleosome positioning by an evolutionarily conserved chromatin remodeler prevents aberrant DNA methylation in neurospora. Genetics 211, 563–578.

Koch C, Moll T, Neuberg M, Ahorn H, Nasmyth K. 1993. A role for the transcription factors Mbp1 and Swi4 in progression from G1 to S phase. Science 261:1551–1557. DOI: https://doi.org/10.1126/science.8372350, PMID: 8372350

Kornberg RD. 1974. Chromatin structure: a repeating unit of histones and DNA. Science 184:868–871. DOI: https://doi.org/10.1126/science.184.4139.868, PMID: 4825889

Krietenstein N, Wal M, Watanabe S, Park B, Peterson CL, Pugh BF, Korber P. 2016. Genomic nucleosome organization reconstituted with pure proteins. Cell 167:709–721. DOI:https://doi.org/10.1016/j.cell.2016.09.045

Kubik S, Bruzzone MJ, Challal D, Dreos R, Mattarocci S, Bucher P, Libri D, Shore D. 2019. Opposing chromatin remodelers control transcription initiation frequency and start site selection. Nature Structural & Molecular Biology 26:744–754. DOI: https://doi.org/10.1038/s41594-019-0273-3, PMID: 31384063

Kurdistani, S. K., & Grunstein, M. (2003). Histone acetylation and deacetylation in yeast. Nature Reviews Molecular Cell Biology, 4(4), 276–284. https://doi.org/10.1038/nrm1075

Lai WKM, Pugh BF. 2017. Understanding nucleosome dynamics and their links to gene expression and DNA replication. Nature Reviews. Molecular Cell Biology 18:548–562. DOI: https://doi.org/10.1038/nrm.2017.47,PMID: 28537572

Langmead B, Salzberg SL. 2012. Fast gapped-read alignment with Bowtie 2. Nature Methods 9:357–359. DOI: https://doi.org/10.1038/nmeth.1923, PMID: 22388286

Larsson J (2020). eulerr: Area-Proportional Euler and Venn Diagrams with Ellipses. R package version 6.1.0, https://cran.r-project.org/package=eulerr.

Lee W, Tillo D, Bray N, Morse RH, Davis RW, Hughes TR, Nislow C. 2007. A high-resolution atlas of nucleosome occupancy in yeast. Nature Genetics 39:1235–1244. DOI: https://doi.org/10.1038/ng2117, PMID: 17873876

Li M, Hada A, Sen P, Olufemi L, Hall MA, Smith BY, Forth S, McKnight JN, Patel A, Bowman GD, Bartholomew B, Wang MD. 2015. Dynamic regulation of transcription factors by nucleosome remodeling. eLife 4:e06249. DOI: https://doi.org/10.7554/eLife.06249

Li, B., & Reese, J. C. (2001). Ssn6-Tup1 Regulates RNR3 by Positioning Nucleosomes and Affecting the Chromatin Structure at the Upstream Repression Sequence. Journal of Biological Chemistry, 276(36), 33788–33797. https://doi.org/10.1074/jbc.M104220200

Li, L., Miles, S., & Breeden, L. L. (2015). A genetic screen for Saccharomyces cerevisiae mutants that fail to enter quiescence. G3: Genes, Genomes, Genetics, 5(8), 1783–1795. https://doi.org/10.1534/g3.115.019091

Lin, X., Yu, A. Q., Zhang, C. Y., Pi, L., Bai, X. W., & Xiao, D. G. (2017). Functional analysis of the global repressor Tup1 for maltose metabolism in Saccharomyces cerevisiae: Different roles of the functional domains. Microbial Cell Factories, 16(1), 1–12. https://doi.org/10.1186/s12934-017-0806-6

Longtine, M.S.; McKenzie, A.; Demarini, D.J.; Shah, N.G.; Wach, A.; Brachat, A.; Philippsen, P.; Pringle, J.R. (1998). Additional modules for versatile and economical PCR-based gene deletion and modification in Saccharomyces cerevisiae Yeast, 14(10), 953-61. https://doi.org/10.1002/(SICI)1097-0061(199807)14:10<953::AID-YEA293>3.0.CO;2-U

Lorch, Y., & Kornberg, R. D. (2017). Chromatin-remodeling for transcription. Quarterly Reviews of Biophysics, 50, 1–15. https://doi.org/10.1017/S003358351700004X

Love MI, Huber W, Anders S. 2014. Moderated estimation of fold change and dispersion for RNA-seq data with DESeq2. Genome Biology 15:550. DOI: https://doi.org/10.1186/s13059-014-0550-8, PMID: 25516281

Lowary PT, Widom J. 1998. New DNA sequence rules for high affinity binding to histone octamer and sequencedirected nucleosome positioning. Journal of Molecular Biology 276:19–42. DOI: https://doi.org/10.1006/jmbi.1997.1494, PMID: 9514715

Ludwigsen J, Pfennig S, Singh AK, Schindler C, Harrer N, Forne´ I, Zacharias M, Mueller-Planitz F. 2017. Concerted regulation of ISWI by an autoinhibitory domain and the H4 N-terminal tail. eLife 6:e21477. DOI: https://doi.org/10.7554/eLife.21477, PMID: 28109157

Luger K, Mader AW, Richmond RK, Sargent DF, Richmond TJ. 1997. Crystal structure of the nucleosome core particle at 2.8 A resolution. Nature 389:251–260. DOI: https://doi.org/10.1038/38444, PMID: 9305837

Luger K, Rechsteiner TJ, Richmond TJ. 1999. Expression and purification of recombinant histones and nucleosome reconstitution. Methods in Molecular Biology 119:1–16. DOI: https://doi.org/10.1385/1-59259-681-9:1, PMID: 10804500

Lusser A, Urwin DL, Kadonaga JT. 2005. Distinct activities of CHD1 and ACF in ATP-dependent chromatin assembly. Nature Structural & Molecular Biology 12:160–166. DOI: https://doi.org/10.1038/nsmb884, PMID: 15643425

Lusser, A., & Kadonaga, J. T. (2003). Chromatin remodeling by ATP-dependent molecular machines. BioEssays, 25(12), 1192–1200. https://doi.org/10.1002/bies.10359

Mai, B., & Breeden, L. (1997). Xbp1, a stress-induced transcriptional repressor of the Saccharomyces cerevisiae Swi4/Mbp1 family. Molecular and Cellular Biology, 17(11), 6491–6501. https://doi.org/10.1128/MCB.17.11.6491

Malavé, T. M., & Dent, S. Y. R. (2006). Transcriptional repression by Tup1-Ssn6. Biochemistry and Cell Biology, 84(4), 437–443. https://doi.org/10.1139/O06-073

Marescal, O., & Cheeseman, I. M. (2020). Cellular Mechanisms and Regulation of Quiescence. Developmental Cell, 55(3), 259–271. https://doi.org/10.1016/j.devcel.2020.09.029

Mavrich TN, Ioshikhes IP, Venters BJ, Jiang C, Tomsho LP, Qi J, Schuster SC, Albert I, Pugh BF. 2008b. A barrier nucleosome model for statistical positioning of nucleosomes throughout the yeast genome. Genome Research 18:1073–1083. DOI: https://doi.org/10.1101/gr.078261.108, PMID: 18550805

Mavrich TN, Jiang C, Ioshikhes IP, Li X, Venters BJ, Zanton SJ, Tomsho LP, Qi J, Glaser RL, Schuster SC, Gilmour DS, Albert I, Pugh BF. 2008a. Nucleosome organization in the Drosophila genome. Nature 453:358–362. DOI: https://doi.org/10.1038/nature06929, PMID: 18408708

Maza, J. C., Nimmo, Z. M., & Young, D. D. (2016). Expanding the scope of alkyne-mediated bioconjugations utilizing unnatural amino acids. Chemical Communications, 52(1), 88–91. https://doi.org/10.1039/c5cc08287k

McKnight JN, Jenkins KR, Nodelman IM, Escobar T, Bowman GD. 2011. Extranucleosomal DNA binding directs nucleosome sliding by Chd1. Molecular and Cellular Biology 31:4746–4759. DOI: https://doi.org/10.1128/MCB.05735-11, PMID: 21969605

McKnight JN, Tsukiyama T, Bowman GD. 2016. Sequence-targeted nucleosome sliding in vivo by a hybrid Chd1 chromatin remodeler. Genome Research 26:693–704. DOI:https://doi.org/10.1101/gr.199919.115, PMID: 26993344

McKnight JN, Tsukiyama T. 2015. The conserved HDAC Rpd3 drives transcriptional quiescence in S. cerevisiae. Genomics Data 6:245–248. DOI: https://doi.org/10.1016/j.gdata.2015.10.008, PMID: 26697386

McKnight, J. N., Boerma, J. W., Breeden, L. L., & Tsukiyama, T. (2015). Global Promoter Targeting of a Conserved Lysine Deacetylase for Transcriptional Shutoff during Quiescence Entry. Molecular Cell, 59(5), 732–743. https://doi.org/10.1016/j.molcel.2015.07.014

McKnight, J. N., Breeden, L. L., & Tsukiyama, T. (2015). A molecular off switch for transcriptional quiescence. Cell Cycle, 14(23), 3667–3668. https://doi.org/10.1080/15384101.2015.1112618

McKnight, J.N., and Tsukiyama, T. (2015). The conserved HDAC Rpd3 drives transcriptional quiescence in S. cerevisiae. Genom. Data 6, 245–248.

McKnight, J.N., Tsukiyama, T., and Bowman, G.D. (2016). Sequence- targeted nucleosome sliding in vivo by a hybrid Chd1 chromatin remodeler. Genome Res. 26, 693–704.

McKnight, L. E., Crandall, J. G., Bailey, T. B., Banks, O. G. B., Orlandi, K. N., Truong, V. N., Donovan, D. A., Waddell, G. L., Wiles, E. T., Hansen, S. D., Selker, E. U., & McKnight, J. N. (2021). Rapid and inexpensive preparation of genome-wide nucleosome footprints from model and non-model organisms. STAR Protocols, 2(2), 100486. https://doi.org/10.1016/j.xpro.2021.100486

Miles, S., Bradley, G. T., & Breeden, L. L. (2021). The budding yeast transition to quiescence. Yeast, 38(1), 30–38. https://doi.org/10.1002/yea.3546

Nagalakshmi, U., Wang, Z., Waern, K., Shou, C., Raha, D., Gerstein, M., and Snyder, M. (2008). The transcriptional landscape of the yeast genome defined by RNA sequencing. Science 320, 1344– 1349.

Nair M, McIntosh PB, Frenkiel TA, Kelly G, Taylor IA, Smerdon SJ, Lane AN. 2003. NMR structure of the DNAbinding domain of the cell cycle protein Mbp1 from Saccharomyces cerevisiae. Biochemistry 42:1266–1273. DOI: https://doi.org/10.1021/bi0205247, PMID: 12564929

O'Farrell, P. H. (2011). Quiescence: Early evolutionary origins and universality do not imply uniformity. Philosophical Transactions of the Royal Society B: Biological Sciences, 366(1584), 3498–3507. https://doi.org/10.1098/rstb.2011.0079

Ocampo J, Chereji RV, Eriksson PR, Clark DJ. 2016. The ISW1 and CHD1 ATP-dependent chromatin remodelers compete to set nucleosome spacing in vivo. Nucleic Acids Research 44:4625–4635. DOI: https://doi.org/10.1093/nar/gkw068, PMID: 26861626

Ogawa, M., Yaginuma, T., Nakatomi, C., Nakajima, T., Tada-Shigeyama, Y., Addison, W. N., Urata, M., Matsubara, T., Watanabe, K., Matsuo, K., Sato, T., Honda, H., Hikiji, H., Watanabe, S., & Kokabu, S. (2019). Transducin-like enhancer of split 3 regulates proliferation of melanoma cells via histone deacetylase activity. Oncotarget, 10(3), 404–414. https://doi.org/10.18632/oncotarget.26552

Papamichos-Chronakis, M., Gligoris, T., & Tzamarias, D. (2004). The Snf1 kinase controls glucose repression in yeast by modulating interactions between the Mig1 repressor and the Cyc8-Tup1 co-repressor. EMBO Reports, 5(4), 368–372. https://doi.org/10.1038/sj.embor.7400120

Papamichos-Chronakis, M., Steven, R., Gounalaki, N., Copf, T., Tzamarias, D., Chem, J. B., & Conlan, R. S. (2000). Hrs1 / Med3 Is a Cyc8-Tup1 Corepressor Target in the RNA Polymerase II Holoenzyme. Journal of Biological Chemistry, 275(12), 8397–8403. https://doi.org/10.1074/jbc.275.12.8397

Parnell, E. J., & Stillman, D. J. (2011). Shields up: The Tup1-Cyc8 repressor complex blocks coactivator recruitment. Genes and Development, 25(23), 2429–2435. https://doi.org/10.1101/gad.181768.111

Peters-Regehr, T., Bode, J. G., Kubitz, R., & Häussinger, D. (1999). Organic osmolyte transport in quiescent and activated rat hepatic stellate cells (Ito cells). Hepatology, 29(1), 173–180. https://doi.org/10.1002/hep.510290111

Pointner J, Persson J, Prasad P, Norman-Axelsson U, Stra˚ lfors A, Khorosjutina O, Krietenstein N, Svensson JP, Ekwall K, Korber P. 2012. CHD1 remodelers regulate nucleosome spacing in vitro and align nucleosomal arrays over gene coding regions in S. pombe. The EMBO Journal 31:4388–4403. DOI: https://doi.org/10.1038/emboj.2012.289, PMID: 23103765

Polak, P., Karlic, R., Koren, A., Thurman, R., Sandstrom, R., Lawrence, M. S., Reynolds, A., Rynes, E., Vlahovicek, K., Stamatoyannopoulos, J. A., & Sunyaev, S. R. (2015). Cell-of-origin chromatin organization shapes the mutational landscape of cancer. Nature, 518(7539), 360–364. https://doi.org/10.1038/nature14221

Ramakrishnan, V. (1997). Histone structure and the organization of the nucleosome. Annual Review of Biophysics and Biomolecular Structure, 26, 83–112. https://doi.org/10.1146/annurev.biophys.26.1.83

Ramani, V., Qiu, R., and Shendure, J. (2019). High sensitivity profiling of chromatin structure by MNase-SSP. Cell Rep. 26, 2465–2476.e4.

Ramírez, F., Ryan, D. P., Grüning, B., Bhardwaj, V., Kilpert, F., Richter, A. S., Heyne, S., Dündar, F., & Manke, T. (2016). deepTools2: a next generation web server for deep-sequencing data analysis. Nucleic Acids Research, 44(W1), W160–W165. https://doi.org/10.1093/NAR/GKW257

Reimand, J., Aun, A., Vilo, J., Vaquerizas, J. M., Sedman, J., & Luscombe, N. M. (2012). M:Explorer: Multinomial regression models reveal positive and negative regulators of longevity in yeast quiescence. Genome Biology, 13(6). https://doi.org/10.1186/gb-2012-13-6-r55

Rhee HS, Pugh BF. 2012. Genome-wide structure and organization of eukaryotic pre-initiation complexes. Nature 483:295–301. DOI: https://doi.org/10.1038/nature10799, PMID: 22258509

Rittershaus, E. S. C., Baek, S. H., & Sassetti, C. M. (2013). The normalcy of dormancy: Common themes in microbial quiescence. Cell Host and Microbe, 13(6), 643–651. https://doi.org/10.1016/j.chom.2013.05.012

Rizzo, J. M., Mieczkowski, P. A., & Buck, M. J. (2011). Tup1 stabilizes promoter nucleosome positioning and occupancy at transcriptionally plastic genes. Nucleic Acids Research, 39(20), 8803–8819. https://doi.org/10.1093/nar/gkr557

Rodriguez J, McKnight JN, Tsukiyama T. 2014. Genome-Wide analysis of Nucleosome positions, occupancy, and accessibility in yeast: nucleosome mapping, high-resolution histone ChIP, and NCAM. Current Protocols in Molecular Biology 108:1–16. DOI: https://doi.org/10.1002/0471142727.mb2128s108, PMID: 25271716

Rothbart, S. B., & Strahl, B. D. (2014). Interpreting the language of histone and DNA modifications. Biochim Biophys Acta., 1839(8), 627–643. https://doi.org/10.1016/j.bbagrm.2014.03.001.Interpreting

Seymour, M., Ji, L., Santos, A.M., Kamei, M., Sasaki, T., Basenko, E.Y., Schmitz, R.J., Zhang, X., and Lewis, Z.A. (2016). Histone H1 limits DNA methylation in neurospora crassa. G3 (Bethesda) 6, 1879–1889.

Shao, N., Singh, N. S., Slade, S. E., Jones, A. M. E., & Balasubramanian, M. K. (2015). Site Specific Genetic Incorporation of Azidophenylalanine in Schizosaccharomyces pombe. Scientific Reports, 5, 1–10. https://doi.org/10.1038/srep17196

Shyh-Chang, N., & Daley, G. Q. (2015). Metabolic switches linked to pluripotency and embryonic stem cell differentiation. Cell Metabolism, 21(3), 349–350. https://doi.org/10.1016/j.cmet.2015.02.011

Sprague, E. R., Redd, M. J., Johnson, A. D., & Wolberger, C. (2000). Structure of the C-terminal domain of Tup1, a corepressor of transcription in yeast. EMBO Journal, 19(12), 3016–3027. https://doi.org/10.1093/emboj/19.12.3016

Steglich, B., Stralfors, A., Khorosjutina, O., Persson, J., Smialowska, A., Javerzat, J.P., and Ekwall,K.(2015). The Fun30 chromatin remodeler Fft3 controls nuclear organization and chromatin structure of insulators and subtelomeres in fission yeast. PLoS Genet. 11, e1005101.

Stockdale C, Flaus A, Ferreira H, Owen-Hughes T. 2006. Analysis of nucleosome repositioning by yeast ISWI and Chd1 chromatin remodeling complexes. Journal of Biological Chemistry 281:16279–16288. DOI: https://doi.org/10.1074/jbc.M600682200, PMID: 16606615

Struhl, K. (1998). Histone acetylation and transcriptional regulatory mechanisms. Genes and Development, 12(5), 599–606. https://doi.org/10.1101/gad.12.5.599

Sun, S., & Gresham, D. (2021). Cellular quiescence in budding yeast. Yeast, 38(1), 12–29. https://doi.org/10.1002/yea.3545

Swygert, S. G., Kim, S., Wu, X., Fu, T., Hsieh, T. H., Rando, O. J., Eisenman, R. N., Shendure, J., McKnight, J. N., & Tsukiyama, T. (2019). Condensin-Dependent Chromatin Compaction Represses Transcription Globally during Quiescence. Molecular Cell, 73(3), 533-546.e4. https://doi.org/10.1016/j.molcel.2018.11.020

Thodberg, M., Thieffry, A., Bornholdt, J., Boyd, M., Holmberg, C., Azad, A., Workman, C.T., Chen, Y., Ekwall, K., Nielsen, O., et al. (2019). Comprehensive profiling of the fission yeast transcription start site activity during stress and media response. Nucleic Acids Res. 47, 1671–1691.

Treitel, M. A., & Carlson, M. (1995). Repression by SSN6-TUP1 is directed by MIG1, a repressor/activator protein. Proceedings of the National Academy of Sciences, 92(8), 3132–3136. https://doi.org/10.1073/pnas.92.8.3132

Tsukiyama T, Palmer J, Landel CC, Shiloach J, Wu C. 1999. Characterization of the imitation switch subfamily of ATP-dependent chromatin-remodeling factors in Saccharomyces cerevisiae. Genes & Development 13:686–697. DOI: https://doi.org/10.1101/gad.13.6.686, PMID: 10090725

Tucker, K.A., Lilly, M.B., Heck, L., Jr., and Rado, T.A. (1987). Characterization of a new human diploid myeloid leukemia cell line (PLB-985) with granulocytic and monocytic differentiating capacity. Blood 70, 372–378.

Tümpel, S., & Rudolph, K. L. (2019). Quiescence: Good and Bad of Stem Cell Aging. Trends in Cell Biology, 29(8), 672–685. https://doi.org/10.1016/j.tcb.2019.05.002

Turner, B. M. (1991). Histone acetylation and control of gene expression. Journal of Cell Science, 99(1), 13–20. https://doi.org/10.1242/jcs.99.1.13

Tyagi, M., Imam, N., Verma, K., & Patel, A. K. (2016). Chromatin remodelers: We are the drivers!! Nucleus, 7(4), 388–404. https://doi.org/10.1080/19491034.2016.1211217

Uppuluri, P.; Perumal, P.; Chaffin, W.L. (2007). Analysis of RNA species of various sizes from stationary-phase planktonic yeast cells of Candida albicans. FEMS Yeast Research, (7), 110-117. https://doi/org/10.1111/j.1567-1364.2006.00143.x

Valcourt, J. R., Lemons, J. M. S., Haley, E. M., Kojima, M., Demuren, O. O., & Coller, H. A. (2012). Staying alive: Metabolic adaptations to quiescence. Cell Cycle, 11(9), 1680–1696. https://doi.org/10.4161/cc.19879

Valencia, A. M., & Kadoch, C. (2019). Chromatin regulatory mechanisms and therapeutic opportunities in cancer. Nature Cell Biology, 21(2), 152–161. https://doi.org/10.1038/s41556-018-0258-1

Vallette, F. M., Olivier, C., Lézot, F., Oliver, L., Cochonneau, D., Lalier, L., Cartron, P. F., & Heymann, D. (2019). Dormant, quiescent, tolerant and persister cells: Four synonyms for the same target in cancer. Biochemical Pharmacology, 162(November 2018), 169–176. https://doi.org/10.1016/j.bcp.2018.11.004

Valouev A, Johnson SM, Boyd SD, Smith CL, Fire AZ, Sidow A. 2011. Determinants of nucleosome organization in primary human cells. Nature 474:516–520. DOI: https://doi.org/10.1038/nature10002, PMID: 21602827

van Velthoven, C. T. J., & Rando, T. A. (2019). Stem Cell Quiescence: Dynamism, Restraint, and Cellular Idling. Cell Stem Cell, 24(2), 213–225. https://doi.org/10.1016/j.stem.2019.01.001

Varadi, M., Anyango, S., Deshpande, M., Nair, S., Natassia, C., Yordanova, G., Yuan, D., Stroe, O., Wood, G., Laydon, A., Zídek, A., Green, T., Tunyasuvunakool, K., Petersen, S., Jumper, J., Clancy, E., Green, R., Vora, A., Lutfi, M., … Velankar, S. (2022). AlphaFold Protein Structure Database: Massively expanding the structural coverage of protein-sequence space with high-accuracy models. Nucleic Acids Research, 50(D1), D439–D444. https://doi.org/10.1093/nar/gkab1061

Varanasi, U. S., Klis, M., Mikesell, P. B., & Trumbly, R. J. (1996). The Cyc8 (Ssn6)-Tup1 corepressor complex is composed of one Cyc8 and four Tup1 subunits. Molecular and Cellular Biology, 16(12), 6707–6714. https://doi.org/10.1128/MCB.16.12.6707

Washburn BK, Esposito RE. 2001. Identification of the Sin3-binding site in Ume6 defines a two-step process for conversion of Ume6 from a transcriptional repressor to an activator in yeast. Molecular and Cellular Biology 21:2057–2069. DOI: https://doi.org/10.1128/MCB.21.6.2057-2069.2001, PMID: 11238941

Watson, A. D., Edmondson, D. G., Bone, J. R., Mukai, Y., Yu, Y., Du, W., Stillman, D. J., & Roth, S. Y. (2000). Ssn6-Tup1 interacts with class I histone deacetylases required for repression. Genes and Development, 14(21), 2737–2744. https://doi.org/10.1101/gad.829100

Weiner, A., Hsieh, T. H. S., Appleboim, A., Chen, H. V., Rahat, A., Amit, I., Rando, O. J., & Friedman, N. (2015). High-resolution chromatin dynamics during a yeast stress response. Molecular Cell, 58(2), 371–386. https://doi.org/10.1016/j.molcel.2015.02.002

Weinstein, J. N., Collisson, E. A., Mills, G. B., Shaw, K. R. M., Ozenberger, B. A., Ellrott, K., Sander, C., Stuart, J. M., Chang, K., Creighton, C. J., Davis, C., Donehower, L., Drummond, J., Wheeler, D., Ally, A., Balasundaram, M., Birol, I., Butterfield, Y. S. N., Chu, A., … Kling, T. (2013). The cancer genome atlas pan-cancer analysis project. Nature Genetics, 45(10), 1113–1120. https://doi.org/10.1038/ng.2764

Wickham H. 2016. Ggplot2: Elegant Graphics for Data Analysis. Springer-Verlag. DOI: https://doi.org/10.1007/978-0-387-98141-3

Wiechens N, Singh V, Gkikopoulos T, Schofield P, Rocha S, Owen-Hughes T. 2016. The chromatin remodelling enzymes SNF2H and SNF2L position nucleosomes adjacent to CTCF and other transcription factors. PLOS Genetics 12:e1005940. DOI: https://doi.org/10.1371/journal.pgen.1005940, PMID: 27019336

Williams, F. E., & Trumbly, R. J. (1990). Characterization of TUP1, a mediator of glucose repression in Saccharomyces cerevisiae. Molecular and Cellular Biology, 10(12), 6500–6511. https://doi.org/10.1128/mcb.10.12.6500

Williams, F. E., Varanasi, U., & Trumbly, R. J. (1991). The CYC8 and TUP1 proteins involved in glucose repression in Saccharomyces cerevisiae are associated in a protein complex. Molecular and Cellular Biology, 11(6), 3307–3316. https://doi.org/10.1128/mcb.11.6.3307

Wong, K. H., & Struhl, K. (2011). The Cyc8-Tup1 complex inhibits transcription primarily by masking the activation domain of the recruiting protein. Genes and Development, 25(23), 2525–2539. https://doi.org/10.1101/gad.179275.111

Wood, V., Gwilliam, R., Rajandream, M.A., Lyne,M., Lyne, R., Stewart, A., Sgouros, J., Peat, N., Hayles, J., Baker, S., et al. (2002). The genome sequence of Schizosaccharomyces pombe. Nature 415, 871–880.

Wu, J., Suka, N., Carlson, M., & Grunstein, M. (2001). TUP1 utilizes histone H3/H2B-specific HDA1 deacetylase to repress gene activity in yeast. Molecular Cell, 7(1), 117–126. https://doi.org/10.1016/S1097-2765(01)00160-5

Yadon AN, Singh BN, Hampsey M, Tsukiyama T. 2013. DNA looping facilitates targeting of a chromatin remodeling enzyme. Molecular Cell 50:93–103. DOI: https://doi.org/10.1016/j.molcel.2013.02.005, PMID: 23478442

Yan C, Chen H, Bai L. 2018. Systematic study of Nucleosome-Displacing factors in budding yeast. Molecular Cell 71:294–305. DOI: https://doi.org/10.1016/j.molcel.2018.06.017, PMID: 30017582

Yan L, Wang L, Tian Y, Xia X, Chen Z. 2016. Structure and regulation of the chromatin remodeller ISWI. Nature 540:466–469. DOI: https://doi.org/10.1038/nature20590, PMID: 27919072

Yanagida, M. (2009). Cellular quiescence: are controlling genes conserved? Trends in Cell Biology, 19(12), 705–715. https://doi.org/10.1016/j.tcb.2009.09.006

Yao, G. (2014). Modelling mammalian cellular quiescence. Interface Focus, 4(3). https://doi.org/10.1098/rsfs.2013.0074

Yates, A.D., Achuthan, P., Akanni, W., Allen, J., Allen, J., Alvarez-Jarreta, J., Amode, M.R., Armean, I.M., Azov, A.G., Bennett, R., et al. (2019). Ensembl 2020. Nucleic Acids Res. 48, D682–D688.

Yen K, Vinayachandran V, Batta K, Koerber RT, Pugh BF. 2012. Genome-wide nucleosome specificity and directionality of chromatin remodelers. Cell 149:1461–1473. DOI: https://doi.org/10.1016/j.cell.2012.04.036, PMID: 22726434

Yuan, D., Yang, X., Yuan, Z., Zhao, Y., & Guo, J. (2017). TLE1 function and therapeutic potential in cancer. Oncotarget, 8(9), 15971–15976. https://d

Zakeri B, Fierer JO, Celik E, Chittock EC, Schwarz-Linek U, Moy VT, Howarth M. 2012. Peptide tag forming a rapid covalent bond to a protein, through engineering a bacterial adhesin. PNAS 109:E690–E697. DOI: https://doi.org/10.1073/pnas.1115485109, PMID: 22366317

Zhang Z, Wippo CJ, Wal M, Ward E, Korber P, Pugh BF. 2011. A packing mechanism for nucleosome organization reconstituted across a eukaryotic genome. Science 332:977–980. DOI: https://doi.org/10.1126/science.1200508, PMID: 21596991

Zhang, Y., Liu, T., Meyer, C. A., Eeckhoute, J., Johnson, D. S., Bernstein, B. E., Nussbaum, C., Myers, R. M., Brown, M., Li, W., & Shirley, X. S. (2008). Model-based analysis of ChIP-Seq (MACS). Genome Biology, 9(9). https://doi.org/10.1186/gb-2008-9-9-r137

Zhang, Z., & Reese, J. C. (2004a). Redundant mechanisms are used by Ssn6-Tup1 in repressing chromosomal gene transcription in Saccharomyces cerevisiae. Journal of Biological Chemistry, 279(38), 39240–39250. https://doi.org/10.1074/jbc.M407159200

Zhang, Z., & Reese, J. C. (2004b). Ssn6-Tup1 requires the ISW2 complex to position nucleosomes in Saccharomyces cerevisiae. EMBO Journal, 23(11), 2246–2257. https://doi.org/10.1038/sj.emboj.7600227

Zhou CY, Johnson SL, Gamarra NI, Narlikar GJ. 2016. Mechanisms of ATP-Dependent chromatin remodeling motors. Annual Review of Biophysics 45:153–181. DOI: https://doi.org/10.1146/annurev-biophys-051013-022819, PMID: 27391925

Zofall M, Persinger J, Bartholomew B. 2004. Functional role of extranucleosomal DNA and the entry site of thenucleosome in chromatin remodeling by ISW2. Molecular and Cellular Biology 24:10047–10057. DOI: https://doi.org/10.1128/MCB.24.22.10047-10057.2004, PMID: 15509805

Zofall M, Persinger J, Kassabov SR, Bartholomew B. 2006. Chromatin remodeling by ISW2 and SWI/SNF requires DNA translocation inside the nucleosome. Nature Structural & Molecular Biology 13:339–346. DOI: https://doi.org/10.1038/nsmb1071, PMID: 16518397